

WORLD METEOROLOGICAL ORGANIZATION



Year of Tropical Convection (YOTC)

The YOTC Implementation Plan

A Joint WCRP – WWRP/THORPEX International Initiative

DRAFT

July 7, 2009

Authors / Contributors will be noted : TBS

WMO/TD-No. TBD



SYNOPSIS

The realistic representation of tropical convection in our global atmospheric models is a long-standing grand challenge for numerical weather forecasts and global climate predictions. Our lack of fundamental knowledge and practical capabilities in this area leaves us disadvantaged in modeling and predicting prominent phenomena of the tropical atmosphere such as the ITCZ, ENSO, TBO, monsoons and their active/break periods, the MJO, subtropical stratus decks, near-surface ocean properties, easterly waves, tropical cyclones, bulk budgets of cloud microphysical quantities, and even the diurnal cycle. Furthermore, tropical weather/climate disturbances strongly influence stratospheric-tropospheric exchange as well as the extratropics, with the latter mediated via poleward migration of synoptic systems or through initiating Rossby wave trains that can involve a range of processes and time scales.

To address this the challenge of tropical convection, WCRP and WWRP/THORPEX propose a Year of coordinated observing, modeling and forecasting of organized tropical convection and its influences on predictability.. This effort is intended to exploit the vast amounts of existing and emerging observations, the expanding computational resources and the development of new, high-resolution modeling frameworks, with the objective of advancing the characterization, diagnosis, modeling, parameterization and prediction of multi-scale convective/dynamic interactions, including the two-way interaction between tropical and extra-tropical weather/climate. This activity and its ultimate success will be based on the coordination of a wide range of ongoing and planned international programmatic activities (e.g., GEWEX/CEOP/GCSS, AMY, EOS, GOOS), strong collaboration among the operational prediction, research laboratory and academic communities, and the construction of a comprehensive data base consisting of satellite data, in-situ data sets and global/high-resolution forecast and simulation model outputs relevant to tropical convection. The proposed timing, focus year approach and integrated framework of this effort is intended to leverage the most benefit from recent investments in Earth Science infrastructure as well as entrain a new generation of young scientists into tackling the outstanding problems in the field of weather and climate prediction.

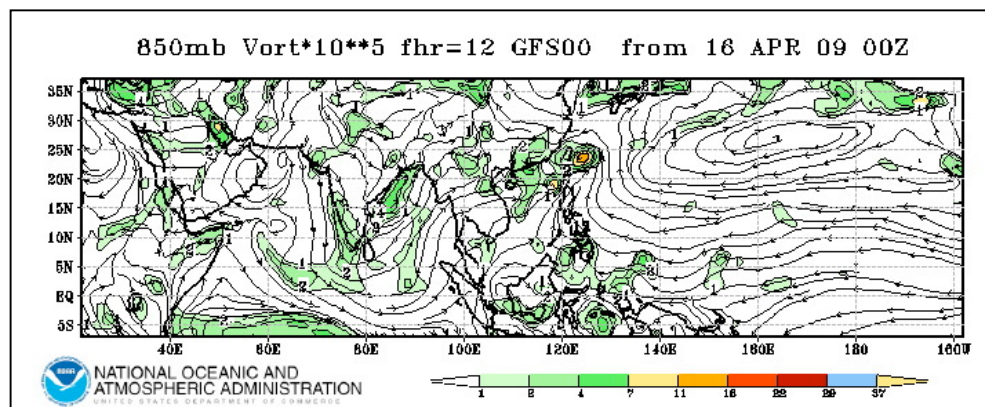
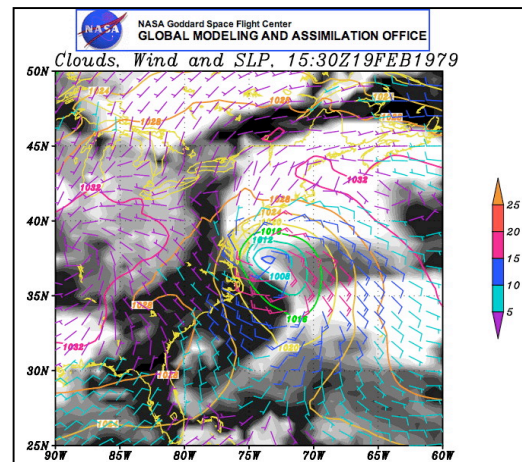
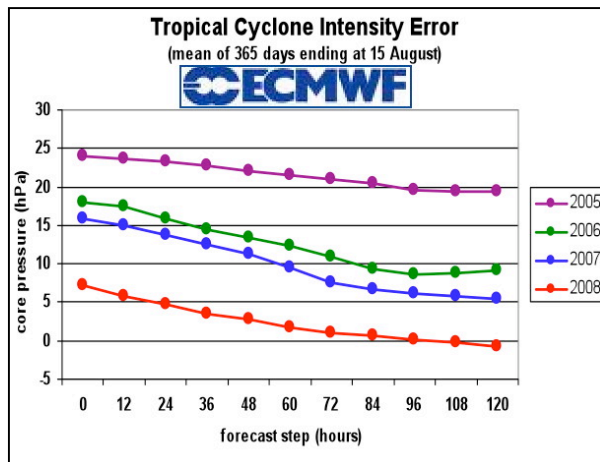
Table of Contents

1	Atmospheric Analyses and Forecasts.....	6
1.1	Introduction	7
1.2	ECMWF	7
1.3	GMAO	11
1.4	NCEP	13
2	Satellite Data.....	15
2.1	Introduction	16
2.2	Dissemination Framework.....	17
2.3	Special A-Train Data Set.....	22
2.4	Data Set Highlights.....	23
2.4.1	AIRS temperature, water vapor, and related products	23
2.4.2	AMSRE surface wind speed, precipitable and cloud-liquid water, SST, and rain rate ..	26
2.4.3	CALIPSO cloud and aerosol products.....	27
2.4.4	CERES cloud properties and radiative fluxes	28
2.4.5	CloudSat cloud and precipitation products	30
2.4.6	GPS temperature and water vapor profiles.....	32
2.4.7	ISCCP cloud products	35
2.4.8	MLS water vapor, cloud ice, composition and temperature profiles.....	36
2.4.9	MODIS Cloud Products.....	38
2.4.10	PEHRRP – high resolution precipitation products	41
2.4.11	QuikScat ocean surface wind/stress.....	43
2.4.12	TRMM/TMI precipitation, SST and related products	46
3	Synoptic Periods of Interest	47
3.1	Introduction	48
3.2	Overarching Periods of Interest.....	48
3.3	MJO and CCEWs	51
3.4	Easterly Waves and Tropical Cyclones.....	54
3.5	MJO Interactions with the Pacific Ocean.....	54
3.6	African Easterly Waves.....	56
3.6.1	Western North Pacific	57
3.7	Regions of Diurnal Cycle Focus	60
3.7.1	Overview.....	60
3.8	Indian Summer Monsoon Evolution and Components	62
3.8.1	2008.....	62
3.8.2	2009.....	64
3.9	Tropical-Extratropical Interactions.....	65
3.9.1	The MAY 2008 MJO	65
3.9.2	Boreal fall intraseasonals: The return of La Nina	67
3.9.3	Initiation of the DJFM 2008-09 MJO activity.....	68
3.9.4	Trend toward a warming equatorial Pacific: MAM 2009	72
3.10	Overlapping Field Campaigns.....	75
3.10.1	THORPEX Pacific Asian Regional Campaign (T-PARC).....	75
3.10.2	Winter THORPEX Pacific Asian Regional Campaign (Winter T-PARC).....	81
3.10.3	AMY	84
3.10.4	VAMOS Ocean-Cloud-Atmosphere-Land Study (VOCALS)	85

4	Modeling Resources and Research Tasks	88
4.1	Overview.....	88
4.1	Global analysis and prediction	88
4.2	Multiscale cloud-system simulation and modeling	89
4.2.1	Cloud-system resolving models.....	90
4.2.2	Superparameterization	90
4.2.3	Nested Regional Climate Models/Tropical Channel Models	90
4.2.4	Global cloud-system resolving models.....	91
4.2.5	Idealized models.....	91
4.3	Key Elements.....	91
4.3.1	Improving convective parameterization	92
4.3.2	Modeling in support of field campaigns	93
4.3.3	Weather as an initial-value problem for climate.....	94
4.4	Research tasks	96
4.4.1	GCSS Pacific Cross-section Intercomparison (GPCI)	96
4.4.2	Madden-Julian Oscillation and Convectively-Coupled Equatorial Waves	98
4.4.3	Easterly Waves and Tropical Cyclones.....	103
4.4.4	Diurnal Cycle	103
4.4.5	Tropical-Extratropical Interaction	104
4.4.6	Monsoons	105
4.4.7	References.....	105
5	Analysis Framework	109
6	Appendices	110
6.1	ECMWF Variables.....	110
6.1.1	Two – Dimensional Analysis Fields.....	110
6.1.2	Three – Dimensional Pressure-Level Analysis Fields	110
6.1.3	Two – Dimensional Forecast Fields	111
6.1.4	Three – Dimensional Pressure-Level Forecast Fields.....	112
6.1.5	Three – Dimensional Model-Level Forecast Fields	112
6.1.6	Three – Dimensional Pressure-Level Physics Forecast Fields	112
6.1.7	Two – Dimensional Physics Forecast Fields.....	113
6.2	GMAO Variables	114
6.2.1	Two-Dimensional, Hourly, Time-averaged Assimilation and Forecast Fields – Single Level Diagnostics Collection	114
6.2.2	Two-Dimensional, Hourly, Time-averaged Assimilation and Forecast Fields – Turbulence Collection	114
6.2.3	Two-Dimensional, Hourly, Time-averaged Assimilation and Forecast Fields – Radiation Collection	114
6.2.4	Two-Dimensional, Hourly, Time-averaged Assimilation and Forecast Fields – Land Surface Collection.....	115
6.2.5	Two-Dimensional, Hourly, Time-averaged Assimilation and Forecast Fields – Ocean Surface Collection.....	115
6.2.6	Three-Dimensional, 3-Hourly, Instantaneous Pressure-Level Assimilation and Forecast Fields (3 Collections)	115
6.2.7	Three-Dimensional, 3-Hourly, Time-averaged Pressure-Level Assimilation and Forecast Fields – 3D Cloud Diagnostics Collection	116
6.2.8	Three-Dimensional, 3-Hourly, Time-averaged Pressure-Level Assimilation and Forecast Fields – 3D Moist Processes Diagnostics Collection.....	116

6.2.9	Three-Dimensional, 3-Hourly, Time-averaged Pressure-Level Assimilation and Forecast Fields – 3D Radiation Diagnostics Collection	116
6.2.10	117
6.2.11	Three-Dimensional, 3-Hourly, Time-averaged Pressure-Level Assimilation and Forecast Fields – 3D Turbulence Diagnostics Collection	117
6.2.12	Three-Dimensional, 3-Hourly, Time-averaged Pressure-Level Assimilation and Forecast Fields – 3D Temperature Tendencies Collection	117
6.2.13	Three-Dimensional, 3-Hourly, Time-averaged Pressure-Level Assimilation and Forecast Fields – 3D Wind Tendencies Collection	117
6.2.14	Three-Dimensional, 3-Hourly, Time-averaged Pressure-Level Assimilation and Forecast Fields – 3D Moisture Tendencies Collection.....	117
6.2.15	Three-Dimensional, 3-Hourly, Time-averaged Pressure-Level Assimilation and Forecast Fields – 3D Ozone Tendencies Collection	117
6.2.16	6-Hourly, Instantaneous, Model-Level Analysis Collection	118
6.2.17	6-Hourly, Instantaneous, Pressure-Level Analysis Collection.....	118
6.2.18	Invariants Collection.....	118
6.2.19	Notes	118
6.3	NCEP Tendencies	120

1 Atmospheric Analyses and Forecasts



1.1 Introduction

The fundamental challenges to overcoming our shortcomings in understanding and modeling/predicting tropical convection have been two fold: I) the need to represent the broad range of scales applicable to the tropical organization problem (i.e. cumulus to planetary), and II) the lack of observations that adequately and simultaneously characterize this broad range of scales, particularly three-dimensional information on thermodynamic, radiative and dynamical interactions, including cloud microphysical processes. Both of these challenges play a direct role in the tropical forecasting problem via the determination of the atmospheric initial conditions for the forecast. However, atmospheric analyses products have advanced considerably over recent years via more and improved observational resources, more advanced data assimilation and physical parameterization schemes, and greater computing capacity (see Science Plan). These products play a key role not only in improving predictions but also by providing best-estimates of the atmospheric state from which in-depth analysis of the dynamic, thermodynamic and hydrologic processes and their interactions can be examined. Moreover, they provide a crucial resource for setting boundary conditions for higher-resolution regional (i.e. cloud-resolving) simulations/predictions that are one of the tools utilized for addressing the multi-scale problem of tropical convection.

This chapter describes the atmospheric analysis and forecast data sets that are being produced and/or made available for YOTC. At the time of this writing, these include products from the European Centre for Medium Range Forecasting (ECMWF), the National Oceanographic and Atmospheric Administration's (NOAA) National Centers for Environmental Prediction (NCEP), and the National Aeronautical and Space Administration's (NASA) Global Modeling and Assimilation Office (GMAO). The forecast data sets described here are only those associated with the systems producing the analyses products; the more research-oriented forecasts are discussed in the Modeling section of the YOTC Implementation Plan. The primary consideration for including the above listed analyses and forecast products in YOTC is the willingness and capability by the given center to make them available. Where possible, efforts by the centers were made to make the products with as high of spatial resolution as possible (and thus the focus here on the deterministic forecasts), include as many physical/diagnostic fields (e.g., diabatic heating profiles) as possible, and provide the means to disseminate the products to the YOTC community. While the use of ensemble forecasts may be of use in some aspects of YOTC, they are already routinely available through the THORPEX Interactive Grand Global Ensemble (TIGGE). The subsections below describe each of the analysis/forecast data sets, the ECMWF, GMAO and NCEP products.

1.2 ECMWF

Overview:

The ECMWF analysis and forecast products are provided from their deterministic forecasting system. This system is comprised of a 4-dimensional variational data assimilation system (4D-Var), the high resolution (T799 ~ 25km) global model and the 51 member Ensemble Prediction System (EPS) at 40 km resolution. The specific contributions provided by ECMWF include the T799 analyses, produced 4 x daily, and the associated 10-day forecasts, output at 3-hourly intervals. The exception to this is that a set of non-

operational 3-dimensional physical process fields were provided, and these extend out to a lead of only 36 hours. The Appendix provides a listing of the variables that are included for both the analyses and the forecasts. The ECMWF YOTC data set begins in May 2008 and will extend through the end of the YOTC period.

Cautions and Caveats:

Regular upgrades are made to the ECMWF operational system also during the Year of Tropical Convection. Such changes may have impact on the analysis and forecast fields and users may see changes in the characteristics of e.g. the fields related to the parametrization schemes. Model and data assimilation changes are listed with a short description in:

http://www.ecmwf.int/products/data/technical/model_id/index.html

Data Policy:

Users of the data are required to agree to the following policy before downloading and/or using the data.

The YOTC data server is sponsored by the YOTC (Year of Coordinated Observing Modelling and Forecasting Tropical Convection) project. Before retrieving data please read the conditions below and acknowledge that you accept them.

Conditions

- Data from the YOTC dataset available on this server are provided without charge and may be retrieved and used solely by members of the YOTC and THORPEX (The Observing System Research and Predictability Experiment) research communities for research and education only. Commercial use of the data is not permitted.
- Research is understood as any project organised by a university, scientific institute or similar (private or institutional), for non-commercial research purposes only. A necessary condition for the recognition of non-commercial purposes is that all the results obtained are openly available at delivery costs only, without any delay linked to commercial objectives, and that the research itself is submitted for open publication.
- Although every care has been taken in preparing and testing the data, ECMWF cannot guarantee that the data are correct in all circumstances; neither does ECMWF accept any liability whatsoever for any error or omission in the data, or for any loss or damage arising from its use.
- Any person extracting data from this server will accept responsibility for informing all data users of these conditions.
- Data must not be supplied as a whole or in part to any third party without the authorisation of ECMWF.

Articles, papers, or written scientific works of any form, based in whole or in part on data supplied by ECMWF, will contain an acknowledgment concerning the supplied data.

This policy can be found at: <http://data-portal.ecmwf.int/data/d/license/yotc/>

Example Figure(s):

ECMWF FORECAST VERIFICATION 12UTC

850hPa VECTOR WIND

ABSOLUTE CORRELATION

FORECAST

TROPICS LAT -20.000 TO 20.000 LON -180.000 TO 180.000

SCORE REACHES 70.00

SCORE REACHES 70.00 MA

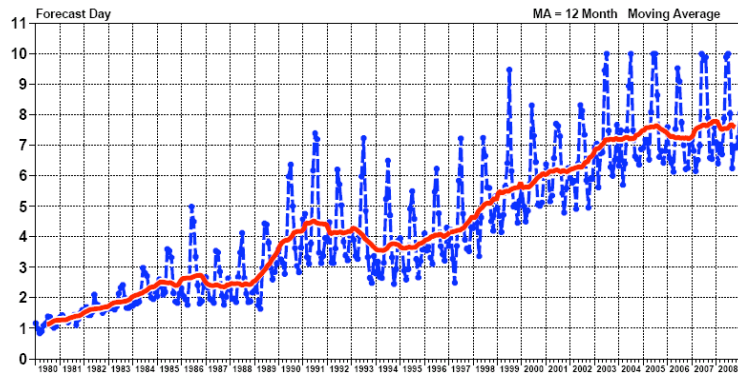


Figure 1. Tropical skill score for wind at 850 hPa of the ECMWF operational system from 1980 to 2009: time in days when the absolute correlation between forecast and analysis drops below 70%.

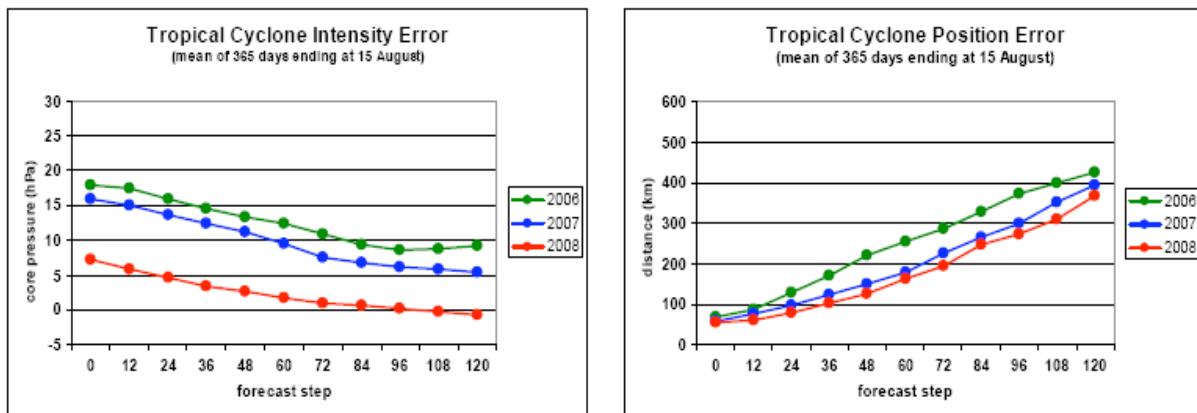


Figure 2. Verification of tropical cyclone predictions from the operational deterministic forecast for three 12-month periods: August 2005 - August 2006 (green), August 2006 - August 2007 (blue) and August 2007 - August 2008 (red). The left panel shows the mean error in core pressure, the right panel the position error. The intensity error is larger in the analyses than in the forecasts because the analysis increments are at lower resolution resulting in damping of tropical cyclones.

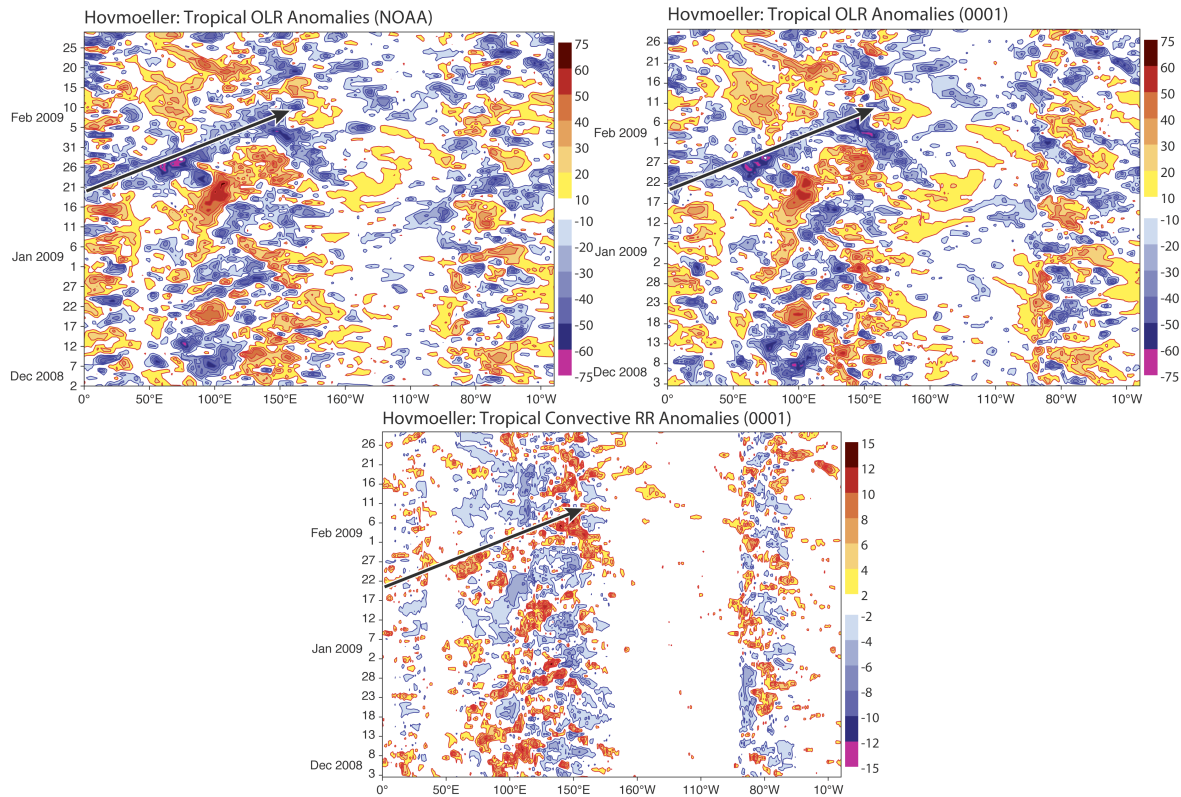


Figure 3. Hovmoeller of averages between 10°N and 10°S of anomalies of Observed OLR (top panel), model OLR (middle panel), and model convective precipitation (bottom panel). The model fields are from the ECMWF daily 24-hour forecasts. The Jan/Feb 2009 MJO event is marked with an arrow.

Web Page(s): <http://data-portal.ecmwf.int/data/d/yotc>

Contact Information: Anton.Beljaars@ecmwf.int

References:

<http://www.ecmwf.int/research/ifsdocs/CY31r1/index.html>

Model diagnostics on recent model versions:

Jung, T., G. Balsamo, P. Bechtold, A. Beljaars, M. Köhler, M. Miller, J.-J. Morcrette, A. Orr, M. Rodwell and A.M. Tompkins (2009): The ECMWF model climate: Recent progress through improved physical parametrizations, in: proceedings of the ECMWF seminar on: Parametrization of Subgrid Physical Processes, 1–4 September 2008. <http://www.ecmwf.int/publications/library/do/references/list/200809>

Recent improvements of convection parametrization:

Peter Bechtold, Martin Köhler, Thomas Jung, Francisco Doblas-Reyes, Martin Leutbecher, Mark J. Rodwell, Frederic Vitart, Gianpaolo Balsamo (2008): Advances in simulating atmospheric variability with the ECMWF model: From synoptic to decadal time-scales, *Q.J.Roy.Meteor.Soc.*, 134, 1337-1351.

1.3 GMAO

Overview:

The GMAO analysis and experimental forecast products for YOTC are provided from an experimental deterministic forecasting system. This system is comprised of a 3-dimensional variational data assimilation system (3D-Var), using the GEOS-5 atmospheric model with the grid-point statistical interpolation (GSI) analysis developed in collaboration with NCEP. The global model's horizontal grid spacing for YOTC is $1/4^\circ \times 1/3^\circ$ —twice the resolution of the routine GEOS-5 products. The specific contributions provided by GMAO include both assimilation and forecast products. The assimilation products consist of $1/4^\circ$ analyses produced every 6 hours by the GSI and higher frequency products produced by the atmospheric model during the corrector segment of the Incremental Analysis Update (IAU). Forecast products are identical to the model generated assimilation products but from once-daily 5-day forecasts from the 0Z analysis. For the model-generated products, the 3D fields are output at 3-hourly intervals and the 2D fields are hourly. The 3D fields are a combination of instantaneous state variables and time averaged diagnostics. All hourly fields are time averages. Section 6.1 provides a listing of the variables that are included for both the analyses and the forecasts. In addition, aerosol products consistent with the analyses are available. The GMAO YOTC data set begins in January 2009 and will extend through the end of the YOTC period. Selected time periods from 2008 may also be available before the completion of the YOTC project. The GEOS-5 products are distributed through a data portal on the NASA Center for Computational Sciences (NCCS). Data are available via anonymous ftp or (preferably) through *opendap*.

Cautions and Caveats:

The GMAO's YOTC products are experimental products that are generated on a best effort basis. The system used to generate the products is part of our parallel validation suite and may be upgraded at any time to correct bugs or deficiencies.

Data Policy:

The GMAO's YOTC data products are openly available to the community. The predictions are experimental and are produced for research purposes only. Use of the forecasts for purposes other than research is not recommended. Publications based in whole or in part on data supplied by GMAO should contain an acknowledgment concerning the supplied data.

Web Page:

<http://gmao.gsfc.nasa.gov/forecasts/yotc>

<http://www.nccs.nasa.gov/>

Additional Contact Information:

Technical: Dr Gi-Kong Kim, GMAO, Gi-Kong.Kim-1@nasa.gov

Science: Dr Max Suarez, GMAO, Max.Suarez@nasa.gov

References:

Rienecker, M.M., M.J. Suarez, R. Todling, J. Bacmeister, L. Takacs, H.-C. Liu, W. Gu, M. Sienkiewicz, R.D. Koster, R. Gelaro, I. Stajner, and J.E. Nielsen, 2008. The GEOS-5 Data Assimilation System - Documentation of Versions 5.0.1, 5.1.0, and 5.2.0. NASA *Technical Report Series on Global Modeling and Data Assimilation*, NASA/TM-2008-104606, Vol. 27, 97 pp. [Available at: http://gmao.gsfc.nasa.gov/pubs/docs/GEOS5_104606-Vol27.pdf].

1.4 NCEP

Overview:

The NCEP analysis and forecasts products are provided from the global and global ensemble forecast systems. These products consist of single (GFS), ensemble (GEFS) and multi-ensemble (NAEFS) forecast products issued 4 times daily. The NCEP GFS is a global spectral numerical model based on the primitive dynamical equations that includes a suite of parameterizations for atmospheric physics (e.g., Sela 1980; Kanamitsu 1989; Kalnay et al. 1990). The model has been under constant development and evaluation (e.g., Moorthi et al. 2001, Yang et al. 2006). The GFS uses spectral triangular truncation in the horizontal and a sigma coordinate in the vertical that extends from the earth's surface to the top of the atmosphere. The current resolution is T384L64 out to 7 days and T190L64 for leads beyond 7 days out to 16 days. T384 is approximately 34 km in horizontal resolution. The ensemble forecast products are based on the GEFS, which generates 20-member ensemble forecasts out to 16 days every 6hr. The forecast model is a low-resolution version (T190L28) of the current operational NCEP GFS. Ensemble initial perturbations are obtained using the Ensemble Transform method (Bishop and Toth, 2001; Wei et al. 2006). The system upgrades at least once a year to allow the latest developments on both modeling improvements and ensemble methods. A new version is planned for implementation by September 2009. Besides the variables contained in the GFS, the GEFS, provides: ensemble mean and spread, 10%, 50% and 90% percentile probability, mode, and anomaly forecast.

Time tendency variables

Beginning sometime in summer 2009, NCEP will be able to produce the tendencies listed in Section 6.3. In addition, it is expected that later this year NCEP will be able to produce the missing physics for tendencies related to convection, which are: mass flux, upward and downward drafts and entrainment. The tendency variables will likely be posted on a server for couple of days in near real time. Archival of these files is not resolved at this time but it is likely to be stored at the National Climate Data Center (NCDC).

Data Access:

GFS

The are being archived at NCDC at half degree resolution (analysis and forecast). The data can be downloaded from the NOMADS system: <http://nomads.ncdc.noaa.gov/data.php>

GEFS

The data are provided in two spatial resolutions 1x1 degree and 2.5x2.5 degrees. Access to the archived data can be made through the NOMADS website: <http://nomads.ncdc.noaa.gov/data.php> Evaluation statistics, including ensemble mean, mode, spread, RMSE, AC are posted at <http://www.emc.ncep.noaa.gov/gmb/yzhu/>.

Contact: Zoltan.Toth@noaa.gov, Malaquias.Pena.Mendez@noaa.gov

References:

Atmos. Sci., **56**, 1748-1765.

Moorthi S., H.-L. Pan, and P. Caplan, 2001: Changes to the 2001 NCEP operational MRF/AVN global analysis/forecast system. Tech. Procedures Bull. 484, Office of Meteorology, National Weather Service, 14 pp.

Kalnay E., M. Kanamitsu, and W. E. Baker, 1990: Global numerical weather prediction at the National Meteorological Center. *Bull. Amer. Meteor. Soc.*, **71**, 1410–1428.

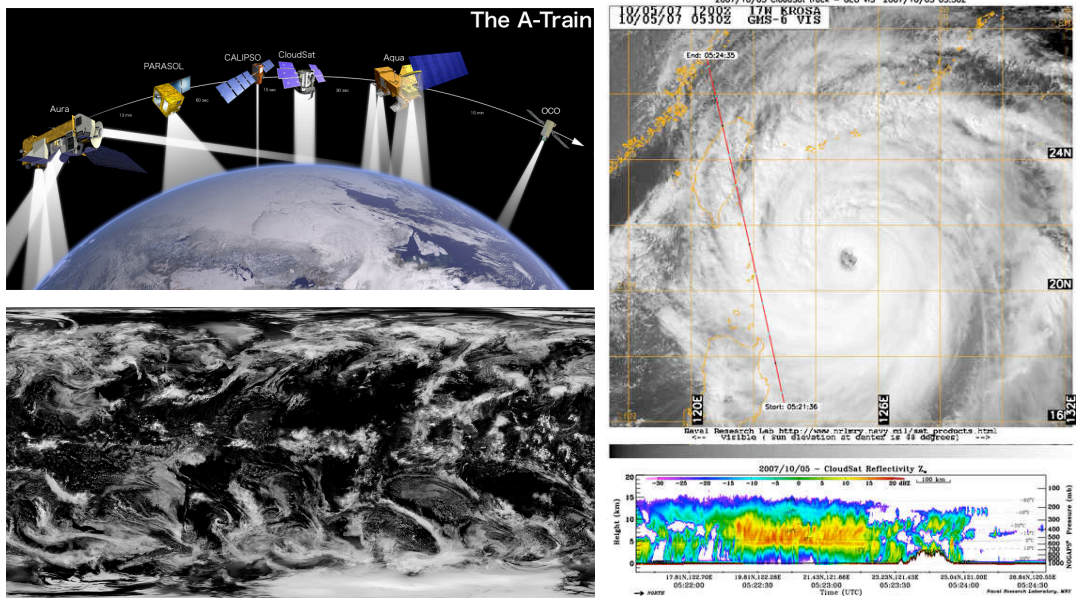
Kanamitsu M., 1989: Description of the NMC global data assimilation and forecast system. *Wea. Forecasting*, **4**, 335–342.

Sela J., 1980: Spectral modeling at the National Meteorological Center. *Mon. Wea. Rev.*, **108**, 1279–1292.

Wei, M., Z. Toth, R. Wobus, and Y. Zhu, 2008: Initial perturbations based on the ensemble transform (ET) technique in the NCEP global operational forecast system. *Tellus*, **60A**, 62–79.

Yang F., H.-L. Pan, S. K. Krueger, S. Moorthi, and S. J. Lord, 2006: Evaluation of the NCEP Global Forecast System at the ARM SGP Site. *Mon. Wea. Rev.*, **134**, 3668–3690.

2 Satellite Data



2.1 Introduction

The fundamental challenges to overcoming our shortcomings in understanding and modeling/predicting tropical convection have been two fold: I) the need to represent the broad range of scales applicable to the tropical organization problem (i.e. cumulus to planetary), and II) the lack of observations that adequately and simultaneously characterize this broad range of scales and that also provide three-dimensional information on thermodynamic, radiative and dynamical interactions, including cloud microphysical processes. In regards to the second challenge, it should be stressed that this problem will not be solved through the production and examination of one or a few high quality long-term records of fundamental quantities (e.g., SST, water vapor, cloud fraction). Rather, an alternative and more comprehensive paradigm is needed, one that integrates the multitude of applicable resources and measures of tropical convection in a manner that that can be better utilized by the diagnostic, modeling and forecasting communities to more completely and coherently focus on the problem. This is the paradigm underlying YOTC in general and is the basis for the satellite data component of the program.

The objective of this component of the YOTC implementation plan is to construct a unique and comprehensive multi-sensor satellite data set that is designed to facilitate the study and model improvement of “tropical convection” and its multi-scale organization. Because the goal of YOTC involves examining a scientifically complex, multi-scale “process”, rather than documenting the characteristics of a single parameter (e.g., SST, cloud cover), YOTC has an IOP perspective that targets a period, May 2008 – October 2009, long enough to encompass many cases of tropical convection activity in many of its most challenging yet influential forms. This includes mesoscale and synoptic variability, easterly waves and hurricanes, convectively coupled waves, the MJO and the culmination of these in terms of the monsoon, their interactions with the extra-tropics, and mean characteristics such as tropical-to-subtropical transitions. The YOTC time period and length are driven in part by the following: 1) keeping the multi-sensor/multi-platform and model-analyses data sets and associated infrastructure manageable, 2) facilitating a focused effort by the research and operational communities on a specific scientific problem, and 3) capitalizing on the recent key additions to the armada of satellites (e.g., CloudSat and CALIPSO). It is worth noting that in regards to item 3), EOS – a constellation of research satellites - is at its peak maturity level with respect to satellite measures characterizing tropical convection.

In addition to the points discussed above, the following are primary to the considerations made in developing the framework and establishing the content of the satellite data component of YOTC:

- Data availability during the YOTC target observation period: May 2008 – October 2009.
- Facilitating data set usage as much as possible – both for observational diagnostic study and model-data comparison/validation.
- Characterization and quantification of primarily tropical convection and secondarily of quantities and processes related to: clouds, thermodynamic structure, dynamics, water and energy fluxes, surface temperature, aerosols and composition.
- Global to near-global spatial coverage to include tropical-extratropical interactions.
- At least daily temporal sampling, and where possible higher resolution sampling [O(hours)] such as from geostationary platforms.
- High spatial resolution [O(km)] and resolving atmospheric vertical structure.

- Characterization of surface land and near-surface ocean conditions relevant to tropical convection processes.
- Having independent data sets not included in operational weather analyses.

Based on the above considerations, the YOTC satellite data archive will nominally include the following products:

- TRMM rainfall and related products, including latent heating profiles.
- ISCCP cloud product data set.
- AIRS profiles of temperature and water vapor, and associated cloud products.
- CloudSat profiles of liquid and ice water, cloud classification, cloud optical depth, surface precipitation flags/estimates, and profiles of radiative fluxes and heating rates.
- CALIPSO profiles of cloud presence, emissivity, and particle size, and associated radiative and geophysical properties (height, optical depth, extinction).
- AMSR-E and/or SSM/I surface wind speed, precipitable and cloud-liquid water, and rain rate.
- PEHRRP – high resolution precipitation products.
- GPS soundings of temperature and water vapor.
- AMSR-E and/or TMI SST.
- CERES cloud properties, TOA and surface fluxes.
- MODIS cloud and aerosol products.
- MLS upper tropospheric profiles of water vapor, temperature and cloud ice.
- Scatterometer (e.g., QuikScat) ocean surface winds.

The specific quantities, characteristics and general strengths and shortcomings of the above satellite data sets are briefly characterized in Section c. These satellite products make up a subset of available data sets that have direct bearing on characterizing tropical convection, and related cloud, dynamic, radiative and thermodynamic properties. While not all products sample the range of scales perceived relevant to the multi-scale organization of tropical convection – in combination they do. Importantly, there are a number of products that have resolution on the order of 1km or less (e.g, MODIS, CloudSat, CALIPSO). While this is a formidable list of quantities, it is worth reiterating and stressing the following:

- 1) Addressing tropical convection will require a comprehensive set of measures, and the solutions to overcoming our shortcomings in understanding and modeling/forecasting it in our global weather and climate models cannot be derived from one or a few parameters – particularly when disjoint in time and/or space.
- 2) The comprehensive nature of the list reinforces the benefits of targeting a relatively short time period – both with respect to resource considerations but also in regards to YOTC's intention to focus community efforts on the tropical convection problem.

2.2 Dissemination Framework

The proposed dissemination framework for the YOTC satellite data archive for most of the data sets listed above is based on the Giovanni system. Giovanni is a web-based application developed by the NASA Goddard Earth Science (GES) Data and Information Service Center (DISC) that provides a simple and intuitive way to visualize, analyze, and access/download vast amounts of Earth science remote sensing data. For a more complete description, see

<http://disc.sci.gsfc.nasa.gov/giovanni/>. A prototype YOTC instance of Giovanni has been constructed¹ and when agreement on the present plan is arrived at and funding is in place, the YOTC Giovanni System (hereafter YOTC-GS) will be completed. YOTC-GS will provide access to level 2 (i.e. swath level data) and/or level 3 (i.e. gridded/mapped data) forms of satellite data, the choice – or both – depending on what is appropriate and relevant. The former is needed and better suited for detailed process examination, exploiting the highest temporal-spatial resolutions available and comparison to regional cloud-system resolving model / cloud resolving model (CSRM/CRM) model output. The latter is needed and more well suited for examination of phenomena, conditions and processes on large to global scales, and for comparisons to global model analyses, prediction and simulation output. In addition to the dissemination strategy of GEOS-5 products discussed in Section 1.3, YOTC-GS *may* (depending on funding) also be a method to disseminate the NASA GEOS5 high-resolution (~20km) atmospheric analysis and forecast products being provided by the NASA Goddard Modeling and Assimilation Office (GMAO); for more details on these analyses and forecast products, see Section 1.3.

An example of the YOTC-GS interface is given in Figure 4. This interface allows for selecting the geographical domain, variables (more than one can be selected at a time and note that not variables available are shown are shown in this figure), height/pressure level or ranges when relevant, date ranges, and type of data slice to be plotted/disseminated. Figure 5 shows the data display page and the features for refinement. Figure 6 shows the data download page illustrating the various output options.

In addition to YOTC-GS, there are other interfaces to satellite data that will be constructed and utilized. For example, the Program to Evaluate High Resolution Precipitation Products (PEHRPP) has provided a web-interface to their products overlapping the YOTC time period – see <http://essic.umd.edu/~msapiano/PEHRPP/YOTC.html>; further details in Section 2.4.10. Besides the above, there are a number of satellite/mission-specific web pages that may of use directly; these are given in the individual data set subsections below.

¹ http://gdata1-ts1.sci.gsfc.nasa.gov/daac-bin/G3/gui.cgi?instance_id=YOTC

Giovanni – Year of Tropical Convection

http://gdata1-ts1.sci.gsfc.nasa.gov/daac-bin/G3/gui.cgi?instance_ic ~ giovanni nasa

Giovanni The Bridge Between Data and Science

+ ABOUT GIOVANNI + NEWS + INSTANCES + FEEDBACK + RELEASE NOTES + HELP

Year of Tropical Convection

Alpha prototype

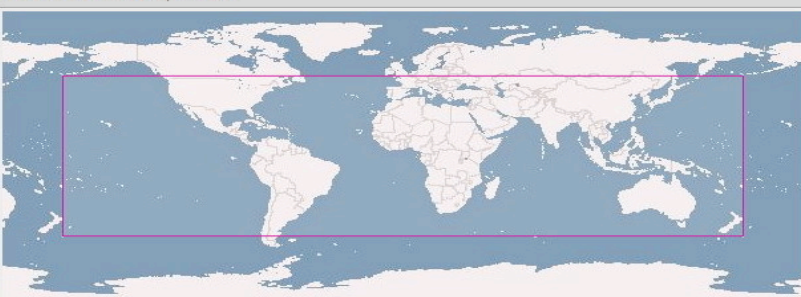
[Home](#) [Remove All](#)

Giovanni for Year of Tropical Convection

Select:

Spatial

Cursor Coordinates: 0.00000, 0.00000



Area of Interest: West: -180 North: 50 South: -50 East: 180 [Update](#) [Select...](#)

Vertical Profile

Select a vertical profile range. The range selection is disabled unless a qualifying parameter is selected. In order to enable this option (and populate the list with values), select a 3D parameter. 3D parameters have at least three dimensions and are labeled with a '3D' in the 'Parameters' section.

NOTE: Selected 3D parameters must have the same vertical (i.e., 3rd dimension) units in order to enable the vertical level menu.

Upper Level

Lower Level

Parameters

Display: ☒ Data Product Info ☐ Units ☐ Parameters with > 2 Dimensions

Ocean

Temperature(1978/11/01 - 2009/03/22)			
<input type="checkbox"/> Surface skin temperature_descending (SurfSkinTemp_D)	AIRX3STD.005	Aqua - AIRS standard	2002/08/31 - 2009/03/22
<input checked="" type="checkbox"/> Total column cloud liquid water ascending (TotCldLiqH2O_A)	AIRX3STD.005	Aqua - AIRS standard	2002/08/31 - 2009/03/22
<input type="checkbox"/> Total column cloud liquid water_descending (TotCldLiqH2O_D)	AIRX3STD.005	Aqua - AIRS standard	2002/08/31 - 2009/03/22
<input checked="" type="checkbox"/> Total column water vapor ascending (TotH2OVap_A)	AIRX3STD.005	Aqua - AIRS standard	2002/08/31 - 2009/03/22

Temporal

Begin Date Year: 2009 Month: Mar Day: 8 (Date Begin: 01 Nov 1978)

End Date Year: 2009 Month: Mar Day: 21 (Date End: 23 Mar 2009)

Animation
 Latitude-Time Hovmöller Diagram
 Longitude-Time Hovmöller Diagram
☒ Lat-Lon map, Time-averaged
 Scatter plot
 Scatter plot, Time-averaged
 Time series

[Edit Preferences](#) [Visualization Help](#)


 Responsible NASA Official: Steven J. Kempler Steven.J.Kempler@nasa.gov
 Web Curator: Anthony Drake web-contact-disc@listserv.gsfc.nasa.gov [+ Contact Us](#)
[+ Privacy Policy and Important Notices](#)

Figure 4. Main YOTC-GS web page provides for selecting geographical region, including global, variable (not all shown), range of vertical levels for applicable quantities, begin and end dates, and type of plot (or data slice) to be constructed/disseminated.

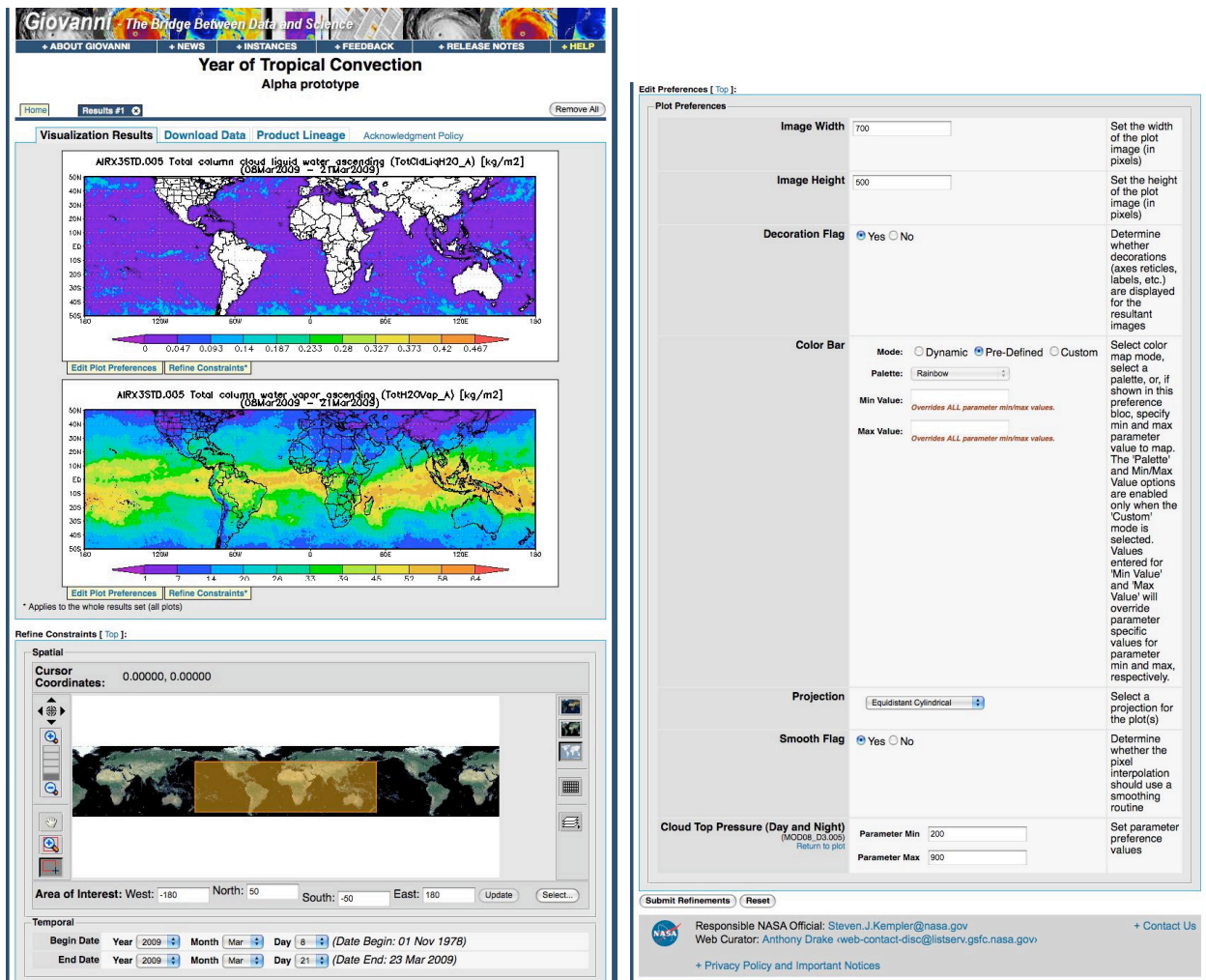


Figure 5. Data selected is displayed, with options to refine geographical area, plotting characteristics (e.g., color, size, projection, dates). In addition, the actual data can be downloaded instead of plotting or following the plotting step.

NASA National Aeronautics and Space Administration

Search DISC
Advanced Search

Giovanni The Bridge Between Data and Science

ABOUT GIOVANNI NEWS INSTANCES FEEDBACK RELEASE NOTES HELP

Year of Tropical Convection
Alpha prototype

Home Results #1 Remove All

Visualization Results **Download Data** Product Lineage Acknowledgment Policy

retrieval and final rendering phases are currently accessible for downloading. Supported download formats are HDF, NetCDF(NCD), ASCII, and KMZ. To download multiple files at once, select the desired files (from any section) by clicking on their associated checkboxes, and then click 'Download in Batch'. Note: that 'n/a' means that a file size or other column value is not available; 'naa' means that a file is exactly the same as the previous one in the list. Also, not all services and data products support all download file formats.

Initial Data Retrieval

Download in Batch

Data Product	Start Time	File Size (b)	HDF	NCD	ASC
AIRX3STD.005 (TropTemp_D)	2009-03-14 00:00:00Z	31408910	<input checked="" type="checkbox"/>	<input checked="" type="checkbox"/>	<input checked="" type="checkbox"/>
AIRX3STD.005 (TropTemp_D)	2009-03-15T00:00:00Z	31507291	<input checked="" type="checkbox"/>	<input checked="" type="checkbox"/>	<input checked="" type="checkbox"/>
AIRX3STD.005 (TropTemp_D)	2009-03-16T00:00:00Z	31673284	<input checked="" type="checkbox"/>	<input checked="" type="checkbox"/>	<input checked="" type="checkbox"/>
AIRX3STD.005 (TropTemp_D)	2009-03-17T00:00:00Z	31792694	<input checked="" type="checkbox"/>	<input checked="" type="checkbox"/>	<input checked="" type="checkbox"/>
AIRX3STD.005 (TropTemp_D)	2009-03-20T00:00:00Z	31878576	<input checked="" type="checkbox"/>	<input checked="" type="checkbox"/>	<input checked="" type="checkbox"/>
AIRX3STD.005 (TropTemp_D)	2009-03-21T00:00:00Z	31988310	<input checked="" type="checkbox"/>	<input checked="" type="checkbox"/>	<input checked="" type="checkbox"/>

Two Dimensional Map Plot

Download in Batch

Input Files	Start Time	File Size (b)	HDF	NCD	ASC
MOD08_D3.005 (Cloud_Top_Pressure_Mean)	2009-03-08T00:00:00Z	148791	<input checked="" type="checkbox"/>	<input checked="" type="checkbox"/>	<input checked="" type="checkbox"/>
AIRX3STD.005 (TotCldLiqH2O_A)	2009-03-08T00:00:00Z	148573	<input checked="" type="checkbox"/>	<input checked="" type="checkbox"/>	<input checked="" type="checkbox"/>
AIRX3STD.005 (TotH2OVap_A)	2009-03-08T00:00:00Z	148570	<input checked="" type="checkbox"/>	<input checked="" type="checkbox"/>	<input checked="" type="checkbox"/>
AIRX3STD.005 (TropTemp_D)	2009-03-08T00:00:00Z	148573	<input checked="" type="checkbox"/>	<input checked="" type="checkbox"/>	<input checked="" type="checkbox"/>

Output Files

☒ KMZ

Output Files	File Size (b)	Download
Cloud_Top_Pressure_Mean.MOD08_D3.005.AreaMap.2009-03-08.gif	61634	<input checked="" type="checkbox"/>
TotCldLiqH2O_A.AIRX3STD.005.AreaMap.2009-03-08.gif	49759	<input checked="" type="checkbox"/>
TotH2OVap_A.AIRX3STD.005.AreaMap.2009-03-08.gif	54032	<input checked="" type="checkbox"/>
TropTemp_D.AIRX3STD.005.AreaMap.2009-03-08.gif	46187	<input checked="" type="checkbox"/>

Responsible NASA Official: Steven J. Kempler nasa.gov
Web Curator: Anthony Drake web-contact-disc@lisaan.gsfc.nasa.gov

+ Contact Us
+ Privacy Policy and Important Notices

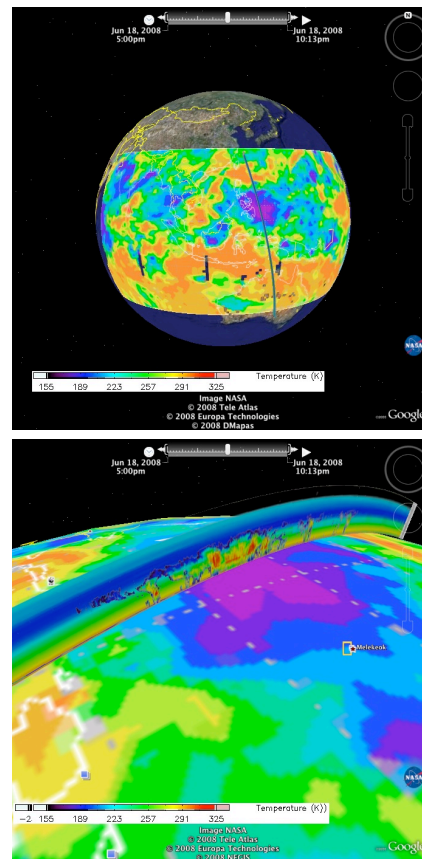


Figure 6. Export options allow for downloading the input data to the operation (e.g., individual days/swaths) and/or the resultant data (e.g. average map). The export formats are hdf, netcdf, and/or ascii. In addition, the map output can be exported into a kmz format for display for example in Google Earth. This capability is shown for a cloud top temperature map and a CloudSat orbit overlaid with each other; note this example does not follow from the previous figures' selections.

2.3 Special A-Train Data Set

The upper-left figure on the cover page for this chapter illustrates what is referred to as the Earth Observing System's (EOS) "A-Train" constellation of satellites. Most relevant to YOTC are the Aqua, CloudSat, CALIPSO and Aura platforms, which when taken together provide near instantaneous (within about 10 minutes) sampling of the same atmospheric region, albeit with different spatial sampling characteristics. For the purposes of YOTC, this combined measurement facility provides an altogether new opportunity to sample, quantify and study cloud and convection processes. Figure 7 illustrates schematically the information that can be put together from the A-Train constellation that is relevant to YOTC's study of tropical convection. Given that CloudSat represents core quantities at issue here and that the CloudSat data processing center has already made large inroads to the development of a multi-sensor data set, including the co-located profiles of temperature and moisture from ECMWF analyses, we propose making this a CloudSat-centric data set. That is to construct a data set for the YOTC period such that every CloudSat profile is matched to, either via interpolation or nearest-neighbor, the retrievals from the other sensors indicated in the diagram. This will facilitate an incredible array of analysis to be performed that involves considerable constraints on the atmospheric thermodynamic and hydrological structure and processes but also includes a rich set of interactions as well (e.g., aerosol, composition, thermodynamics).

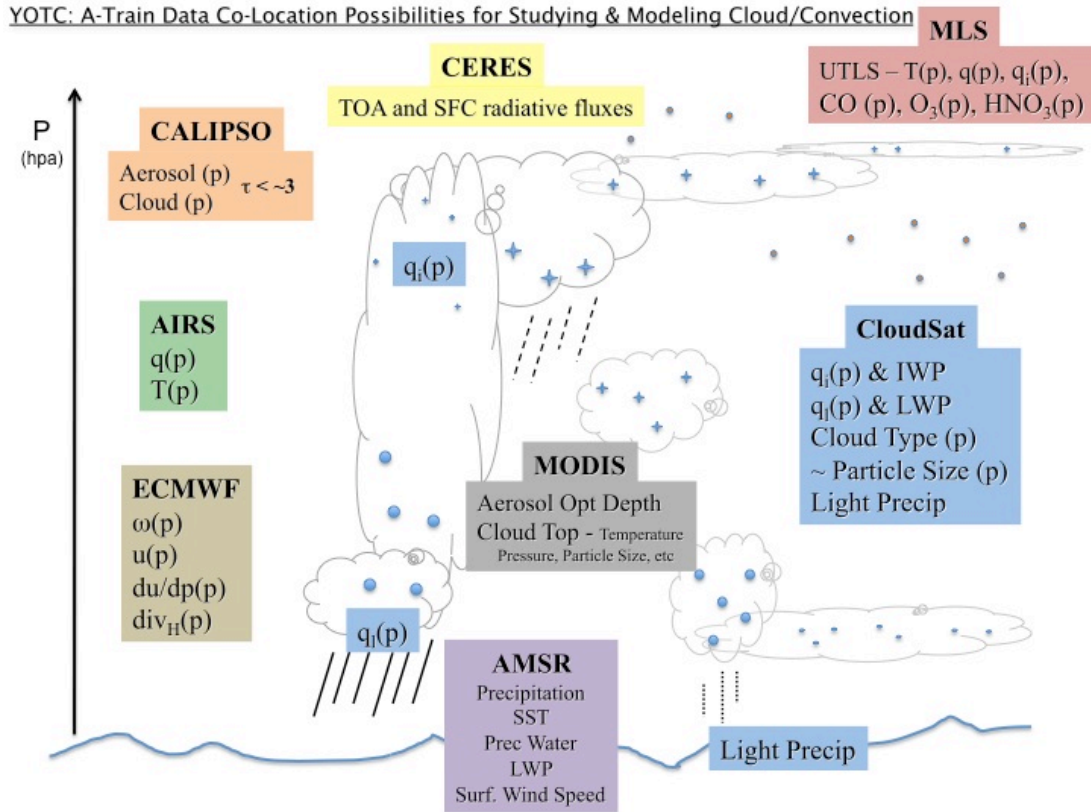


Figure 7. Schematic illustrating the opportunity for developing a co-located satellite retrieval dataset from the EOS A-Train. Note that not all sensors sample identically; the proposal is to produce for each CloudSat profile a nearest-neighbor and/or interpolated value from each of the other products.

2.4 Data Set Highlights

2.4.1 AIRS temperature, water vapor, and related products

Overview and Relevance to YOTC: The Atmospheric Infrared Sounder (AIRS) is a nadir-viewing combined infrared and microwave instrument suite for profiling atmospheric temperature, water vapor and trace gases, along with cloud top properties and surface temperature. AIRS is carried on the Aqua spacecraft, launched in May 2002, with the AIRS record beginning in September 2002.

AIRS provides up to 324,000 profiles daily over the globe, and about 70% of these extend to the surface. This provides nearly 100,000 profiles daily in the ± 30 degree latitude bands. An overview of instrument performance is given in Chahine et al. (2006), the instrument suite is describe in Aumann et al. (2003), and the retrieval algorithm described in Susskind et al. (2006) AIRS is primarily a tropospheric sounder, with nominal resolution of 1 K in 1 km layers for temperature, and 15% in 2 km layers for water vapor. The AIRS temperature and water vapor products are well validated for a range of conditions in Divakarla et al. (2006) and Tobin et al. (2006) and other studies. Vertical coverage for temperature extends from the surface to the mesosphere, with best resolution in the lower troposphere. Vertical coverage for water vapor extends from the surface to about 200 hPa in the tropics (lowest sensitivity is ~ 10 ppmv). AIRS vertical resolution appears superior to reanalyses, especially in the boundary layer (Tian et al., 2006). Biases are ~ 0.5 K or less in temperature and a few percent in humidity. AIRS performs particularly well for partially cloudy conditions over tropical oceans, though it cannot sound into areas of continuous thick clouds (see Caveats below). AIRS cloud top properties are in good agreement with in situ and satellite observations (Kahn et al. 2007, 2007a; 2008), and cloud uncertainties are lowest for thick clouds. With the exception of stratospheric ozone, AIRS trace gas observations contain significantly less information than those of temperature, water vapor or clouds, though this is offset by near-global coverage; see Chahine et al. (2006) for discussion.

Cautions and Caveats: Because of complex surface emissivity, AIRS profiles generally have lower information content over land within 2-3 km of the surface (Divakarla et al., 2006; Tobin et al. 2006). However, retrieval uncertainties are generally small over land in the free troposphere.

Because extensive thick clouds are opaque in the infrared, AIRS sampling is compromised in their presence. (The preponderance of information in AIRS retrievals is obtained from the infrared radiances, with microwave providing low-resolution constraints on temperature and total water vapor.) Conversely, AIRS sampling is quite good in the presence of thin cirrus or low scatter clouds. Fetzer et al. (2006) found only small sampling biases in total water vapor relative to the Advanced Microwave Scanning Radiometer for EOS (also on Aqua) in regions of deep convection in the Western Pacific, despite AIRS cloud-induced sampling rates as low as 15%. Recent studies using CloudSat cloud classes shows significant differences in AIRS sampling with cloud type. Note that poor sampling does not imply retrieval performance, and the instrument error characteristics cited above are independent of cloud type to first order.

The AIRS instrument is not sensitive to stratospheric water vapor.

Example Figure(s):

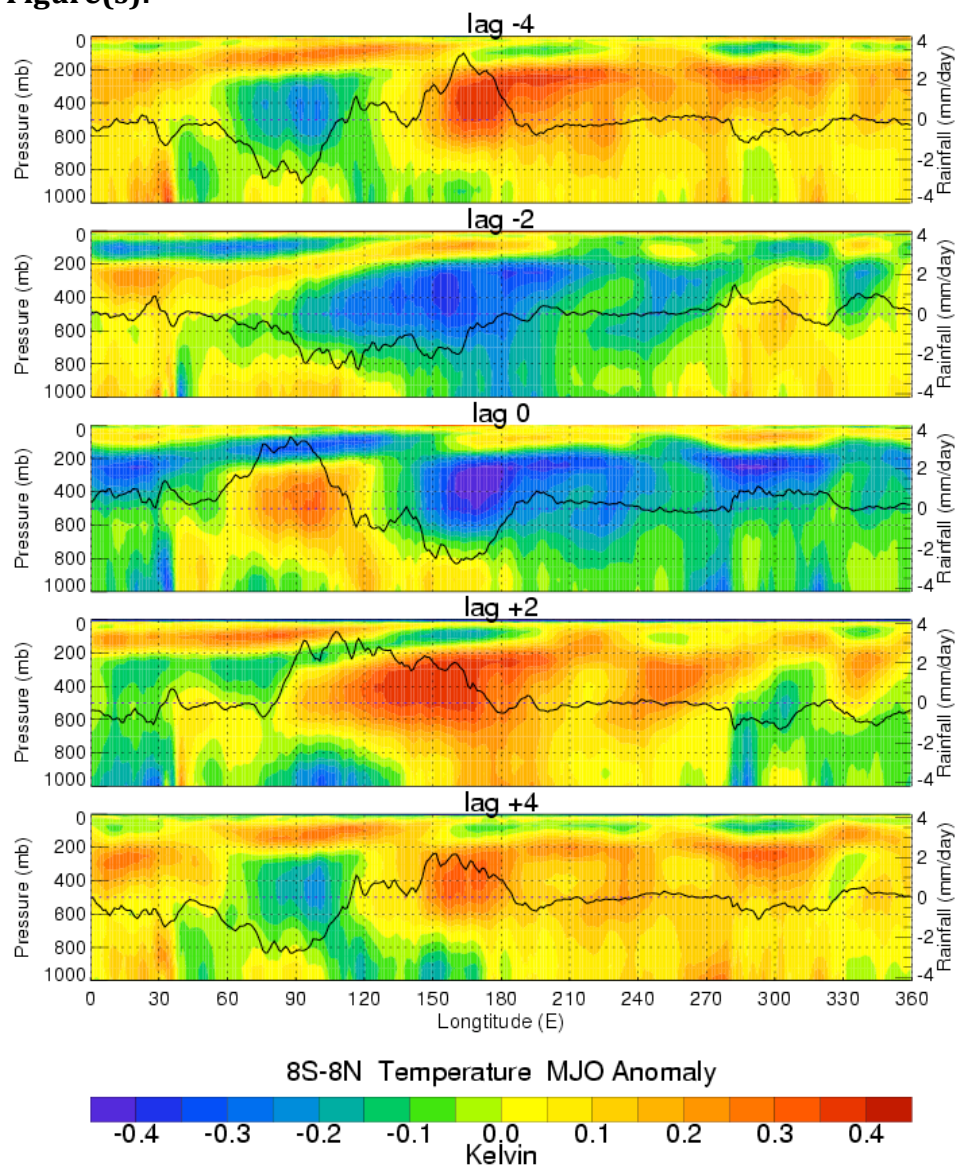


Figure 8. Pressure-longitude cross sections of temperature anomaly (Kelvin) for the composite MJO cycle based on AIRS data. For simplicity, only lags of -4 , ± 2 , and 0 pentads of the MJO cycle are shown. The color red denotes positive temperature anomalies, i.e., warming, while the color blue indicates negative temperature anomalies, i.e., cooling. The superimposed solid black line denotes the associated TRMM rainfall anomaly at the AIRS spatial resolution ($1^\circ \times 1^\circ$). The anomalies are averaged from 8°S - 8°N . From Tian et al. 2006.

Web Page(s): <http://www.jpl.nasa.gov/airs>

Additional Contact Information: Eric.J.Fetzer@jpl.nasa.gov;
Bjorn.H.Lambrigtsen@jpl.nasa.gov.

References:

- Aumann, H. H., M. T. Chahine, C. Gautier, M. D. Goldberg, E. Kalnay, L. M. McMillin, H. Revercomb, P. W. Rosenkranz, W. L. Smith, D. H. Staelin, L. L. Strow and J. Susskind (2003), AIRS/AMSU/HSB on the Aqua mission: design, science objectives, data products and processing system, *IEEE Trans. Geosci. and Remote Sensing*, 41, 253-264.
- Chahine, M. T., T. S. Pagano, H. H. Aumann, R. Atlas, C. Barnet, L. Chen, M. Divakarla, E. J. Fetzer, M. Goldberg, C. Gautier, S. Granger, F. W. Irion, R. Kakar, E. Kalnay, B. H. Lambrigtsen, S.-Y. Lee, J. Le Marshall, W. McMillan, L. McMillin, E. T. Olsen, H. Revercomb, P. Rosenkranz, W. L. Smith, D. Staelin, L. L. Strow, J. Susskind, D. Tobin and W. Wolf, 2006, The Atmospheric Infrared Sounder (AIRS): improving weather forecasting and providing new insights into climate, *Bulletin of the American Meteorological Society*, 87, 891–894, DOI: 10.1175/BAMS-87-7-891.
- Divakarla, M., C. Barnet, M. D. Goldberg, L. McMillin, E. S. Maddy, W. W. Wolf, L. Zhou, and X. Liu (2006), Validation of Atmospheric Infrared Sounder temperature and water vapor retrievals with matched radiosonde measurements and forecasts, *J. Geophys. Res.*, 111, doi:10.1029/2005JD006116.
- Fetzer, E. J., B. H. Lambrigtsen, A. Eldering, H. H. Aumann, and M. T. Chahine (2006), Biases in total precipitable water vapor climatologies from Atmospheric Infrared Sounder and Advanced Microwave Scanning Radiometer, *J. Geophys. Res.*, 111, D09S16, doi:10.1029/2005JD006598.
- Kahn, B. H., A. Eldering, A. J. Braverman, E. J. Fetzer, J. H. Jiang, E. Fishbein and D. L. Wu, (2007), Towards the characterization of upper tropospheric clouds using AIRS and MLS observations, *J. Geophys. Res.*, 112, D05202, doi:10.1029/2006JD007336.
- Kahn, B. H., E. Fishbein, S. L. Nasiri, A. Eldering, E. J. Fetzer, M. J. Garay and S.-Y. Lee, (2007a), The radiative consistency of AIRS and MODIS cloud retrievals, *J. Geophys. Res.*, 112, D09201, doi:10.1029/2006JD007486.
- Kahn et al. (2008), Cloud type comparisons of AIRS, CloudSat, and CALIPSO cloud height and amount, *J. Atmos. Chem. Phys.*, 8, 1231-1248.
- Susskind, J., C. Barnet, J. Blaisdell, L. Iredell, F. Keita, L. Kouvaris, G. Molnar, and M. Chahine (2006), Accuracy of geophysical parameters derived from Atmospheric Infrared Sounder/Advanced Microwave Sounding Unit as a function of fractional cloud cover, *J. Geophys. Res.*, 111, D09S17, doi:10.1029/2005JD006272.
- Tian, B., D. E. Waliser, E. J. Fetzer, B. H. Lambrigtsen, Y. L. Yung and B. Wang, (2006), Vertical moist thermodynamic structure and spatial-temporal evolution of the Madden-Julian oscillation in Atmospheric Infrared Sounder observations, *J. Atmos. Sci.*, 63, 2462-2485.
- Tobin, D.C., H. E. Revercomb, R. O. Knuteson, B. Lesht, L. L. Strow, S. E. Hannon, W. F. Feltz, L. Moy, E. J. Fetzer, and T. Cress (2006), Atmospheric Radiation Measurement site atmospheric state best estimates for Atmospheric Infrared Sounder temperature and water vapor retrieval validation, *J. Geophys. Res.*, 111, doi:10.1029/2005JD006103.

2.4.2 AMSR-E surface wind speed, precipitable and cloud-liquid water, SST, and rain rate

Overview and Relevance to YOTC:

Cautions and Caveats:

Example Figure(s):

Web Page(s):

Additional Contact Information:

References:

2.4.3 CALIPSO cloud and aerosol products

Overview and Relevance to YOTC:

Cautions and Caveats:

Example Figure(s):

Web Page(s):

Additional Contact Information:

References:

2.4.4 CERES cloud properties and radiative fluxes

Overview and Relevance to YOTC: CERES provides integrated climate data records of the Earth's Radiation Budget (ERB) from the surface to the top-of-atmosphere that accounts for the regional and global diurnal cycle of radiative fluxes. CERES data products also include coincident MODIS-derived cloud, aerosol and surface properties, as well as meteorological data so that changes in ERB and climate system components can be investigated in an integrated manner. The CERES instruments measure broadband radiances in three channels: (i) shortwave from 0.3 to 5 μm ; (ii) window from 8 to 12 μm ; (iii) total from 0.3 to 200 μm (Wielicki et al, 1995). CERES provides global coverage daily with a spatial resolution of 20 km at nadir. A total of 25 unique input data sources are used to produce 18 CERES data products that cover a range of time (from instantaneous to monthly mean) and space (footprint level to global) scales, making these data products ideal for studying cloud radiative effects by cloud type.

Cautions and Caveats: All CERES data products have undergone extensive validation. Users should carefully read the Data Quality Summary accompanying each CERES data product for information on data accuracy and any cautions/helpful hints.

Example Figure(s):

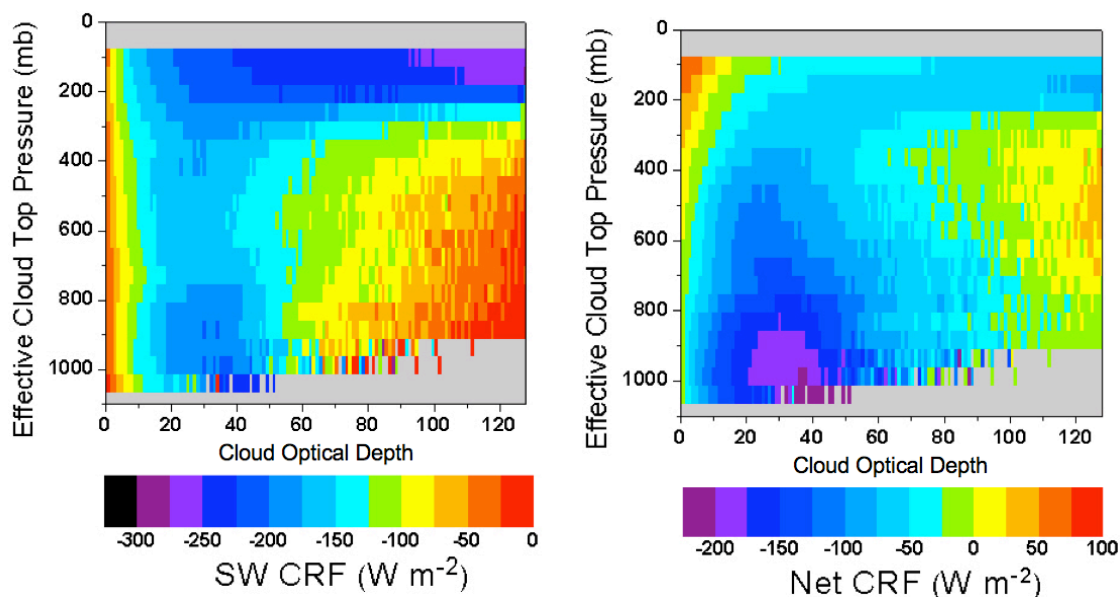


Figure 9. CERES-Terra top-of-atmosphere Cloud Radiative Forcing by MODIS effective cloud top pressure and cloud optical depth for (left) SW and (right) Net radiation from December 2001.

Web Page(s):

Home Page: <http://science.larc.nasa.gov/ceres/index.html>

Data Processing Page: http://eosweb.larc.nasa.gov/project/ceres/table_ceres.html

Additional Contact Information:

Dr. Norman G. Loeb, Mail Stop 420, NASA Langley Research Center, Hampton, VA, 23681.
Email: norman.g.loeb@nasa.gov

References:

Wielicki, B. A., B. R. Barkstrom, E. F. Harrison, R. B. Lee III, G. L. Smith, and J. E. Cooper, 1996: Clouds and the Earth's Radiant Energy System (CERES): An Earth Observing System Experiment, *Bull. Amer. Meteor. Soc.*, 77, 853-868.

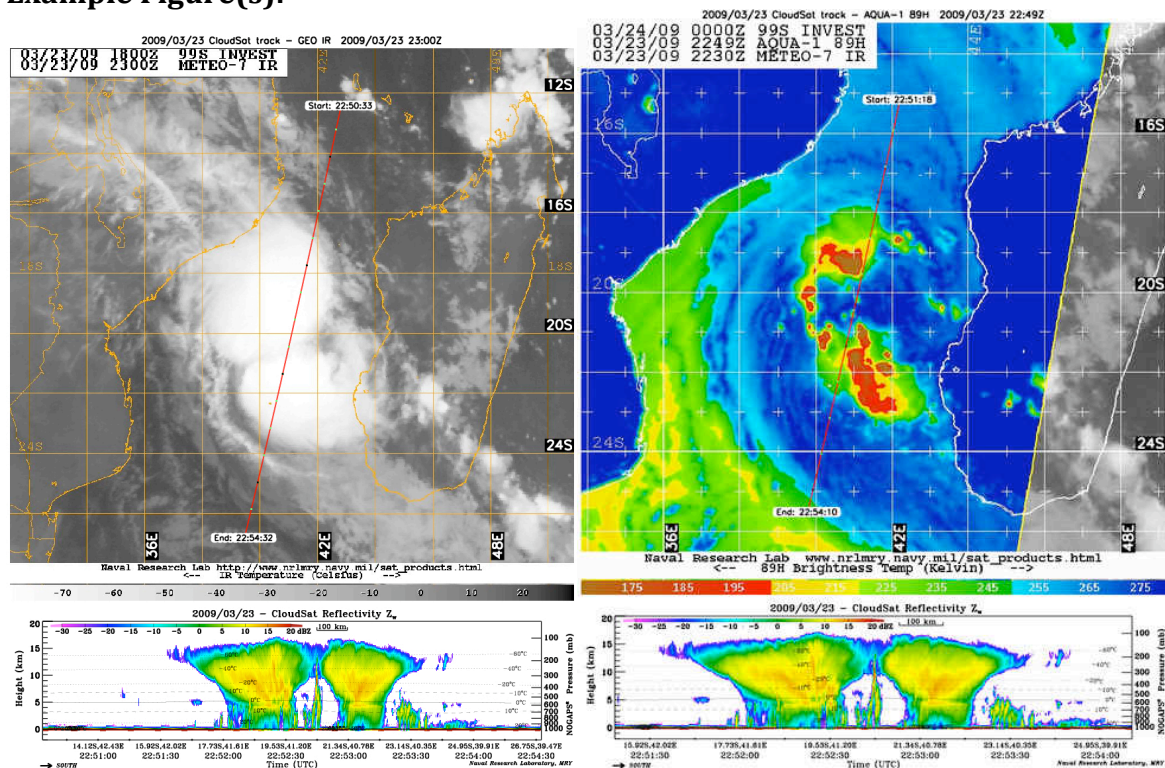
2.4.5 CloudSat cloud and precipitation products

Overview and Relevance to YOTC: CloudSat uses a 94 GHz, nadir-viewing radar to measure backscattered power. These measurements are used to retrieve cloud properties, such as liquid and ice water content profiles, and some precipitation characteristics (Stephens et al. 2002, 2008). In some cases, the retrieval algorithms utilize auxiliary information from other co-located sensor information (e.g., MODIS) and estimates of temperature from ECMWF analysis. The data sampling is based on a nadir-pointing ground track, with a sensor footprint of approximately 1.5km, and a vertical resolution of about 250-500m depending on the quantity.

Cautions and Caveats: Due to effects of ground clutter, the CPR under samples low clouds. The liquid water content of low clouds available from either 2B-CWC-RO or 2B-CWC-RVOD products has not properly excluded effects of precipitation from the product and thus has a tendency to bias the liquid water contents (LWC) high. Similarly the particle size information in these products is too highly constrained. Analysis and improvements to the LWC and related microphysics are forthcoming. The ice water content information for deep convective clouds is also unreliable and should be interpreted with caution. The over-ocean precipitation information from 2C-PRECIP-COLUMN underestimates the heavy precipitation above about 5 mm/hr. Analysis and validation of all data products continues.

For information about data products, contact the Cloudsat Data Processing Center through the home page given.

Example Figure(s):



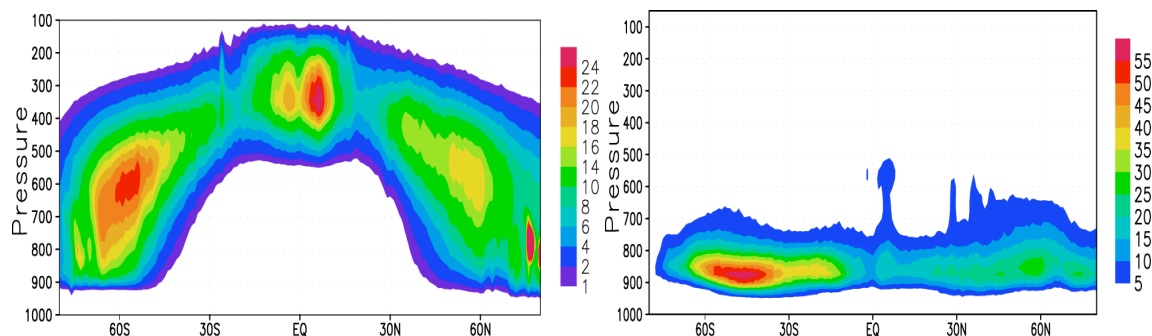


Figure 10. (middle panels) CloudSat reflectivity for Caribbean hurricane Dean in August 19, 2009. (top panels) Collocated maps of CloudSat overpass showing IR temperature (left) and 89H Ghz emission (right). (lower panels) Annual mean zonal average ice (left) and liquid (right) water content from CloudSat (Waliser et al. 2009; Li et al. 2008, respectively).

Web Page(s):

Home Page: <http://cloudsat.atmos.colostate.edu/>

Data Processing Page: <http://www.cloudsat.cira.colostate.edu/>

Additional Contact Information: TBD

References:

- Li, J.-F., D. E. Waliser, C. Woods, J. Teixeira, J. Bacmeister, J. Chern, B. W. Shen, A. Tompkins, and M. Kohler (2008), Comparisons of Satellites Liquid Water Estimates with ECMWF and GMAO Analyses, 20th Century IPCC AR4 Climate Simulations, and GCM Simulations. *Geophys. Res. Lett.*, 35, L19710, doi:10.1029/2008GL035427.
- Stephens, G. L., D. G. Vane, R. J. Boain, G. G. Mace, K. Sassen, Z. E. Wang, A. J. Illingworth, E. J. O'Connor, W. B. Rossow, S. L. Durden, S. D. Miller, R. T. Austin, A. Benedetti, and C. Mitrescu, 2002: The cloudsat mission and the a-train - A new dimension of space-based observations of clouds and precipitation. *Bulletin of the American Meteorological Society*, 83, 1771-1790.
- Stephens, G. L., D. G. Vane, S. Tanelli, E. Im, S. Durden, M. Rokey, D. Reinke, P. Partain, G. G. Mace, R. Austin, T. L'Ecuyer, J. Haynes, M. Lebsock, K. Suzuki, D. Waliser, D. Wu, J. Kay, A. Gettleman, and Z. Wang, 2008: The CloudSat Mission: Performance and early science after the first year of operation. *Journal of Geophysical Research*, In Press.
- Waliser, D.E., J. F. Li, J. Bacmeister, J. Chern, A. Del Genio, J. Jiang, M. Kharitondov, K.N. Liou, H. Meng, P. Minnis, W.B. Rossow, G. Stephens, S. Sun-Mack, W.K. Tao, A. Tompkins, D. Vane, C. Woods, D. Wu, 2009: Cloud Ice: A Climate Model Challenge With Signs and Expectations of Progress, *J. Geophys. Res.*, 114, D00A21, doi:10.1029/2008JD010015.

2.4.6 GPS temperature and water vapor profiles

Overview and Relevance to YOTC: GPS radio occultation (RO) is an active limb sounding method whereby a GPS receiver onboard a low-earth-orbiting satellite measures the phase delays and amplitudes of the L-band dual-frequency radio signals from the GPS satellites as the signals traverse the atmosphere. With the assumption of local spherical symmetry, the measurements can be directly inverted to yield quasi-vertical profiles of microwave refractivity. The refractivity is related to the temperature, pressure, and water vapor. Above the upper troposphere (about 10 km in the tropics), water vapor contribution can be neglected so that temperature and pressure profiles can be determined unambiguously through hydrostatic equation and ideal gas law. In the middle to lower troposphere, water vapor can be retrieved by assuming temperature from ancillary data (usually ECMWF or NCEP analyses) [Hajj et al. 2002].

The current fleet of GPS RO instruments includes the six-satellite COSMIC/FORMOSAT-3 constellation [Anthes et al. 2008], CHAMP, SAC-C, and GRACE-A. About 2500 profiles are available daily across the globe. The GPS RO technique has the following advantages. First, it provides global coverage with sampling over diurnal cycle (Figure 11). (2) It yields temperature and water vapor profiles with very high vertical resolution (about 200 m below 20 km altitude). Horizontal resolution is estimated to be about 100-200 km. (3) The measurements are unaffected by clouds and precipitation. (4) The measurements are self-calibrated, meaning that they are not subject to inter-satellite biases or time-dependent instrumental drifts [Hajj et al. 2004]. Comparisons between GPS and other measurements as well as ECMWF and NCEP analyses have provided strong validations that the temperature profiles are accurate to within 1 K in the altitude range of 10-25 km [e.g., Rocken et al. 1997, Wang et al. 2004, Schwartz et al. 2008, Yunck et al. 2008]. An example of tropical GPS temperature and water vapor profiles from COSMIC is illustrated in Figure 12 showing excellent agreement with collocated radiosonde sounding as well as the NCEP and ECMWF analyses.

Cautions and Caveats: Not all profiles reach the surface due to measurement errors, although they perform better with COSMIC and SAC-C [Ao et al. 2009]. A dry bias might exist below about 2 km over regions with strong inversion at the top of the planetary boundary layer [Sokolovskiy, 2003]. Validation of the tropospheric water vapor retrieval is somewhat lacking, although a recent study comparing collocated GPS, AIRS, and radiosonde measurements showed similar levels of accuracy [Mannucci et al. 2009]. Temperature retrievals above 25 km are not sufficiently well validated.

Example Figure(s):

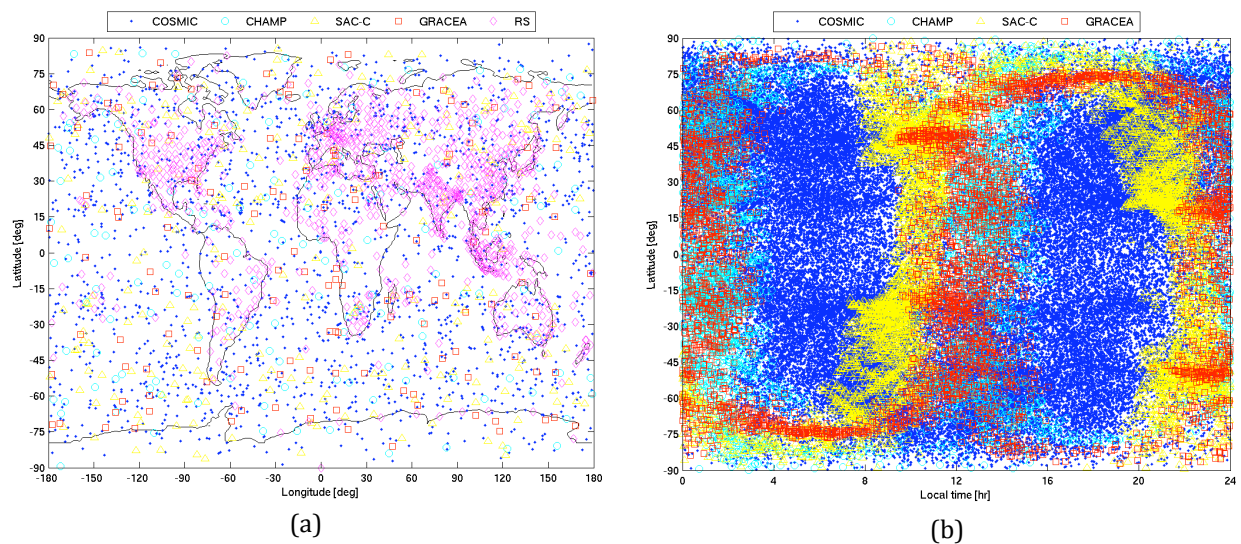


Figure 11. (a) Spatial coverage in one day from COSMIC, CHAMP, SAC-C, and GRACE-A. Also shown for comparison are the routine radiosonde sounding locations. (b) Local time coverage in one month showing good sampling of the diurnal cycle at all latitudes.

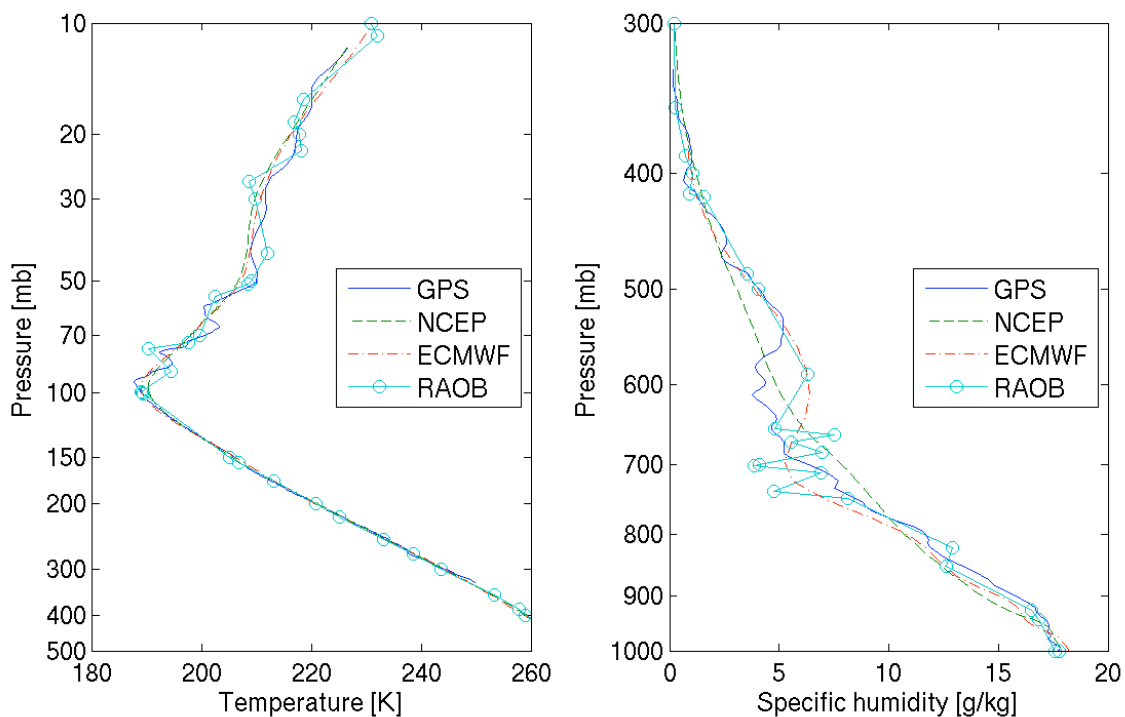


Figure 12. An example of temperature and water vapor profiles retrieved from a COSMIC occultation. Results from NCEP, ECMWF, and a nearby radiosonde sounding (8.52 S, 179.22 E) are also shown for comparison.

Web Page(s): <http://genesis.jpl.nasa.gov/>

Additional Contact Information: chi.o.ao@jpl.nasa.gov

References:

- Anthes, R. A., et al. (2008), The COSMIC/FORMOSAT-3 Mission: Early Results. *Bull. Am. Meteorol. Soc.*, 89, 313-333.
- Ao, C. O., G. A. Hajj, T. K. Meehan, D. Dong, B. A. Iijima, A. J. Mannucci, and E. R. Kursinski (2009), Rising and setting GPS occultations by use of open-loop tracking, *J. Geophys. Res.*, 114, D04101, doi:10.1029/2008JD010483.
- Hajj, G. A., E. R. Kursinski, L. J. Romans, W. I. Bertiger, and S. S. Leroy (2002), A Technical Description of Atmospheric Sounding by GPS Occultation. *J. Atmospheric and Solar-Terrestrial Physics*, 64, 451-469.
- Hajj, G. A., et al. (2004), CHAMP and SAC-C Atmospheric Occultation Results and Intercomparisons, *J. Geophys. Res.*, 109, D06109, doi:10.1029/2003JD003909.
- Mannucci, A. J., C. O. Ao, E. J. Fetzer, B. A. Iijima, F. W. Irion, B. D. Wilson, and T. P. Yunck (2009), Cross Validation of Water Vapor Retrievals from GPS Radio Occultations, AIRS and Radiosondes. AMS Annual Meeting, Phoenix, AZ.
- Schwartz, M. J. et al. (2008), Validation of the Aura Microwave Limb Sounder Temperature and Geopotential Height Measurements. *J. Geophys. Res.*, 113, D15S11, doi:10.1029/2007JD008783.
- Wang, D.-Y. et al. (2004), Cross-Validation of MIPAS/ENVISAT and GPS-RO/CHAMP Temperature Profiles. *J. Geophys. Res.*, 109, D19311, doi:10.1029/2004JD004963.
- Sokolovskiy, S. V. (2003), Effect of Super Refraction on Inversions of Radio Occultation Signals in the Lower Troposphere, *Radio Sci.*, 38(3), 1058, doi:10.1029/2002RS002728.
- Yunck, T. P., E. J. Fetzer, A. J. Mannucci, C. O. Ao, F. W. Irion, B. D. Wilson, and G. J. M. Maniön (2008), Use of Radio Occultation to Evaluate Atmospheric Temperature Data from Spaceborne Infrared Sensors. *Terr, Atmos. Ocean. Sci.*, 20, 71-85, doi: 10.3319/TAO.2007.12.08.01(F3C).

2.4.7 ISCCP cloud products

Overview and Relevance to YOTC:

Cautions and Caveats:

Example Figure(s):

Web Page(s):

Additional Contact Information:

References:

2.4.8 MLS water vapor, cloud ice, composition and temperature profiles

Overview and Relevance to YOTC: The Microwave Limb Sounder (MLS) on Aura observes atmospheric thermal microwave emission in the limb at 118, 190, 240, 640 and 2500 GHz. MLS products include vertical profiles of atmospheric composition (including water vapor), cloud and temperature from the upper troposphere to the mesosphere (Waters et al., 2006). Vertical profiles are measured every ~ 160 km along the orbit track with a cross track width of ~ 7 km and a vertical resolution that varies between about 1.5 km to 5 km depending on the product. Following the A-train reconfiguration in April 2008, the MLS and CloudSat/Calispo measurement tracks have been coincident to within ~ 10 km. MLS measurements relevant for YOTC include profiles of temperature and specific and relative humidity for pressures of 316 hPa and smaller, and profiles of cloud Ice Water Content (IWC), carbon monoxide (CO), ozone (O_3) and nitric acid (HNO_3) for pressures of 215 hPa and smaller.

Cautions and Caveats: Data users should obey all the quality screening instructions given in the MLS data quality document (Livesey et al., 2007). The current (v2.2) MLS dataset includes some biases, notably a persistent $\sim 2\times$ high bias in carbon monoxide at 215 hPa, and a negative bias in HNO_3 at the same pressure. These are ameliorated in the version 3 algorithms to be released in summer 2009.

Example Figure:

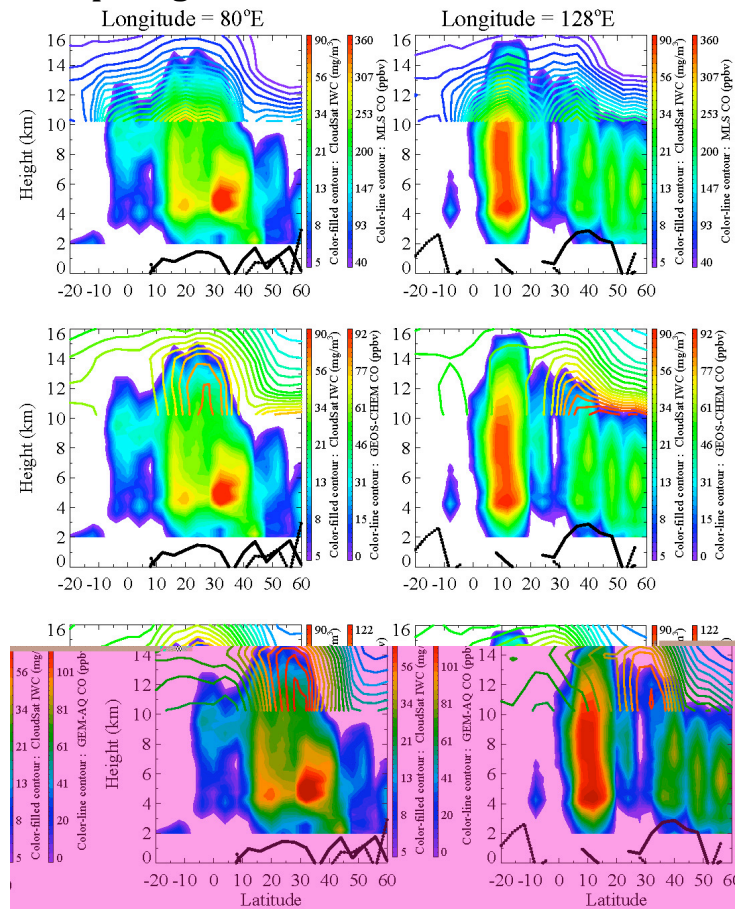


Figure 13. Deep convection can rapidly loft polluted air (enriched in Carbon Monoxide – CO) from the boundary layer into the upper troposphere, with implications for upper tropospheric chemistry and radiative balance (both water vapor and pollution ozone are strong greenhouse gases). The figures show latitude/height sections of the Aura MLS observed (top), and GEOS-CHEM / GEM-AQ simulated (middle, bottom) upper tropospheric CO abundance (line-contours) and CloudSat cloud water content in the troposphere (filled contours) at two longitudes. At 80°E, both models show high CO roughly correlated with the convection. At 128°E, however, neither model captures the impact of deep convection at 10°N. CloudSat and MLS provide observations that can be used to validate improvements to model convective parameterizations.

Web Page(s): <http://mls.jpl.nasa.gov/>

Additional Contact Information:

Nathaniel Livesey
Jet Propulsion Laboratory
Mail Stop 183-701
4800 Oak Grove Drive,
Pasadena,
California 91109,
USA

Email: *Nathaniel.J.Livesey@jpl.nasa.gov*

References:

Waters, J.W., et al., 2006: The Earth Observing System Microwave Limb Sounder (EOS MLS) on the Aura satellite, IEEE Trans. Geosci. Remote Sensing 44, no. 5, 2006.

Livesey, N.J., et al., 2007: Earth Observing System (EOS) Microwave Limb Sounder (MLS) Version 2.2 Level 2 data quality and description document. JPL technical report D-33509. Available from <http://mls.jpl.nasa.gov/> under EOS Aura MLS, Documentation.

Waliser, D.E., et al., 2009: Cloud ice: A climate model challenge with signs and expectations of progress, J. Geophys. Res. 114, D00A21, doi:10.1029/2008JD010015.

Read, W.G., et al., 2008: The roles of convection, extratropical mixing, and in situ freeze-drying in the tropical tropopause layer, Atmos. Chem. Phys. 8, 6051-6067.

2.4.9 MODIS Cloud Products

Overview and Relevance to YOTC: The Moderate Resolution Imaging Spectroradiometer (MODIS) was developed by NASA and launched onboard the Terra spacecraft on December 18, 1999 and Aqua spacecraft on May 4, 2002. MODIS scans a swath width sufficient to provide nearly complete global coverage every two days from each polar-orbiting, sun-synchronous, platform at an altitude of 705 km, and provides images in 36 spectral bands between 0.415 and 14.235 μm with spatial resolutions of 250 m (2 bands), 500 m (5 bands) and 1000 m (29 bands). Aqua MODIS is a member of the afternoon constellation (i.e., the “A-Train”). A comprehensive set of operational algorithms for the retrieval of cloud physical (cloud masking, cloud-top) and optical properties (optical thickness, effective particle radius, water path, thermodynamic phase) have enabled over nine years of continuous observations of cloud properties from Terra and seven years from Aqua. The archived products from these algorithms include pixel-level (Level-2) products at nadir spatial resolutions of: 250m and 1 km (cloud mask), 1 km (optical properties), and 5 km (cloud-top). All atmosphere team gridded (Level-3) products are aggregated to a 1° global grid and include 1- and 2-D histograms in addition to scalar statistics.

Cautions and Caveats: Cloud detection and cloud-top products have been validated vs. ground-based and satellite lidars (see references below). Validation for optical properties (liquid water and ice clouds) is problematic as both optical thickness and effective particle sizes are not trivially measured in situ or from other remote systems (cirrus reference below); efforts are ongoing.

Example Figure(s):

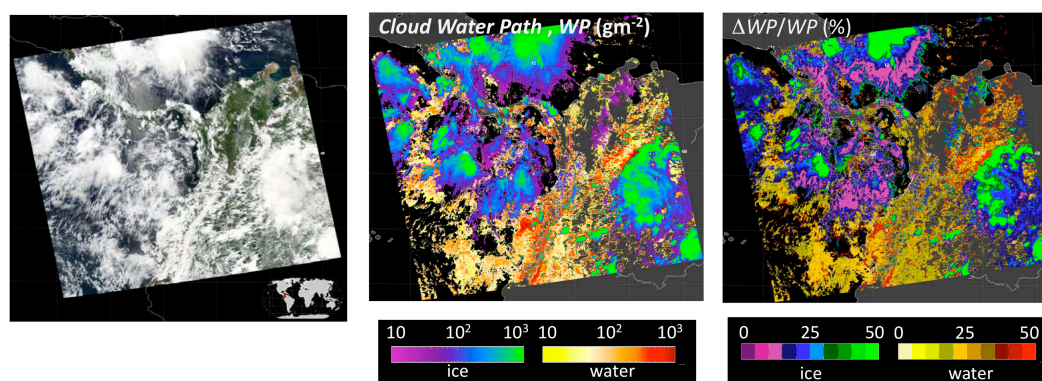


Figure 14. MODIS Aqua true color data granule image for 20 August 2006, over Central America (left panel); corresponding cloud water path retrievals, with liquid water and ice cloud phase shown separately via dual color bars (center panel); water path pixel-level *rms* retrieval uncertainty calculated for a subset of error sources (calibration/model, atmospheric correction, and specification of spectral surface albedo) (right panel).

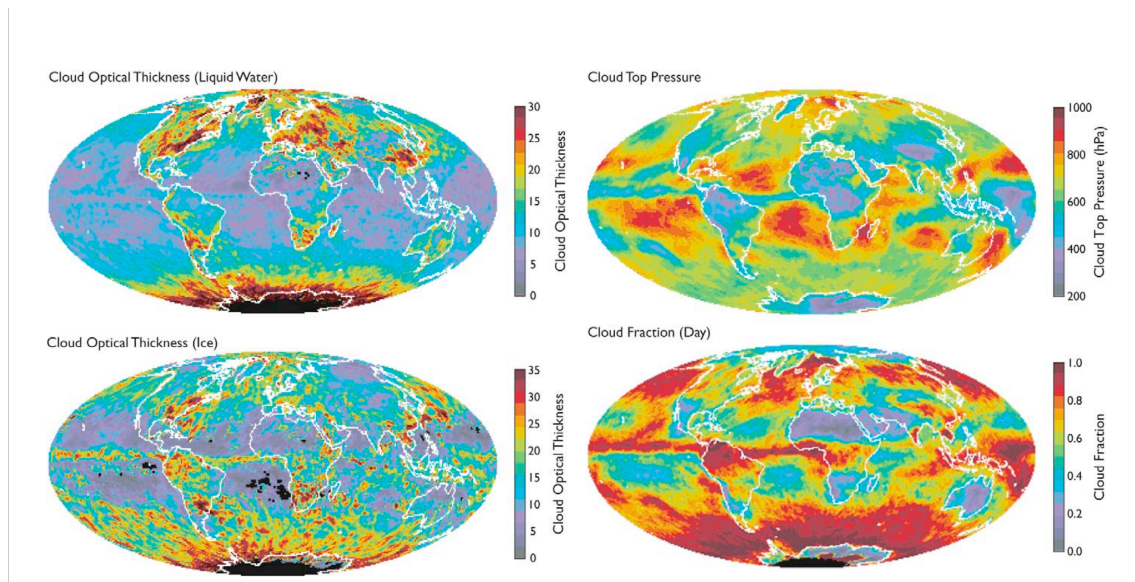


Figure 15. Example MODIS Level-3 cloud aggregations for April 2005, MODIS Aqua.

Web Page(s):

MODIS Atmosphere Team: modis-atmos.gsfc.nasa.gov/

Collection 5 Documentation: modis-atmos.gsfc.nasa.gov/products_C005update.html

References, presentations, ATBDs: modis-atmos.gsfc.nasa.gov/reference/

Known problems: modis-atmos.gsfc.nasa.gov/validation.html

Additional Contact Information:

Cloud Masking and Cloud-top Properties: S. A. Ackerman, W. P. Menzel, University of Wisconsin, Madison WI, USA.

Cloud Optical Properties: M. D. King, University of Colorado, Boulder CO, USA; S. Platnick, NASA Goddard Space Flight Center, Greenbelt MD, USA.

References:

- Ackerman, S. A., R. E. Holz, R. Frey, E. W. Eloranta, B. C. Maddux, M. McGill, 2008: Cloud detection with MODIS. Part II: Validation. *J. Atmos. Oceanic Tech.*, 25, doi: 10.1175/2007JTECHA1053.1.
- Holz R. E., S. A. Ackerman, F. W. Nagle, R. Frey, S. Dutcher, R. E. Kuehn, M. A. Vaughan, B. Baum, 2008: Global Moderate Resolution Imaging Spectroradiometer (MODIS) cloud detection and height evaluation using CALIOP. *J. Geophys. Res.*, 113, doi: 10.1029/2008JD009837.
- Jiang, J. H., H. Su, M. Schoeberl, S. T. Massie, P. Calarco, S. Platnick, N. J. Livesey, 2008: Clean and polluted clouds: relationships among pollution, ice cloud and precipitation in South America. *Geophys. Res. Letters*, 35, doi:10.1029/2008GL034631.
- King, M. D., W. P. Menzel, Y. J. Kaufman, D. Tanre, B.-C. Gao, S. Platnick, S. A. Ackerman, L. A. Remer, R. Pincus, and P. A. Hubanks, 2003: Cloud and aerosol properties, precipitable water, and profiles of temperature and humidity. *IEEE Trans. Geosci. Remote Sens.*, 41, 442-458.

- Mace, G. G., Zhang, Y., S. Platnick, M. D. King, P. Yang, 2005: Evaluation of cirrus cloud properties derived from MODIS radiances using cloud properties derived from ground-based data collected at the ARM SGP site. *J. Appl. Meteor.*, **44**, 221-240.
- Platnick, S., M. D. King, S. A. Ackerman, W. P. Menzel, B. A. Baum, J. C. Riedi, and R. A. Frey, 2003: The MODIS cloud products: Algorithms and examples from Terra. *IEEE Trans. Geosci. Remote Sens.*, **41**, 459-473.
- Waliser, D.E., J. F. Li, J. Bacmeister, J. Chern, A. Del Genio, J. Jiang, M. Kharitondov, K.N. Liou, H. Meng, P. Minnis, S. Platnick, W.B. Rossow, G. Stephens, S. Sun-Mack, W.K. Tao, A. Tompkins, D. Vane, C. Woods, D. Wu , 2009: Cloud Ice: A Climate Model Challenge With Signs and Expectations of Progress, *J. Geophys. Res.*, 114, D00A21, doi:10.1029/2008JD010015.

2.4.10 PEHRRP – high resolution precipitation products

Overview and Relevance to YOTC: Microwave estimates of precipitation from polar orbiting satellites are the most reliable estimates over the global oceans and over many land areas. However, the polar orbiting nature of these instruments means that they lack the sampling required for the production of high resolution estimates. In recent years, several merged estimates have become available which blend high quality passive microwave (PMW) estimates with information from geostationary infrared (geo-IR) satellites which give observations as frequently as every 15 minutes. The Program to Evaluate High Resolution Precipitation Products (PEHRPP; Turk et al. 2008) was established by the International Precipitation Working Group (IPWG) to coordinate the validation of these merged high resolution products which give rain-rates on a 0.25° near-global grid every three hours.

Two datasets have become commonly used and have performed well in validation studies (Ebert et al. 2007; Tian et al. 2007; Sapiiano and Arkin 2009): the CPC Morphing technique (CMORPH; Joyce et al. 2004) and the TRMM Multi-satellite Precipitation Analysis (TMPA; Huffman et al. 2007). Both preferentially use PMW estimates when available and use Geo-IR to fill gaps in the record. CMORPH uses motion vectors derived from Geo-IR information to morph PMW estimates in time between available PMW overpasses. The TMPA fills gaps in the PMW record with rain rates from Geo-IR which are calibrated to match the PMW estimates. Both datasets give three-hourly coverage of the complete tropics (land and ocean) over the YOTC period.

A webpage has been established by PEHRPP which contains three-hourly maps of tropical precipitation with IR data included to indicate the approximate location of clouds. Links to download the datasets are also included on this page; CMORPH is available from CPC/NOAA and the TMPA is available from GSFC/NASA.

Cautions and Caveats:

Both datasets perform well over the tropics, but skill is diminished in mid-latitudes. CMORPH has been shown to have biases over some land areas; TMPA includes a monthly gauge correction over land and has small biases, although these do not necessarily translate to higher skill. TMPA sometimes displays spatial discontinuities arising from the switch between PMW and IR data, whereas CMORPH tends to be smoother than TMPA due to the morphing; it is unclear which is “correct”. Oceanic precipitation may be too low over the oceans, although this is based on very limited validation observations. Users should try to use both estimates (which are based on basically the same inputs) to get a sense for algorithm errors.

Example Figure(s):

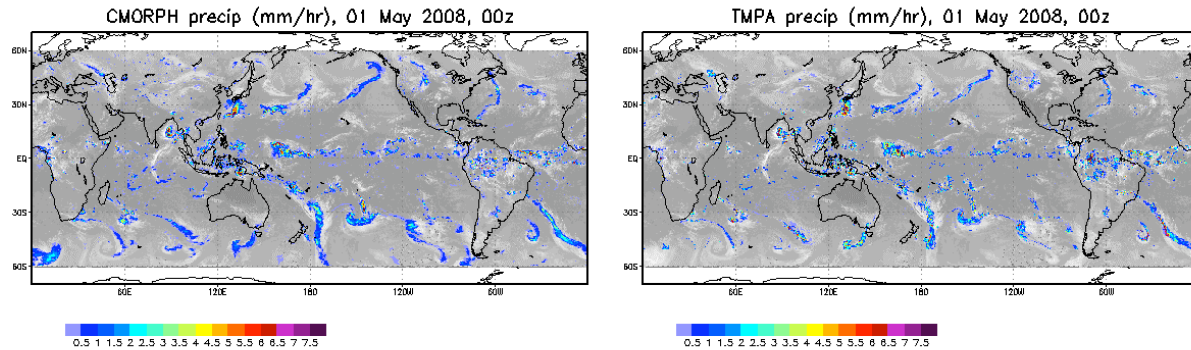


Figure 16. Rain-rate maps for 00z on May 1st 2008 from CMORPH and TMPA with Geo-IR estimates included to denote clouds.

Web Page(s):

PEHRPP: <http://essic.umd.edu/~msapiano/PEHRPP/>

YOTC images: <http://essic.umd.edu/~msapiano/PEHRPP/YOTC.html>

Additional Contact Information:

Mathew Sapiano (IPWG evaluation co-chair): msapiano@essic.umd.edu

References:

- Ebert, E. E., J. E. Janowiak and C. Kidd, 2007: Comparison of Near-Real-Time Precipitation Estimates from Satellite Observations and Numerical Models. *Bull. Amer. Meteor. Soc.*, **88**(1), 47-64.
- Huffman, G. J., R. F. Adler, D. T. Bolvin, G. Gu, E. J. Nelkin, K. P. Bowman, Y. Hong, E. F. Stocker and D. B. Wolff (2007). The TRMM Multisatellite Precipitation Analysis (TMPA): Quasi-Global, Multiyear, Combined-Sensor Precipitation Estimates at Fine Scales. *J Hydromet*, **8**(1), 38-55.
- Joyce, R. J., J. E. Janowiak, P. A. Arkin and P. Xie (2004). CMORPH: A Method that Produces Global Precipitation Estimates from Passive Microwave and Infrared Data at High Spatial and Temporal Resolution. *Journal of Hydrometeorology*, **5**(3), 487-503.
- Sapiano, M. R. P. and P. A. Arkin, 2009: An inter-comparison and validation of high resolution satellite precipitation estimates with three-hourly gauge data. *J. Hydrometeor.*, **10**(1), 149-166.
- Tian, Y., C. D. Peters-Lidard, B. J. Choudhury and M. Garcia, 2007: Multitemporal Analysis of TRMM-Based Satellite Precipitation Products for Land Data Assimilation Applications. *J. Hydrometeor.*, **8**, 1165-1183.
- Turk, F. J., P. Arkin, E. Ebert and M. Sapiano, 2008: Evaluating High Resolution Precipitation Products: The First Workshop of the Program for the Evaluation of High Resolution Precipitation Products. *Bull. Amer. Meteorol. Soc.*, **89**(12), 1911-1916.

2.4.11 QuikScat ocean surface wind/stress.

Overview and Relevance to YOTC

Wind is air in motion and is basically a vector quantity with a magnitude (speed) and a direction. Ocean surface stress is another vector quantity closely related to wind; it is the turbulent transfer of momentum between the ocean and the atmosphere (Liu, 2009). Convergence of surface wind-stress provides the vertical velocity for convection (Hsu et al., 1997). Scatterometer send microwave pulses to the earth's surface and measure the power backscattered from the surface roughness. Over the ocean, which covers over three-quarters of the earth's surface, the surface roughness is largely due to the small centimeter waves on the surface. These surface waves are believed to be in equilibrium with the local stress. The backscatter depends not only on the magnitude of the stress but also the stress direction relative to the direction of the radar beam (azimuth angle). The capability of measuring both stress magnitude and direction is the major unique characteristic of the scatterometer. (Liu and Xie, 2005). Over the large expanse of ocean, which is quasi-stationary and horizontally homogeneous under near neutral conditions, surface stress and the geophysical product of the scatterometer, the so-called equivalent neutral wind, have been used as the actual wind (Liu and Tang, 1996). From the two-dimensional field of surface vector wind/stress, surface convergence could be monitored over global oceans.

QuikSCAT, which was launched in 1999, covers 90% of the Earth each day, with 12.5 km spatial resolutions, and examples of research applications in convective systems, tropical cloud cluster, Madden-Julian waves, and monsoon in the tropics are abound. Liu et al. (2000) related surface wind convergence to the vertical rain profile in the rainbands in Hurricane Floyd. Liu and Xie (2002) relate surface wind convergence and sea surface temperature in the double inter-tropical convergence zone. The vertical extent of mesoscale-system over the meanders of western-boundary currents was examined by Liu et al. (2005). Scatterometers on tandem mission, providing more than twice daily overpasses have been used to improve our understanding of diurnal cycles of convection (Liu et al., 2007). During the YOTC period, we have another scatterometer flying with QuikSCAT, the Advanced Scatterometer (ASCAT) flying on a European platform. Fig. 1 shows that by adding ASCAT to QuikSCAT, the zonally-average revisit time interval decreases to shorter the 12 hours for all latitudes.

Cautions and Caveats

Heavy rain disturbs roughness at the ocean surface and also affects microwave transmission through the atmosphere. Flow separation (surface stress does not increase with wind speed) may cause saturation of the microwave backscatter at wind speed above 35 m/s. There is large uncertainty in the accuracy of wind-stress retrieved under the rainy and strong wind conditions of marine storms. Land contamination of scatterometer footprint may limit wind retrieval in coastal region.

Contact Information: W.Timothy.Liu@jpl.nasa.gov

Web Page: <http://airsea.jpl.nasa.gov>, <http://winds.jpl.nasa.gov>

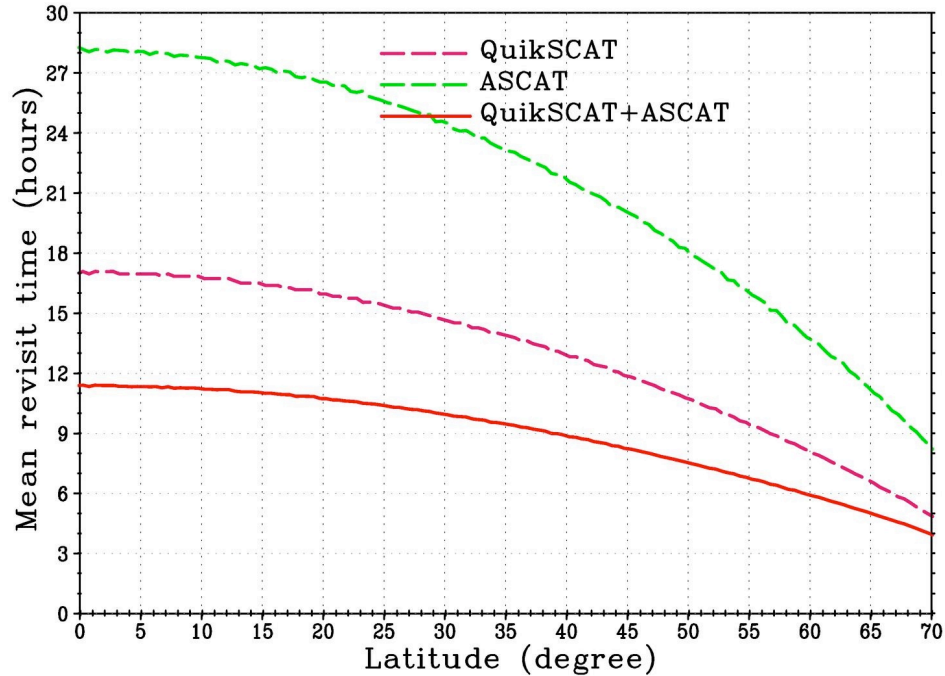


Figure 17. The latitudinal variation of zonally-averaged revisit interval for various scatterometer missions.

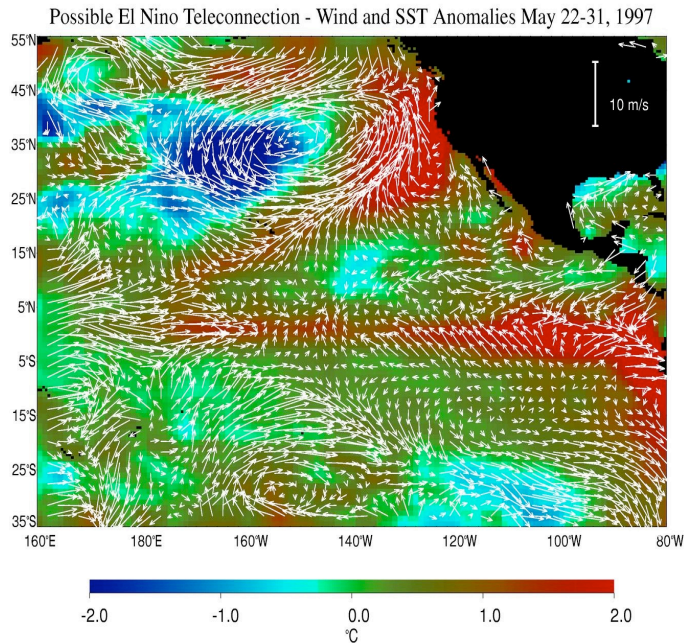


Figure 18. This figure, which appeared in Liu et al, Eos, Trans. of AGU, Vol. 79, No. 21, p249, 1998, and also in National Geographic, Vol. 195, No. 3, p 87, 1999, displays multi-scale air-sea interactions in the tropical Pacific. Surface wind anomalies from NSCAT (white arrows) are superimposed on sea surface temperature anomalies from AVHRR. The data are averaged over the period of May 22-31, 1997, with the climatological mean for this period removed. Eastward extension of the intraseasonal westwind anomalies from the equatorial western Pacific is shown to be associated with the interannual warming of the central and eastern equatorial Pacific. The equatorial west wind anomalies appear to branch north to form what is known as the 'pineapple express' that brings warm and moist air to North America, and is part the unusual cyclone flow that modifies the decadal SST dipole in subtropical Pacific.

References

- Hsu, C.S., W.T. Liu, and M.G. Wurtele, 1997: Impact of scatterometer winds on hydrologic forcing and convective heating through surface divergence. *Mon. Wea. Rev.*, **125**, 1556-1576.
- Liu, W.T., 2008: Sea surface wind/stress vector. *Encyclopedia of Remote Sensing*. Springer Press, Heidelberg, in press.
- Liu, W.T., X. Xie, and P.P. Niiler, 2007: Ocean-atmosphere interaction over Aquilhas Extension Meanders. *J. Climate*, **20**(23), 5784-5797.

- Liu, W.T. and W. Tang, 1996: *Equivalent Neutral Wind*. JPL Publication 96-17, Jet Propulsion Laboratory, Pasadena, 16 pp.
- Liu, W.T. and X. Xie, 2002: Double Intertropical Convergence Zones – a new look using scatterometer. *Geophys. Res. Lett.* 29(22), 2072, doi:10.1029/2002GL015431.
- Liu, W.T., and X. Xie 2006: Measuring ocean surface wind from space. Remote Sensing of the Marine Environment, Manual of Remote Sensing, Third Edition, Vol. 6, J. Gower (ed.), Amer. Soc. for Photogrammetry and Remote Sens. Chapter 5, 149-178.
- Liu, W.T., H. Hu, and S. Yueh, 2000: Interplay between wind and rain observed in Hurricane Floyd. *Eos, Trans. of AGU*, **81**, 253 & 257.
- Liu, W.T., W. Tang, X. Xie, R. Navalgund, and K. Xu, 2007: Power density of ocean surface wind-stress from International scatterometer tandem missions. *Int. J. Remote Sens.*, 29(21), 6109-6116.

2.4.12 TRMM/TMI precipitation, SST and related products

Overview and Relevance to YOTC:

Cautions and Caveats:

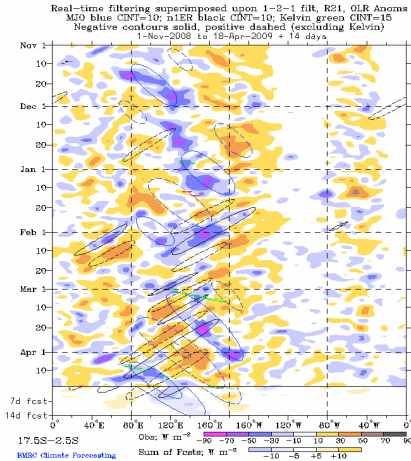
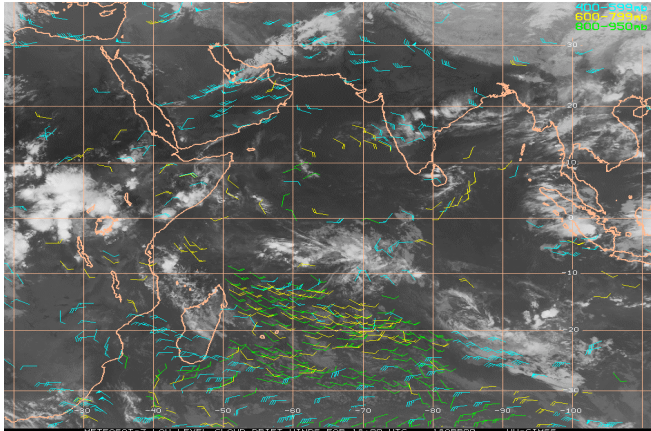
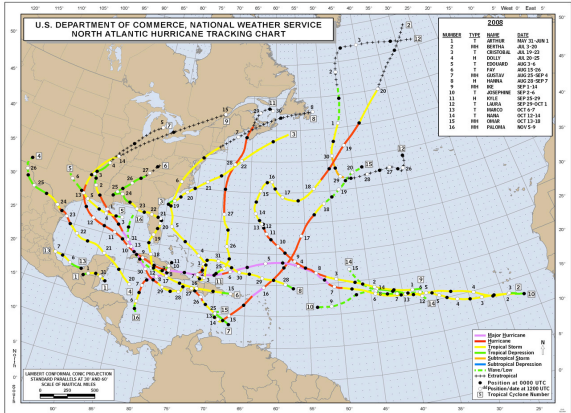
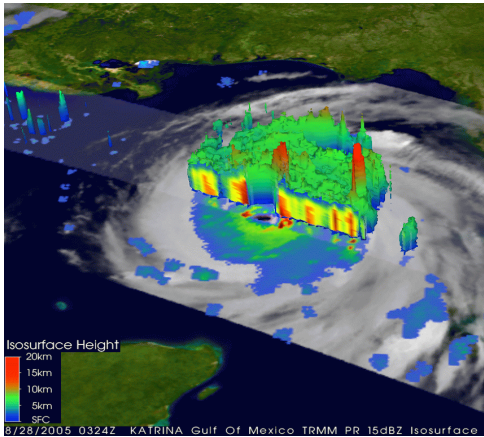
Example Figure(s):

Web Page(s):

Additional Contact Information:

References:

3 Synoptic Periods of Interest



3.1 Introduction

A key aspect of the framework of YOTC is to focus community effort and expertise on a specific time period, i.e. May 2008 to October 2009 – the YOTC period. Associated with this focus is the development of a comprehensive observational database (i.e. see Satellite and Model Analysis and Forecast Data Sections) in conjunction with a targeted research/process modeling component. Within the focus year, there is need to further identify specific “periods of interest” (POI) in order that the most can be gained by the concerted efforts associated with YOTC. As outlined in the Science Plan, YOTC has identified five phenomena / processes that arise and/or are heavily influenced by tropical convection. These include: 1) the Madden-Julian Oscillation (MJO) and other convectively-coupled equatorial waves (CCEWs), 2) the diurnal cycle, 3) easterly waves and tropical cyclones, 4) the summer monsoons, and 5) tropical-extratropical interactions. The objective of this component of the YOTC implementation plan is to highlight specific periods of interest and cases that occurred in the YOTC period which can serve as potential focal points for community discussion, research and hindcasting studies. The sections below provide illustration and motivation for the proposed cases / periods of interest along with brief descriptions of tropical field campaigns that overlap the YOTC period. This component of the Implementation Plan is expected to grow at least until the conclusion of the YOTC observation period, i.e. October 2009. An additional point of reference is NOAA’s hazards and climate extremes web site: www.ncdc.noaa.gov/oa/climate/research/hazards.

3.2 Overarching Periods of Interest

Overview and Motivation:

Figure 1 provides an illustrative example of the interactions between the global scale and synoptic scale disturbances that have significant influence on high impact weather (e.g. monsoon, tropical cyclones) and their mediation by tropical CCEWs. The upper left panel displays the equatorial wave modes during the middle part of 2008. Evident in late May through mid-June is a modestly organized eastward propagating MJO event in the Indian Ocean (see red lines in upper left panel). The event appears to dissipate, with a faster, less-convective signal continuing to propagate in the mid-to-latter part of June, and then re-emerging as a strongly disturbed period in the eastern Pacific. While in the Indian Ocean, this disturbance(s) developed a northward propagating component that initiated the onset of the Indian summer monsoon (upper right, middle left panels). In the eastern Pacific, a number of tropical cyclones were initiated (lower left panel) as well as precipitation up the Gulf of California and an impact on the North American summer monsoon (lower right panel). The illustrative part of this period is that the disturbance(s) exhibit aspects of the MJO, CCEWs, tropical cyclones, and monsoon onsets amongst other variability – all within the course of about 5 weeks, and across two ocean basins.

Illustrating Figure(s):

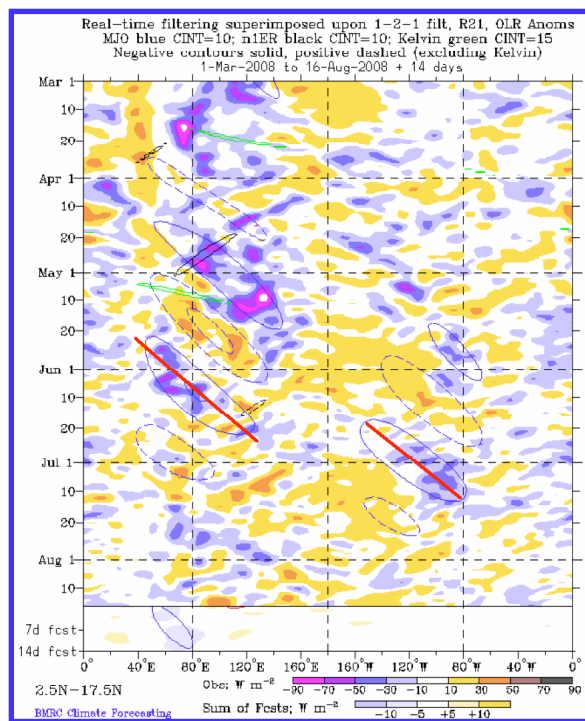
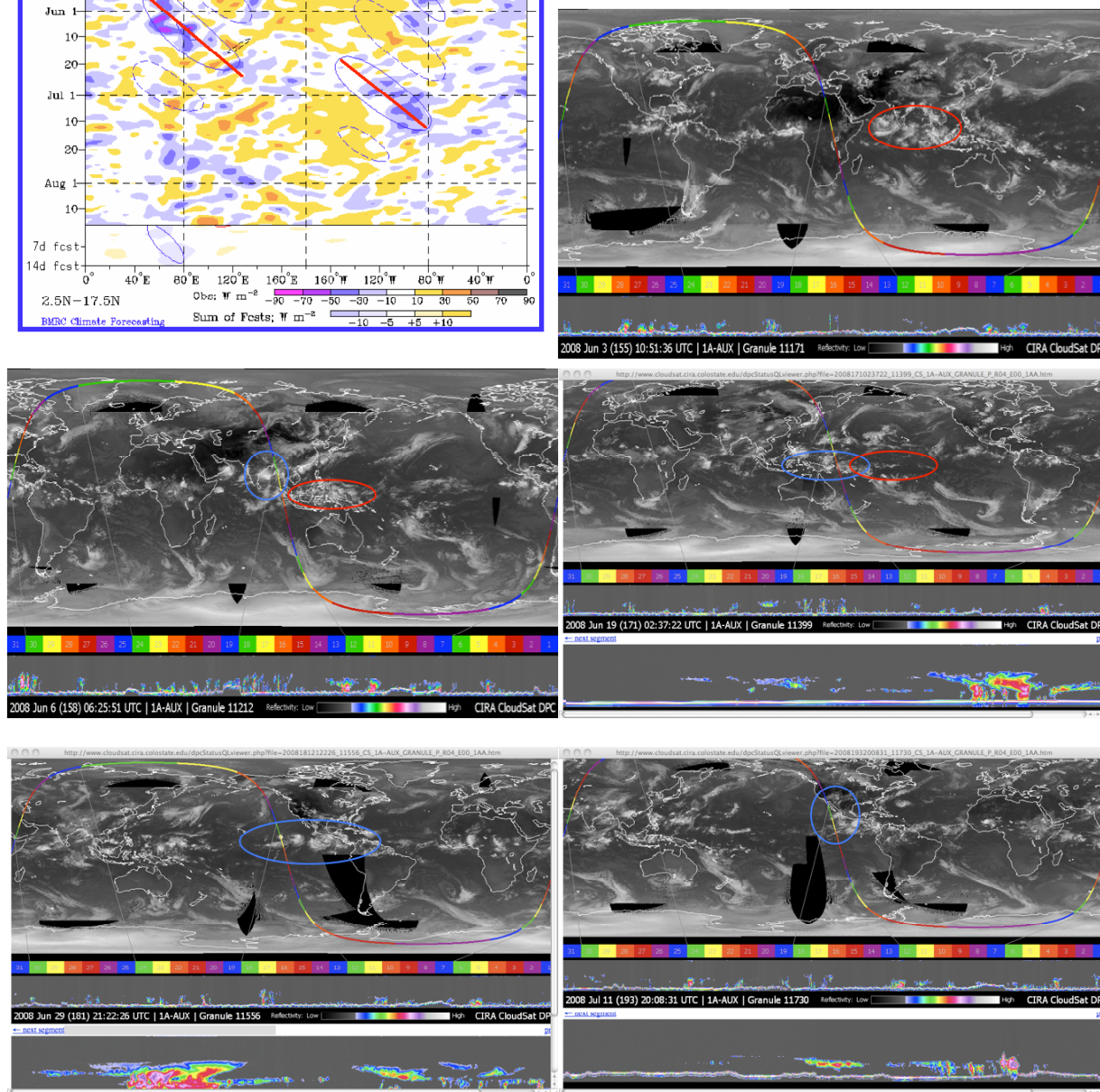


Figure 19 (upper left) Modes of coherent tropical variability (Wheeler and Weickmann, 2001) for the period Mar-Aug'08. Red lines indicate period of interest. (other panels) MODIS images of cloud variability from CloudSat website (see below); date and time of the given images are given in the lower left part the panel. The colored line is the CloudSat satellite ground track location for the given date and time, and the subpanel underneath the global images are the CloudSat radar reflectivity images for the given orbit.



Relevant Web Page(s):

http://www.bom.gov.au/bmrc/clfor/cfstaff/matw/maproom/OLR_modes/

<http://www.cloudsat.cira.colostate.edu/>

Provided By: Matt Wheeler and Jon Gottschalck

References:

Wheeler, M. and K. M. Weickmann 2001: Real-Time Monitoring and Prediction of Modes of Coherent Synoptic to Intraseasonal Tropical Variability, *Monthly Weather Review*, 129, 2677-2694.

3.3 MJO and CCEWs

Figure 20 provides a large-scale view of the near-equatorial convective variability occurring during the period from June 2007 to May 2009. On the interannual time scale, it can be seen that this period was characterised by generally suppressed convection (indicated by positive OLR anomalies) in the central Pacific and enhanced convection (negative OLR anomalies) in the vicinity of the Maritime Continent, as is symptomatic of the weak La Nina conditions that appeared throughout most of the period. Superimposed on this interannual pattern were a number of cases of eastward propagating MJO events highlighted by the contours showing the wavenumber-frequency filtered OLR.

Compared to the very strong MJO activity that occurred during December 2007 and January 2008, the period since the start of YOTC in May 2008 has been relatively weaker. Nevertheless, modest MJO activity occurred from the outset of YOTC in May, June, and early July 2008, with the latter MJO event influencing the eastern Pacific ITCZ (see Section 3.2). Two weak MJO events can be identified in the filtered OLR over the Indo-Pacific warm pool in September-October, but then little MJO-like activity occurred until the beginning of January (2009). Then, a clear eastward progression of enhance convection occurred from the Indian ocean into the Pacific from late January to early February, culminating in

enhanced convection that persisted around 140°E until mid-March. The next well-defined event began around mid-March, with a suppressed phase of convection moving to the east to reach the western Pacific in early April, followed by enhanced convection reaching the western Pacific in late April. The January/February and March/April events are discussed further in Section **Error! Reference source not found.** below.

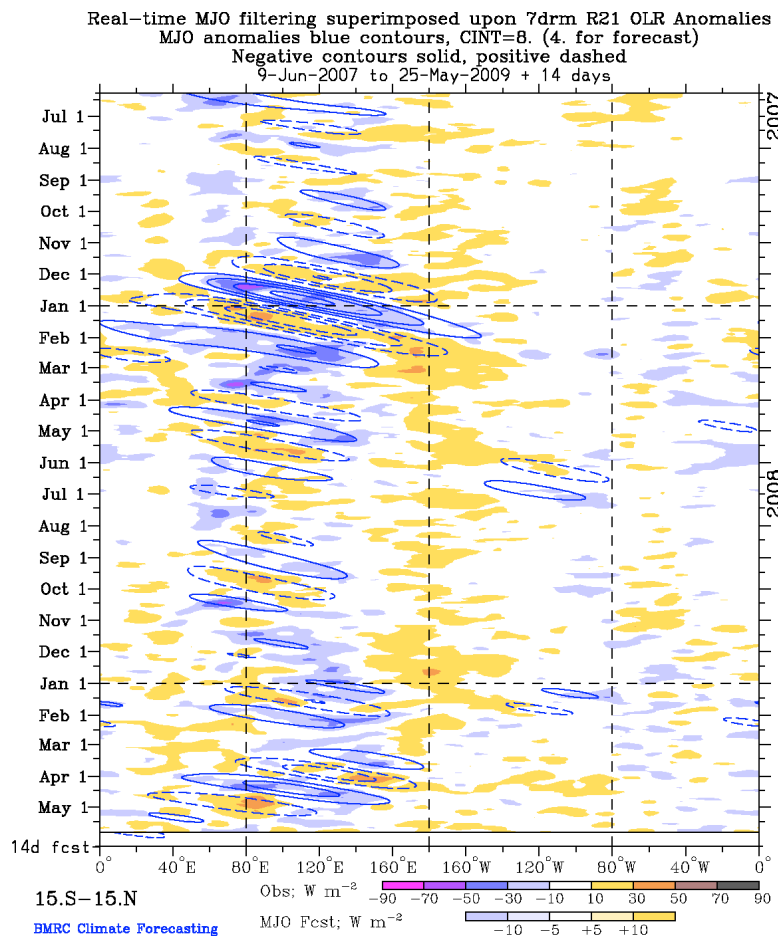


Figure 20. Time-longitude diagram of large-scale OLR anomalies (shading) for the period 9 June 2007 to 25 May 2009, averaged for the latitudes 15°S–15°N. Thick blue contours show the OLR that has been filtered for the characteristic wavenumbers and frequencies of the MJO (e.g. Wheeler and Weickmann 2001). Solid contours are for negative OLR anomalies (enhanced convection), and dashed for

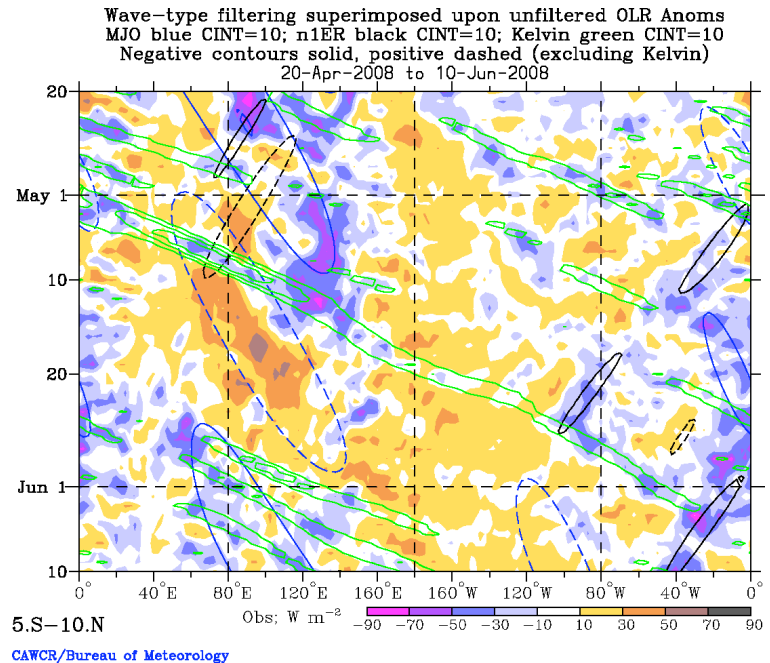
positive (suppressed convection).

Other interesting case studies for YOTC are several good examples of convectively-coupled equatorial waves. Two periods that are described below are: (1) The convectively-coupled wave event of May 2008; and (2) the multiple interacting waves of March-April 2009.

(1) May 2008 convectively-coupled Kelvin wave

Figure 21 shows that this event began over the eastern Atlantic (near 20°W) on 1 May and continued eastwards across the Indian Ocean to reach the main centre of enhanced convective activity near 120°E by 12 May. It then continued as a weaker signal across the Pacific to reach the eastern Pacific ITCZ on about 24 May, and then continued to progress into the Atlantic. Consistent with what is typical of a convectively-coupled Kelvin wave, its eastward phase speed was near 15 m s⁻¹. On potentially interesting aspect of this event were the associated westerly wind anomalies that occurred across the Pacific (Figure 22) and the SST warming they caused. This warming provided a temporary end to the La Nina of 2007-08.

Figure 21. Time-longitude diagram of OLR anomalies (shading) for the period 20 April 2008 to 10 June 2008, averaged for the latitudes 5°S-10°N. Blue contours show filtered OLR for the MJO, green contours for convectively-coupled Kelvin waves, and black contours for convectively-coupled n=1 equatorial Rossby waves (Wheeler and Weickmann 2001). Solid contours are for negative OLR anomalies (enhanced convection), and dashed for positive (suppressed convection). Only negative contours shown for the Kelvin waves.



(2) The multiple interacting waves of March-April 2009

Figure 23 shows the interesting period during March-April 2009 when there was strong evidence of the co-existence of the MJO, convectively-coupled n=1 equatorial Rossby (ER) waves, and convectively-coupled Kelvin waves. The convection of the ER waves was mostly maximized off the equator in both hemispheres, whereas the Kelvin wave convection was concentrated closer to the equator, consistent with their theoretical structures. Thus, when viewing a rather wide range of latitudes (as in Figure 21), both the eastward propagation of the Kelvin waves and westward propagation of the ER waves can be seen. In particular, an apparently linear interaction between the waves can sometimes be observed, such as the occurrence of a ER wave passing through a Kelvin wave on 1 March near 110°E. Modelling this interaction is of particular interest to YOTC.

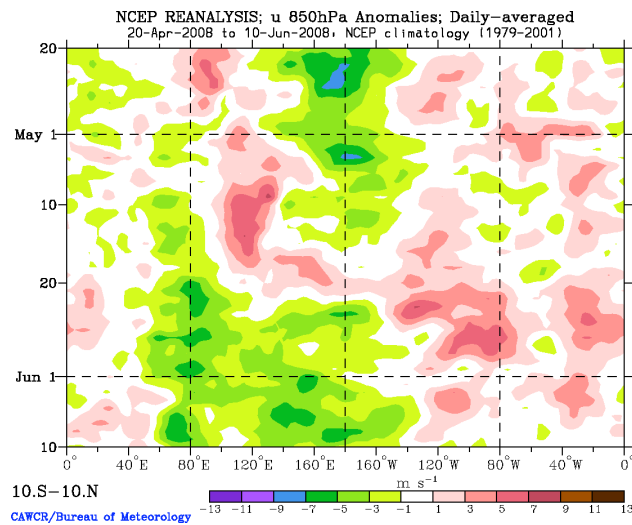
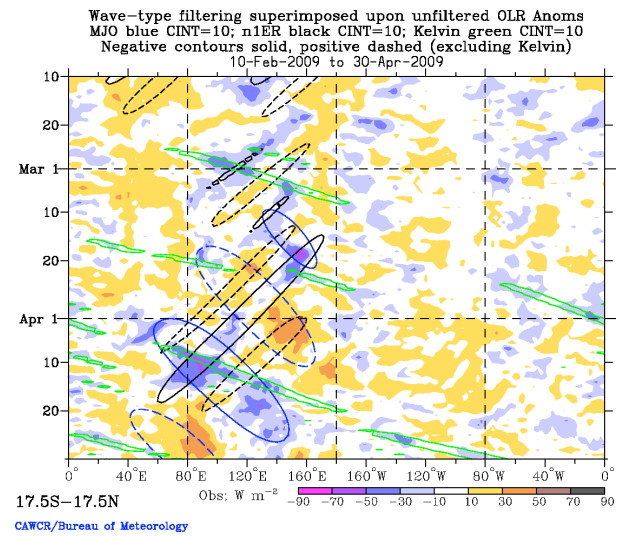


Figure 22. Time-longitude diagram of 850-hPa zonal wind anomalies for the same period as **Figure 21**, averaged for the latitudes 10°S-10°N.

Figure 23. As in Figure **Figure 21**, except for the period 10 February 2009 to 30 April 2009, and averaged for the latitudes 17.5°S to 17.5°N.



3.4 Easterly Waves and Tropical Cyclones

3.5 MJO Interactions with the Pacific Ocean

Intraseasonal Kelvin waves in the equatorial Pacific Ocean have been linked to westerly wind events associated with the MJO (e.g., Hendon et al. 1998). These waves increase in amplitude and overall activity during periods of adjustment toward El Niño (e.g., Roundy and Kiladis 2006). Nevertheless, their specific roles in the development of El Niño remain a matter of debate (e.g., Kessler and Kleeman 2000; Bergman et al. 2001; Eisenman et al. 2005; Hendon et al. 2007; etc.). The structure of the MJO changes as it interacts with these Kelvin waves during different phases of ENSO, allowing MJO activity during different phases of ENSO to yield different impacts on the ocean that might act to alter the progress of ENSO itself (Roundy and Kravitz 2009). However, the precise mechanisms whereby ENSO, the MJO, and these Kelvin waves combine to influence their collective evolution in oceanic and atmospheric circulations are poorly understood.

As previously noted, the state of the global coupled atmosphere-ocean system during Boreal winter 2008-2009 was consistent with La Niña conditions. Although MJO activity can sometimes become enhanced during such conditions, associated westerly wind burst activity over the interior West Pacific tends to be weaker than average, because the active convective phase of the MJO in that region tends to propagate far to the south of the equator under these conditions. Further, La Niña is associated with enhanced trade winds over most of the equatorial Pacific. The enhanced background easterly winds during La Niña come into approximate equilibrium with the geopotential of the ocean surface. Although westerly winds tend not to develop with the westerly phase of the MJO under such conditions, its arrival into the region is associated with temporary weakening of the trade winds. When the winds relax, gravity becomes unbalanced, and Kelvin waves form. How these waves evolve subsequently depends on the intraseasonal wind patterns that they encounter as they propagate eastward (Shinoda et al. 2008). Intraseasonal westerly anomalies along a wave trajectory tend to amplify the wave, whereas intraseasonal easterly anomalies cause the waves to attenuate.

Figure 24a shows OLR anomalies (shading) with contours of 20-120 day bandpass filtered dynamic height from the Tropical Atmosphere Ocean (TAO) buoy array (dynamic height serves as a proxy for sea surface height). The 20-120 day filter band effectively isolates the signal of intraseasonal Kelvin waves. Heavy black lines drawn on positive dynamic height anomalies represent subjective estimates of the trajectories of downwelling Kelvin waves (so named because they push the thermocline down). Active convective anomalies associated with MJO events are labeled. Figure 24b shows 1000 hPa zonal wind anomalies from the NCEP/NCAR reanalysis shaded together with the same dynamic height anomalies plotted in Figure 24a. Consistent with previous results, Figure 24b suggests that positive height anomalies (contoured in red) associated with downwelling Kelvin waves are triggered by westerly wind anomalies that frequently occur within the local active convective phases of the MJO. These results suggest that active MJO convection and low-level westerly winds preceded the development of at least 4 downwelling Kelvin waves during the YOTC period thus far, including September 2008, and January, early April, and May 2009.

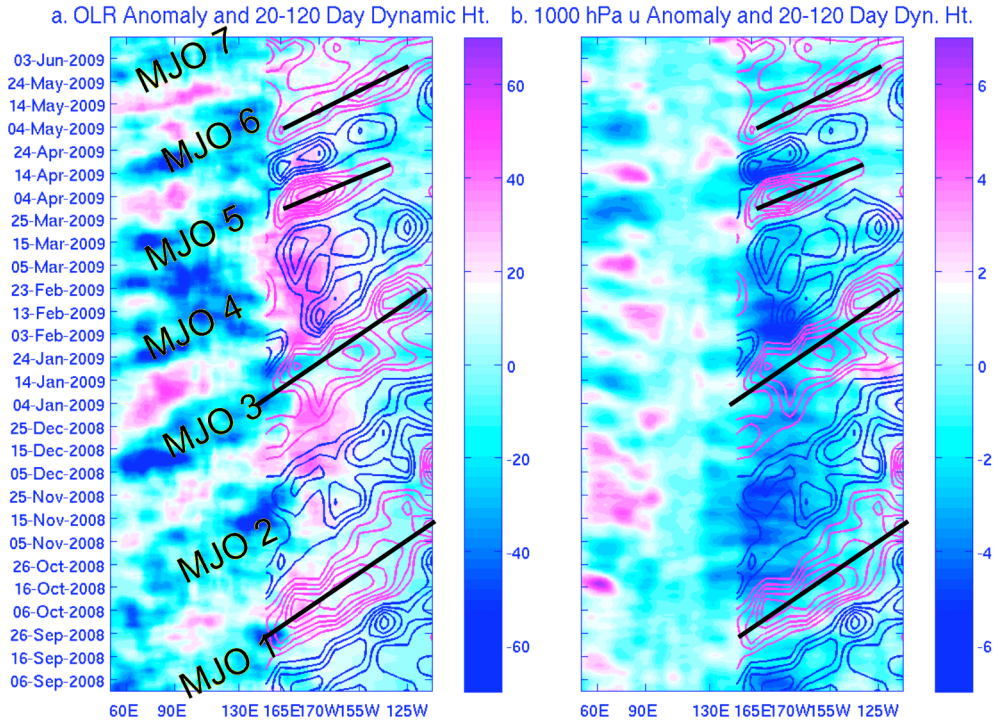


Figure 24. OLR anomalies averaged from 5°N to 5°S (shaded, Wm^{-2} , with active convection suggested in blue), and contours of TAO dynamic height (plotted each cm, with the zero contour omitted, and positive anomalies are red). MJO events discussed in the text are labeled. Heavy black lines approximate the trajectories of the downwelling Kelvin waves. b. Same as a., except that zonal wind anomalies (ms^{-1}) are shaded.

MJO events occurred more frequently over the YOTC period than Kelvin waves, apparently because some MJO events did not induce westerly wind anomalies over the western Pacific basin. Figure 24 suggests that MJO events 1, 3, 5, 6, and 7 induced downwelling Kelvin waves that propagated across most of the basin, whereas MJO events 2 and 4 did not. The Kelvin wave that was triggered in association with MJO 5 encountered intraseasonal easterly wind anomalies across the eastern basin that apparently caused the wave to attenuate (following the pattern that Roundy and Kravitz demonstrated tends to occur in association with intraseasonal events during adjustment toward La Niña conditions). Those Kelvin waves associated with MJO events 3 and 6 amplified over the eastern basin, presumably because they encountered intraseasonal westerly wind anomalies, following a pattern consistent with many similar events observed during adjustment away from La Niña. Gradual adjustment away from La Niña conditions is apparent in the weakening of the zonal wind anomalies beginning in early February, following the transit of the Kelvin wave induced by MJO 3. Mean zonal wind anomalies across the equatorial central Pacific were easterly prior to the Kelvin wave associated with MJO 6 and westerly following. The relevance of this MJO-Kelvin wave event to the adjustment in ENSO amplitude is unknown, and seasonal weakening of La Niña at the close of boreal winter is also consistent with the observed trends. Quick Scat winds suggest that the Kelvin wave associated with MJO 7 is

also evolving with zonal wind anomalies in a pattern consistent with adjustment away from La Niña (not shown).

References:

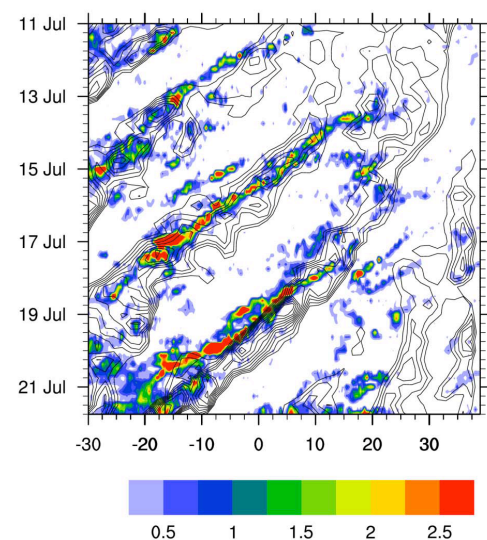
- Bergman, J. W., H. H. Hendon, and K. M. Weickman, 2001: Intraseasonal air-sea interactions at the onset of El Niño. *J. Climate*, **14**, 1702-1718.
- Eisenman, I., L. Yu, and E. Tziperman, 2005: Westerly wind bursts: ENSO's tail rather than the dog? *J. Climate*, **18**, 5224-5238.
- Hendon, H. H., B. Liebmann, and J. D. Glick, 1998: Oceanic Kelvin waves and the Madden-Julian Oscillation. *J. Atmos. Sci.*, **55**, 88-101.
- Kessler, W. S., and R. Kleeman, 2000: Rectification of the Madden-Julian Oscillation into the ENSO cycle. *J. Climate*, **13**, 3560-3575.
- Roundy, P. E., and G. N. Kiladis, 2006: Observed relationships between intraseasonal oceanic Kelvin waves and atmospheric forcing. *J. Climate*, **19**, 5253-5272.
- Roundy, P. E., and J. R. Kravitz, 2009: The association of the evolution of intraseasonal oscillations with ENSO phase. *J. Climate*, **22**, 381-395.
- Shinoda, T., P. E. Roundy, and G. N. Kiladis, 2008: Variability of intraseasonal Kelvin waves in the equatorial Pacific Ocean. *J. Phys. Oceanogr.*, **38**, 921-944.

3.6 African Easterly Waves

Following Berry and Thorncroft (2005) the typical African easterly wave (AEW) life-cycle can be described in terms of three phases: (i) Initiation, (ii) Baroclinic developments and (iii) West coast developments. Central to all three phases is the 2-way interactions between the synoptic scale AEW and convection especially the ubiquitous Mesoscale Convective Systems (MCSs). During the summer of 2008 there were a number of coherent AEWs that were also associated with distinctive convective patterns and MCSs and the most interesting periods are highlighted here. This summary also highlights several cases of East Atlantic tropical cyclogenesis that were clearly related to the passage of an AEW as well as some potentially interesting non-developing cases.

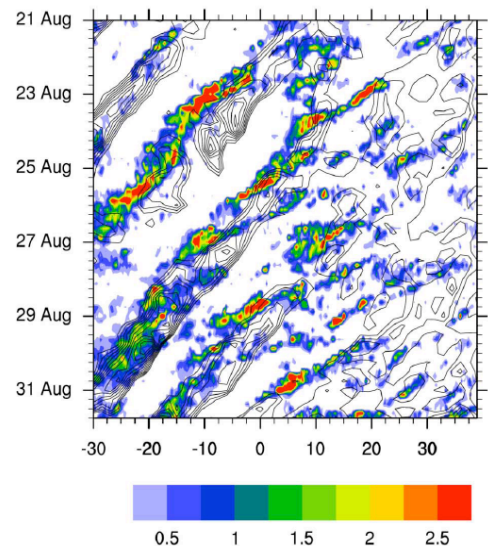
The nature of AEWs and their associated convective signature is illustrated here using curvature vorticity at 700hPa (contoured) based on ERA-Interim Reanalysis and TRMM rainfall (color shaded); both averaged between 5-15°N. A few waves are highlighted in the figures below for further study but many others may also be interesting.

Figure 25. Mid-July Waves. Two coherent AEWs characterized the West African region in mid-July. The most coherent of these originated around 30°E on the 14th (although the precise genesis location and time should be verified). What is striking about this AEW is the initiation of an MCS (or a number of MCSs) just east of the trough center around 15°E. This convective signal clearly moves through the wave and appears to “hug” the region just ahead of the trough after this (the climatological location). The AEW strengthens as it propagates westward. The growth mechanism should be explored taking account of the relative roles of diabatic and adiabatic processes as well as the 2-way interactions between the MCSs and the synoptic environment. This was one of the



strongest AEWs of the season and yet it did not develop into a tropical cyclone. The reasons for this should be explored.

Figure 26. End of August Waves. A very dramatic AEW started around the 23rd August close to about 10°E. This event was special in the sense that it was associated with multiple interactions with convection and associated MCSs. At least four convective streaks appear to have been initiated east of the trough, and subsequently passed through the trough and stalled ahead of the trough. This is possibly a very interesting case for studying scale interactions between the synoptic AEW and convection including propagating MCSs. This system also appears to have been associated with significant convection close to the West African coast. This system became named tropical cyclone Ike on September 1st and was likely strongly impacted by the events which took place over the continent. The wave to follow this, also characterized by significant interactions with convection subsequently became tropical cyclone Josephine close to West Africa on the 6th September.



Relevant Web Page(s):

http://www.atmos.albany.edu/student/janiga/weather_maps.htm

<http://moe.met.fsu.edu/cyclonephase/ecmwf/fcst/index.html>

<http://cimss.ssec.wisc.edu/tropic2>

Reference:

Berry, G., and Thorncroft, C. 2005: Case study of an intense African easterly wave. *Mon. Wea. Rev.*, 133, 752-766.

3.6.1 Western North Pacific

The potential high-impact weather impacts of a tropical cyclone make it one of the primary synoptic-scale foci in YOTC. As described in section 3.8.1.1 below, the combined Tropical Cyclone Structure (TCS-08) and THORPEX Pacific Asian Regional Campaign (T-PARC) field phase during 1 August – 4 October 2008 collected special observations and operational and experimental model fields related to western North Pacific tropical cyclone formation, structure change, motion, extratropical transition, and downstream impacts. These special observations and model analyses and forecast provide an unique opportunity to study the role of convective processes in this ocean basin that has the largest number of tropical cyclones.

Tropical cyclone formation involves circulations and physical processes on space scales from the global (as in the MJO) to the turbulence scale (as in the atmospheric and oceanic boundary layer fluxes that ultimately provide the heat and moisture for the tropical cyclone). It is the tropical convective processes that distinguish the tropical cyclone structure and energetics from the extratropical cyclone. Even the large-scale environmental flow that is the primary determinant in the motion of a tropical cyclone is

determined by the horizontal and vertical distributions of the tropical convection. Indeed, a major contribution to the remarkable improvement in tropical cyclone track prediction has been the use of consensus of multiple skillful global models in which tropical convective processes are better analyzed and forecast.

The tropical cyclone activity during the TCS-08/T-PARC field phase period was much affected by interannual (specifically La Niña), intraseasonal (specifically MJO), and convectively-coupled equatorial waves (CCEWs). The 2008 typhoon season was the third consecutive below-average seasonal activity (and this trend has continued through 1 July 2009). Whereas a persistent La Niña is generally attributed as the cause, a preliminary study suggests that a change in phase of the Pacific Decadal Oscillation may also be a contributing factor. The MJO convective phase did not propagate into the western North Pacific during the combined TCS-08/T-PARC field phase. The normal monsoon trough was also absent during the field phase, so that the modulation of tropical cyclone activity by the 10-20 day monsoon trough oscillation was missing.

Instead, the western North Pacific was under a reverse-oriented monsoon trough regime in which trade easterlies penetrated to the Philippines during most of the period. Vigorous midlatitude troughs were present during the field phase and interacted strongly with the convection in the reverse-oriented monsoon trough. Whereas CCEWs with diurnally-modulated convective activity persisted in the 0°N - 10°N band throughout the combined TCS-8/T-PARC field phase, they had no contribution to the tropical cyclone activity. A complete understanding of tropical cyclone formation and overall activity must include knowledge of why the CCEWs do not contribute in some years. If current predictions that an El Niño will develop during 2009 come true, the latter YOTC period through October 2009 will provide an excellent opportunity to study contrasting large-scale environmental conditions in the western North Pacific. *This aspect of tropical-midlatitude interaction can be studied with the YOTC observation/ model data sets because it led to baroclinic "tropical transition" type formations (and non-formations) that were poorly predicted.*

The showcase tropical cyclone during the combined TCS-08/T-PARC period was Typhoon Sinlaku. A total of 28 aircraft missions totaling more than 500 h were flown, including eight tropical cyclone structure missions in which the Naval Research Lab P-3 with the ELDORA radar, the U. S. Air Force Reserve C-130 with Stepped Frequency Microwave Radiometer, and the Taiwan DOTSTAR participated. On one of these days, the German DLR Falcon also participated, although this was considered to be a targeting flight. A total of six Falcon missions for targeted observations were made to improve tropical cyclone track forecasts. Finally, 14 missions were flown by the P-3, C-130, and Falcon to study the extratropical transition of Sinlaku from a tropical cyclone to an extratropical cyclone.

One topic of keen interest to many modeling groups is the capability to predict the interaction of Sinlaku with the Taiwan Central Mountain Range. Many theoretical studies have been done of this interaction, but the TCS-08/T-PARC observations when Sinlaku was upstream of Taiwan will provide excellent initial conditions for future modeling studies. A second topic of interest is the re-formation of Sinlaku at relatively high latitudes after its structure had been drastically modified while over northern Taiwan. Finally, the TCS-08/T-PARC observations provide a unique opportunity to study the extratropical transition stage over the western North Pacific. Whereas some forecast models indicate Sinlaku

contributed to significant downstream impacts, the analyses do not support such a contribution. At least the in situ TCS-08/T-PARC observations in Sinlaku will provide information on the tropical cyclone structure contribution to the downstream impacts of the extratropical transition. This will contribute to a YOTC goal of understanding tropical-midlatitude interaction.

Although fewer aircraft missions during the formation stage were acquired than anticipated, the ELDORA observations of cloud characteristics in the western North Pacific during the combined TCS-08/T-PARC field experiment may be a unique data set for YOTC studies. That is, high-quality radar sets were obtained in cloud clusters, developing tropical cyclones, and in two tropical cyclones undergoing extratropical transition. These observations in conjunction with hourly satellite atmospheric motion vectors provide insights into western North Pacific convection and its impact on the environment.

3.7 Regions of Diurnal Cycle Focus

3.7.1 Overview

The global distribution of annual rainfall in the tropics, derived from ten years of the Tropical Rainfall Measuring Mission (TRMM) 3B42 merged satellite product at $0.25^\circ \times 0.25^\circ$ resolution, is shown in Figure 27. The regions of greatest rainfall – the intertropical convergence zone (ITCZ), the maritime continent, and the monsoon regions – are known to exhibit strong diurnal cycles.

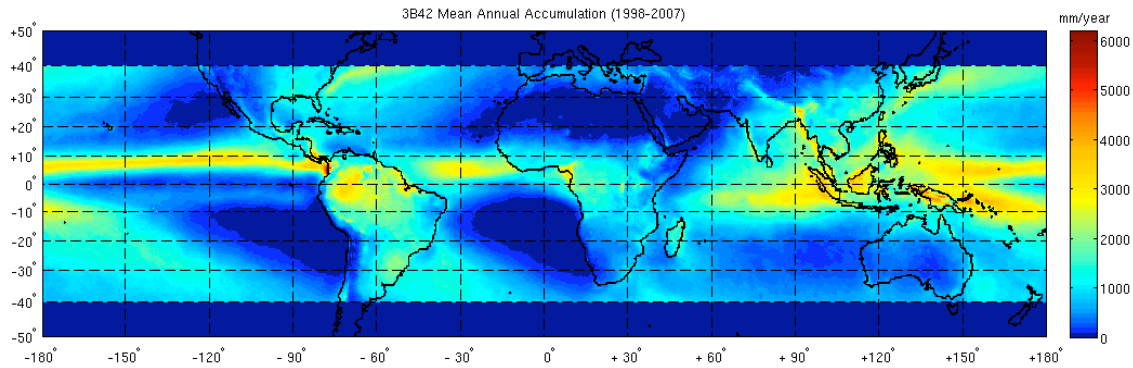


Figure 27. Ten-year (1998-2007) TRMM 3B42 annual precipitation climatology.

To illustrate the diurnal cycle of precipitation using the TRMM 3B42 data set, a simple procedure is adopted, namely, to produce analyses of afternoon/evening (1200 to 2300 LT average) minus morning (0000 to 1100 LT average) rainfall normalized by the mean annual rainfall at each location (). The amplitude of the diurnal variability is largest over the regions of the maritime continent, the Asian monsoon, the North and South American monsoons, and portions of the African monsoon. The signal is very large near coastlines, where there is typically a maximum in precipitation over the land during the afternoon and evening, and a maximum just offshore during the morning.

The analysis in Figure 28 clearly shows the general preference for afternoon/evening rainfall over the all of the land areas and morning rainfall over the ocean. However, there are important exceptions to this rule, namely, certain land areas have a morning maximum of rainfall (e.g., areas downstream of the Rocky Mountains, Andes, and Tibetan Plateau; the coastal interior of Brazil; areas south and north of the Tibetan Plateau; and the interior of Borneo), while certain ocean areas have an afternoon/evening maximum (e.g., the SPCZ, the South Atlantic Convergence Zone, areas of the west coasts of the equatorial Americas and Africa, and enclosed ocean basins of the Americas and the Asian monsoon). Some of these exceptions are associated with propagating signals of convection, e.g., eastward propagation of convection from the Rocky Mountains, Andes, and Tibetan Plateau and southward propagation of convection over the Bay of Bengal and South China Sea.

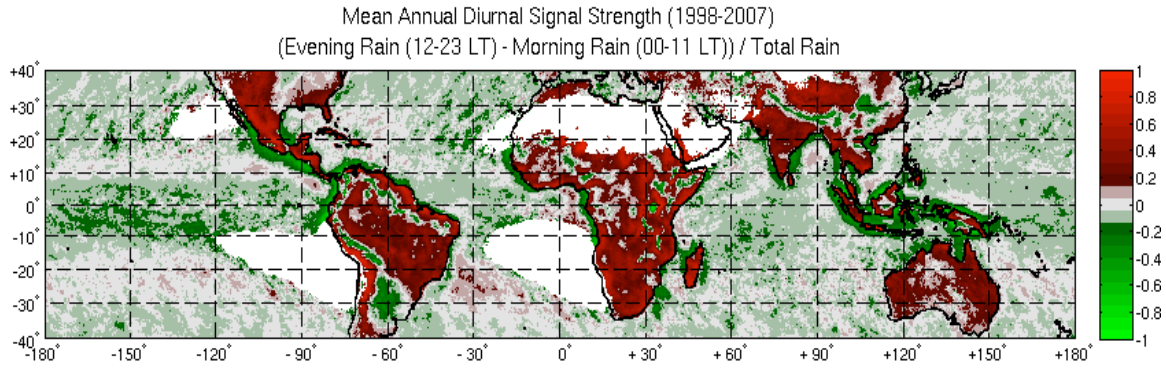


Figure 28. Evening (1200-2300 LT) minus morning (0000-1000 LT) rainfall normalized by annual mean rainfall from ten years (1998-2007) of TRMM 3B42 data. White regions denote areas having less than 100 mm rain per year.

To better view the global patterns of propagation, a plot of the time of maximum rainfall has been prepared (Figure 29). Once again, it can be seen that in general, rainfall maxima occur over land during the afternoon/evening and over the ocean during the morning hours. Over land, prominent signals of eastward propagation of convection can be seen downstream of the Rocky Mountains, the Andes, and the Tibetan Plateau from the afternoon and evening to the early morning hours. Also, inland propagation of precipitation can be seen along the northeast coast of Brazil. Also evident from this global map are signals of propagation westward from the coast of central America, equatorial Africa, and Sumatra; and northward from Papua New Guinea, with convection initiating near the coastline in the morning and moving seaward in the afternoon. Squall lines over West Africa propagate westward over great distances in association with African easterly waves; however, a persistent phasing with the diurnal cycle cannot be seen until the convective systems emerge from the west coast of Africa.

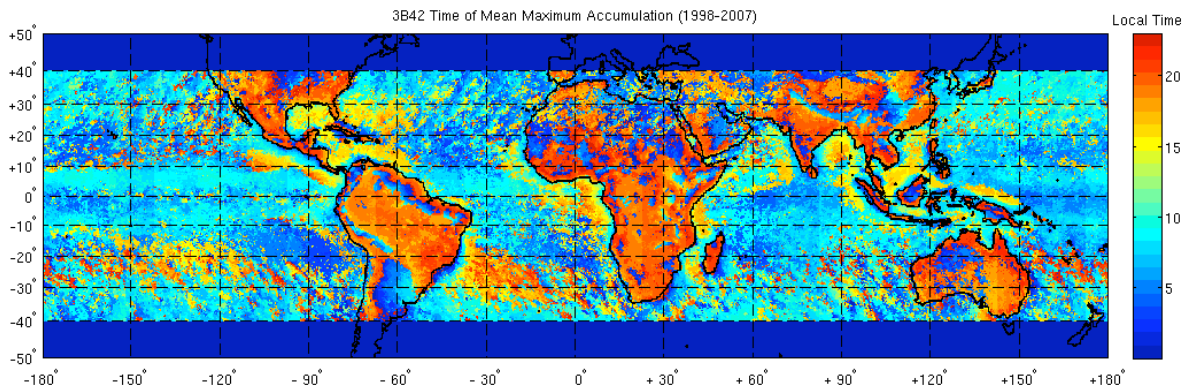


Figure 29. Time of maximum rainfall (LT) for ten years (1998-2007) using TRMM 3B42 data.

3.8 Indian Summer Monsoon Evolution and Components

3.8.1 2008

Northward progression of the Indian summer monsoon, after onset over Kerala (MOK) is associated with the northward propagation of a Boreal summer intraseasonal oscillation (BISO) event (Goswami, 2005). An interesting feature of the 2008 summer monsoon season was the very rapid progression of the monsoon after MOK. While it normally takes more than a month for monsoon to progress from southern tip of India to New Delhi, it took less than 15 days during 2008. This is associated with rather unusually rapid northward propagation of the BISO event associated with the onset (Figure 30a). The MOK during 2008 was on 28 May and the first episode of BISO reached 25N by 15 June with a northward phase speed of approximately 2° lat/day. This is nearly twice as fast as the average speed of northward propagation ($\sim 1^{\circ}$ lat/day). The second episode of BISO starting at 5S on 16th July and reaching 25N on 16th July indeed has the average northward propagating speed. The third northward propagating episode starts at 5N only on 10th Sept. and propagates rather fast. Prior to that, there was a southward propagating event starting at 5N on 23rd Aug. and reaching 10S on 1st Sept.

As the date of establishment of Indian monsoon over northern India has important implications in starting various agricultural practices, it is important to understand the cause of the unusual fast northward propagation of the first episode of BISO during 2008 YOTC period. It may be noted from Figure 19 that the first northward propagating episode is associated with a moderate eastward propagating MJO episode along the equator. Also it may be noted that the second slow northward propagating episode starting 16th July was associated with a rather fast eastward propagating weak MJO episode (Figure 19). What is the link between the eastward propagating MJO and northward propagating BISO?

The heating associated with stratiform rain seems to play an important role in the northward propagation of the BISO (Chattopadhyay et al, 2009). 20-90 day filtered stratiform and convective rain anomalies composited for different phases of the BISO from TRMM product 3G68 indeed shows that the stratiform contributes much more than the convective rain to the total rain anomaly during the first episode (Figure 30b). What was the role of the stratiform rain in making the northward propagation of the first episode fast?

Also during the first episode and during the third episode (10-25 Sept), the easterly vertical shear was stronger than normal helping the northward propagation (Figure 30c). What was the role of convective/stratiform organization on generating and maintaining the easterly shear over the south Asian monsoon region?

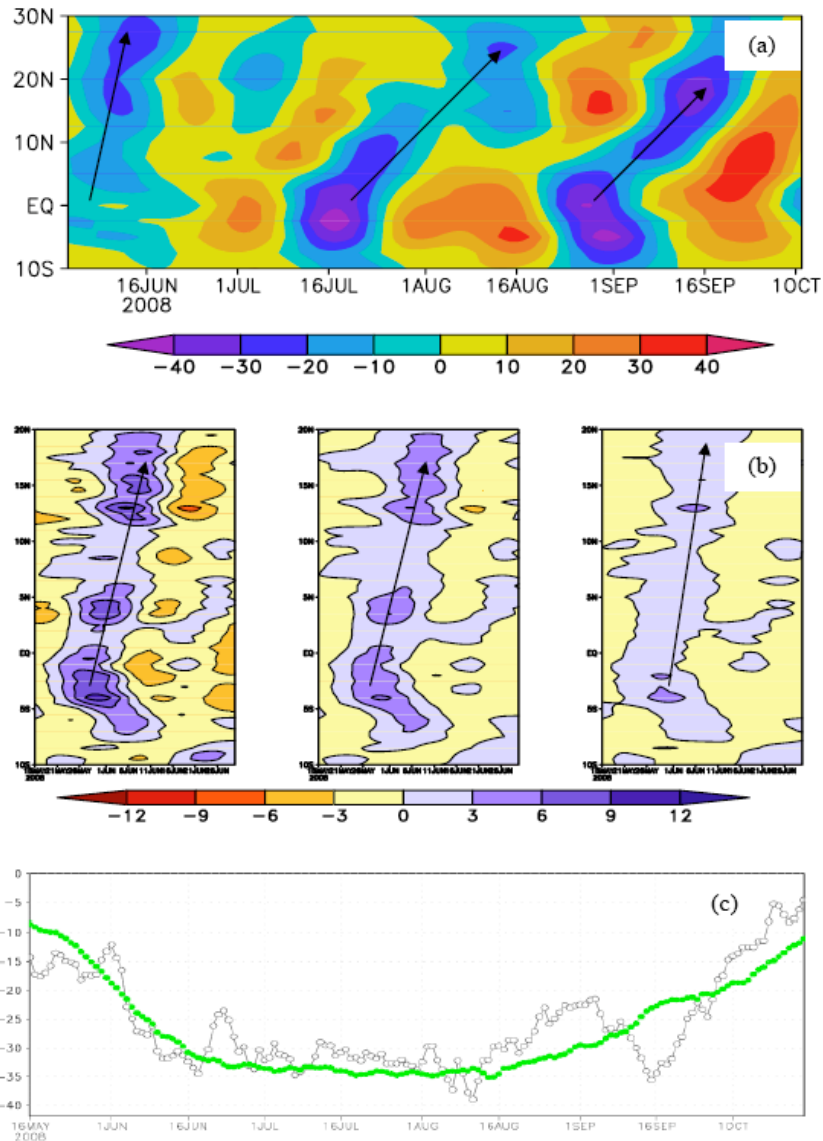


Figure 30. (a) Latitude-time section of 20 to 90 day filtered OLR anomalies averaged over the region 70-90E (b) Latitude-time section of 20 to 90 day filtered total (left panel), stratiform (middle panel) and convective (right panel) TRMM rainfall anomalies (c) Vertical easterly shear (200 hPa minus 850 hPa) averaged over 50-100E; 5-15N.

References:

Goswami B. N., 2005, South Asian Monsoon, in Intraseasonal Variability in the Atmosphere-Ocean Climate System, Lau K. M. and Waliser Duane (Eds). Praxis Publishes, Chichster, UK, pp 19-62

Chattopadhyay Rajib, B N Goswami, Atul Sahai, and Klaus Fraedrich, 2009, The Role of Stratiform Rainfall in modifying the northward propagation of Monsoon Intraseasonal Oscillation, J. Geophys. Res. (to appear)

3.8.2 2009

Placeholder – taken from an email from:

Dr. D. R. Pattanaik

Meteorologist-I

O/o Director General of Meteorology

India Meteorological Department

Mausam Bhawan, Lodhi Road

New Delhi - 110003

India

The June rainfall over India during 2009 is very unusual as similar deficit in June has occurred only long time back in 1926. One of the feature that is directly responsible for deficit June during 2009 is that the southwest monsoon although arrived over southern tip of India few days early, there was complete stagnation in progress of monsoon northward from the south Peninsula (around the latitude 15 N) during the period from **8th June to 20th June**.

The monsoon only started slowly progressing northward after 21st. Thus, for 13 days the features must be very adverse for the monsoon progress.

As suggested by Dr. Ding, Prof Wang and others there was the influence of mid latitude westerly over the Indian region. Looking at the wind and temperature anomalies at middle and upper troposphere during this stagnation period from 8-20 June (please see the attachment) it is seen that large cold cyclonic circulation anomalies was prevailing over NW India, which was responsible for the stagnation of monsoon for a quite long time.

Similar stagnation of monsoon progress associated with the influence of mid latitude westerly has also been noticed in some other years (like 2005) (Reference; DR Pattanaik & H.R. Hatwar Analysis and Impact of Delayed Onset of Monsoon Over Northeast India During 2005 : Jan-Jun, 2006, 3-9.

With regards,

DR Pattanaik

3.9 Tropical-Extratropical Interactions

Synoptic events related to the Madden-Julian oscillation (MJO) and the global wind oscillation (GWO; Weickmann and Berry, 2009) during the YOTC period are described. The events generally involved important forecast challenges on a variety of time scales based on monitoring and predicting the weather-climate state in real time during YOTC. Interestingly, subseasonal events that in real time seemed significant for the prediction can in hindsight be lost in subseasonal noise.

3.9.1 The MAY 2008 MJO

The MJO activity weakened after 2007-08 winter but a significant event still occurred during the start of YOTC in May 2008, and contributed to the severe weather over the US Great Plains and major flooding along the upper Mississippi Valley during May-June 2008; e.g., Cedar River,

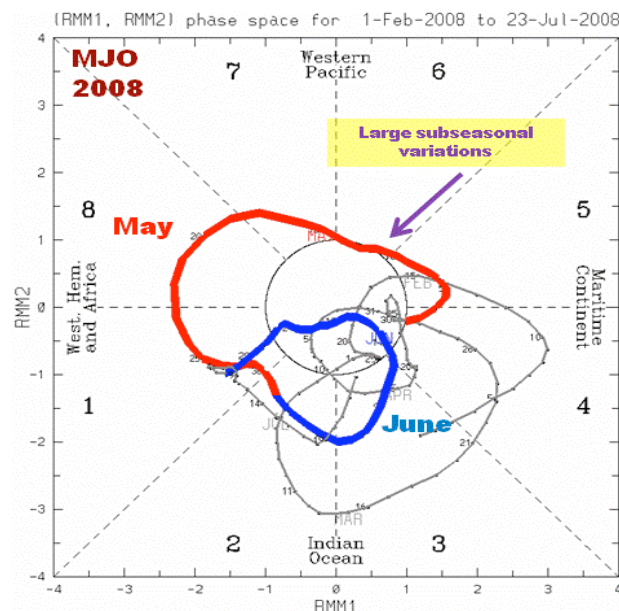


Figure 31. The WH-phase space with EOFs projected on total anomalies of wind and OLR. The persistent La Nina convection anomalies (> 1 sigma projection) during Feb-April 2008 are disrupted by the May (red line) and June 2008 (blue line) MJO.

Cedar Rapids, Iowa. The MJO in question has already been mentioned in connection with an interacting Kelvin wave in Section 3.3. Here, the link between the MJO and severe weather outbreaks over the Great Plains is described.

The May MJO (red line in Figure 31) has a strong projection in phases 7-8-1 of the WH-phase space, a region associated with a well known synoptic evolution that operational forecast models still cannot simulate properly. A further, related contribution by the large-scale circulation is seen in where La Nina conditions with weak subtropical flow and low AAM for much of the preceding winter become close to normal in May and June 2008. Global relative AAM anomalies increase by > 1 sigma, mostly from stronger tropical westerly flow.

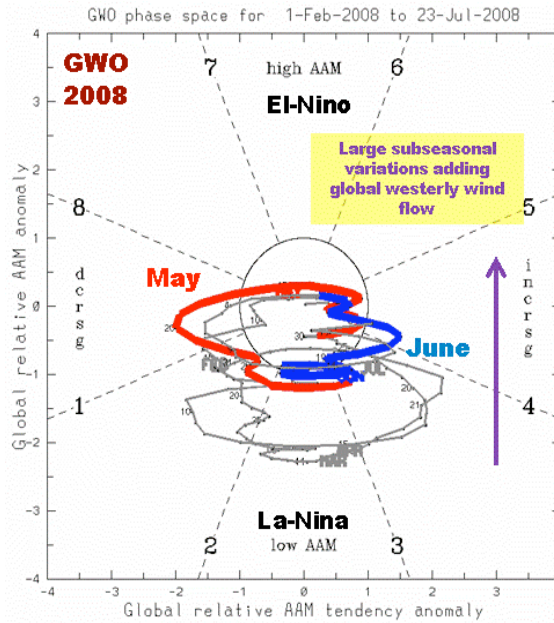


Figure 32. A phase space representation of global relative AAM anomaly (ordinate) and its time tendency (abscissa) for the same time period as **Figure 31**. May and June 2008 are highlighted as in **Figure 31**. See Weickmann and Berry (2009).

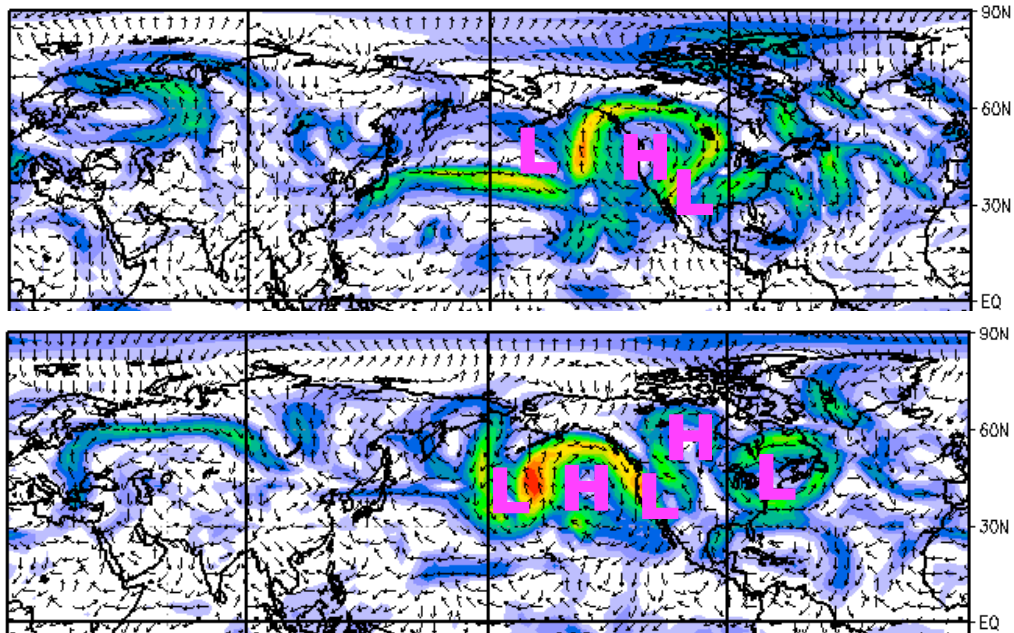


Figure 33. Daily mean vector wind anomaly at 250 mb for 16 May 2008 (top) and 22 May 2008 (bottom). The arrows show direction only while the contours are the vector magnitude.

An illustration of the synoptic sequence during MJO phases 7-8-1 is shown in Figure 33. Simply put, a strong jet and west coast ridge on 16 May (top panel) is replaced by a weaker jet and a southwest US trough by 22 May. Arguably, the mid-latitude anomaly pattern retrogrades as tropical convection with the MJO comes back into the eastern hemisphere

through Africa by 22 May (see Figure 31). Numerical model guidance failed to predict at week 2 the deep trough that developed in the southwest USA.

3.9.2 Boreal fall intraseasonals: The return of La Nina

The September MJO was the last disturbance to produce a weak positive convective signal just west of the dateline before strong suppression developed there during and after October 2008. The October MJO started with a strong convective flare-up over the Indian Ocean around 15 October 2008. It progressed east but was truncated in its eastward move to the west Pacific as convection redeveloped back over the Indian Ocean only 30 days later. A large orbit in the GWO was observed that contributed to a well-defined poleward movement of zonal mean easterly and westerly wind anomalies during October. A distinct series of “jumps” northward of anomalies is observed and linked to three wave-breaking events that “broke” at successively higher latitudes.

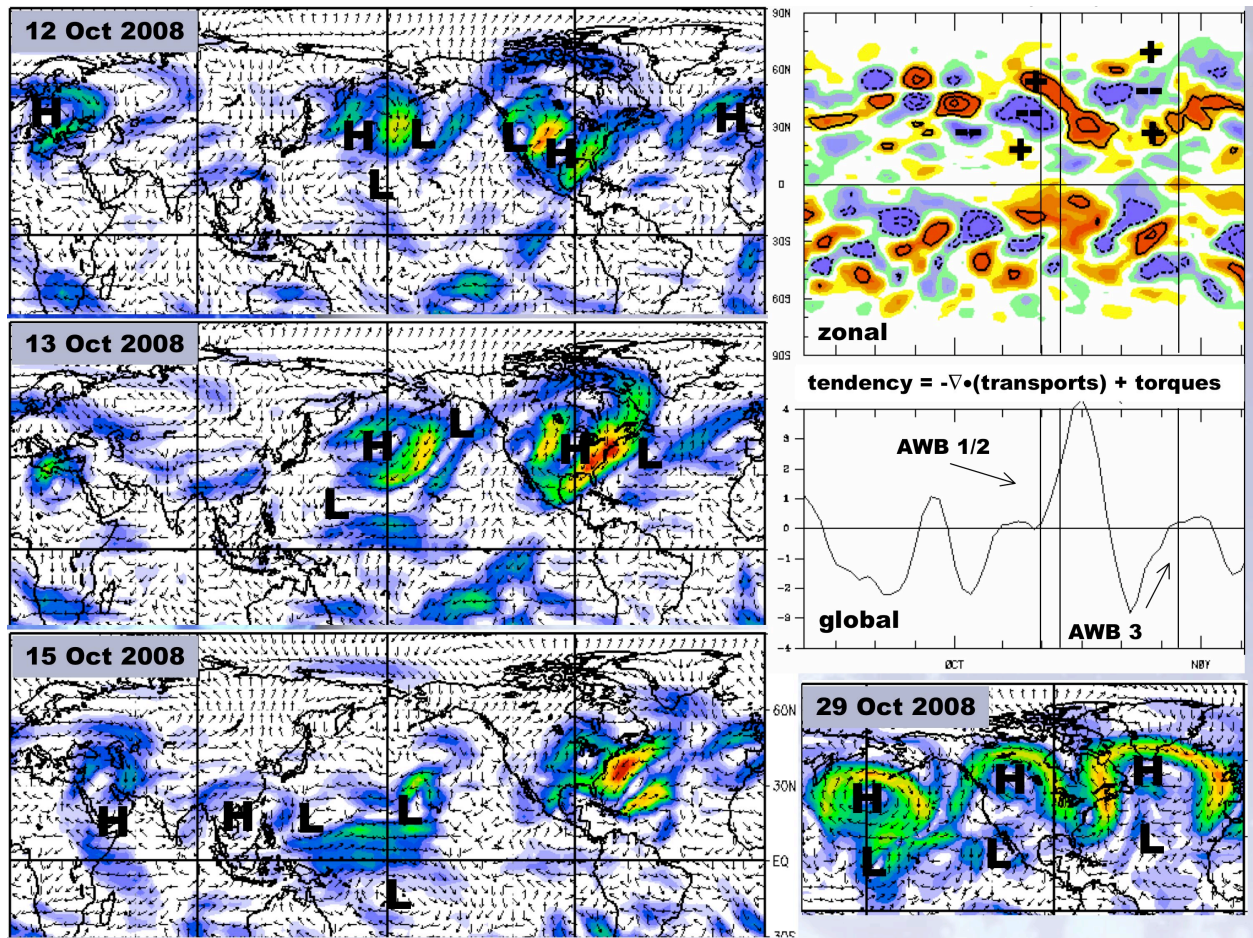


Figure 34. Daily plots of the anomaly wind field at 250 mb during the poleward movement of zonal mean zonal AAM anomalies during October 2008. The left column shows selected daily maps that imply the strong poleward transport of momentum across 35N. The tendency of zonal AAM during October is shown at the top right, the global tendency in the middle time series (only torques can contribute). The first two lines on the time series plot bracket the left column maps while the third line is for 29 October 08 (last map, right column) when the zonal westerly flow anomalies reached farthest poleward.

Zonal mean wave breaking signatures appeared around 20 September 2008 as synoptic activity returned to the 30-60N band. As an example, Figure 34 shows aspects of the poleward transport of momentum across 35N during the middle of October. The transport was concentrated in two sequential baroclinic wave packets (BWP) that developed over the west Pacific Ocean region and propagated energy eastward across North America. Figure 34 (left, middle) for 13 October 2008 shows both BWPs simultaneously and the tilt of the eddies leaves little doubt that momentum is being transported northward across ~35N. The zonal AAM budget provides useful clues about the importance of different physical processes that together produce the observed global and zonal AAM tendency.

3.9.3 Initiation of the DJFM 2008-09 MJO activity

The 2008-09 winter was characterized by weak MJO activity especially in comparison to the previous 2007-08 season. The dominant interannual climate state was again La Nina, continuing an atmosphere-initiated trend that started in the middle of the 2006-07 El Nino. After weakening in the Northern Hemisphere during summer 2008, well-defined asymmetric circulation anomalies characteristic of La Nina re-developed by October 2008 and tropical Pacific SSTs cooled in early December 2008. Despite the weak MJO season, two cases of interest occurred whose diagnosis could further understanding of the initiation of the MJO.

Figure 35 and Figure 36 below show some preliminary analysis of the MJOs, one that developed in late December 2008 and the other in mid-March 2009. Figure 35 quantifies their evolution in the Wheeler and Hendon (2004; hereafter WH04) phase space, where, in contrast to WH04, the EOFs are projected onto the total anomalies of OLR and wind. Both MJOs start around the Maritime Continent region as a fast smaller loop before settling into an anticlockwise second bigger loop at the MJO time scale. The April MJO has about twice the amplitude of the first. It is proposed the early loops represent a disruption of the dominant La Nina base state by baroclinic wave packets from mid-high latitudes. These disturbances move into and interact with persistent La Nina

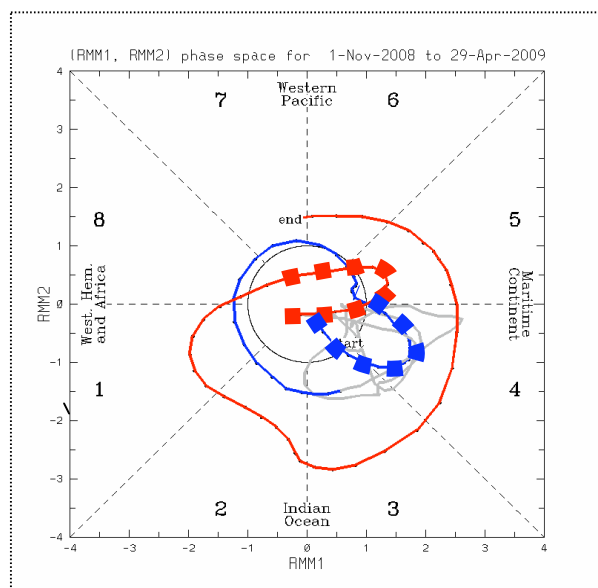


Figure 35: The MJO phase space is highlighted to show the initiation and subsequent propagation of two MJOs. The blue line starts on 19 Dec, goes through a small unclosed loop until 3-4 Jan 2009 (blue squares) and then follows a more conventional MJO trajectory until ~ 6 Feb 2009. The red line tracks the second MJO; it starts ~12 March, shows another unclosed loop to 25 March (red squares) and then a large MJO trajectory signal to the end of the record on 29 April 2009.

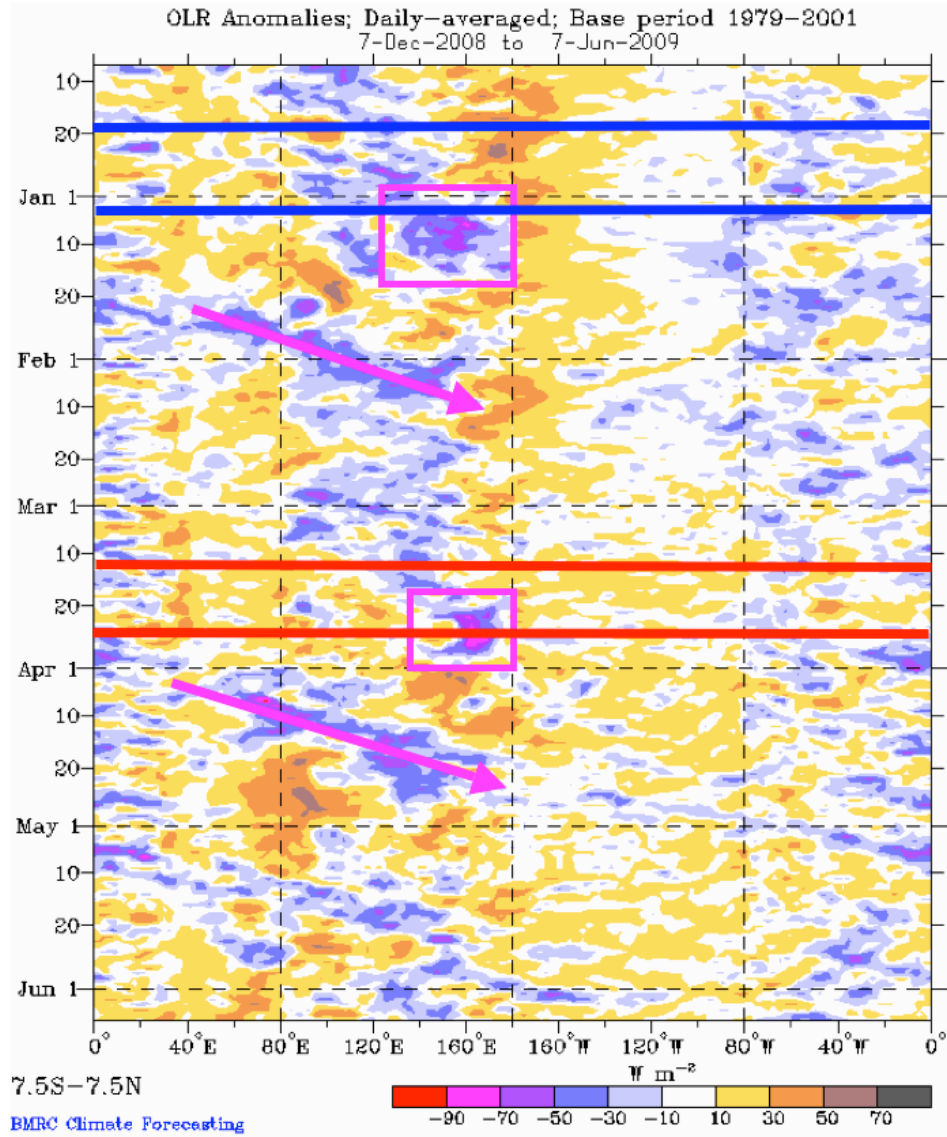


Figure 36. Hovmoller of OLR anomalies along the equator with boxes cut out from a similar Hovmoller south of equator superimposed. The arrows represent the propagating MJOs initiated by an apparent La Nina-orchestrated tropical-extratropical interaction. The heavy blue and red lines correspond approximately to the small, unclosed loops described and shown in **Figure 31**.

convective activity between 80-140E, which helps move the dominant convection eventually eastward. This initiates the MJOs. The movements are seen in Figure 36 as an eastward shift of convection anomalies to $\sim 10\text{S}$, 160E (see boxes Figure 36), which are preceded by a month of persistent 80-140E convection anomalies, with embedded fast events. The initiation is followed by a fast well-defined MJO-Kelvin wave that propagates back into the Indian Ocean in late January and early-mid April 2009. The Indian Ocean convective initiation is linked with the propagation of the MJO and does not develop out of a persistent background anomaly pattern. One hypothesis says the initiation was forced by direct interaction and feedback between the background or base state convection and circulation, and the baroclinic wave packets moving into and through the tropics from mid-latitudes. The latter produced large signals in the zonal mean zonal wind through their northward momentum transports.

Figure 37 shows the MJO initiations also aligned with maxima in anomalous, zonal mean cyclonic vorticity between the equator and 30N. The zonal mean westerlies around the equator signify a stronger Walker Circulation (see also Figure 38), which then weakens as the MJO is initiated and anomalous convection shifts from the Maritime Continent to the southern tropical west Pacific Ocean (see boxes in Figure 36). After initiation, the large deceleration of easterly flow around 30N signifies a weakening of the La Nina base state flow as the MJO goes through its life cycle. Both the periods centered on the vertical lines in Figure 37 are favorable for the dispersion of

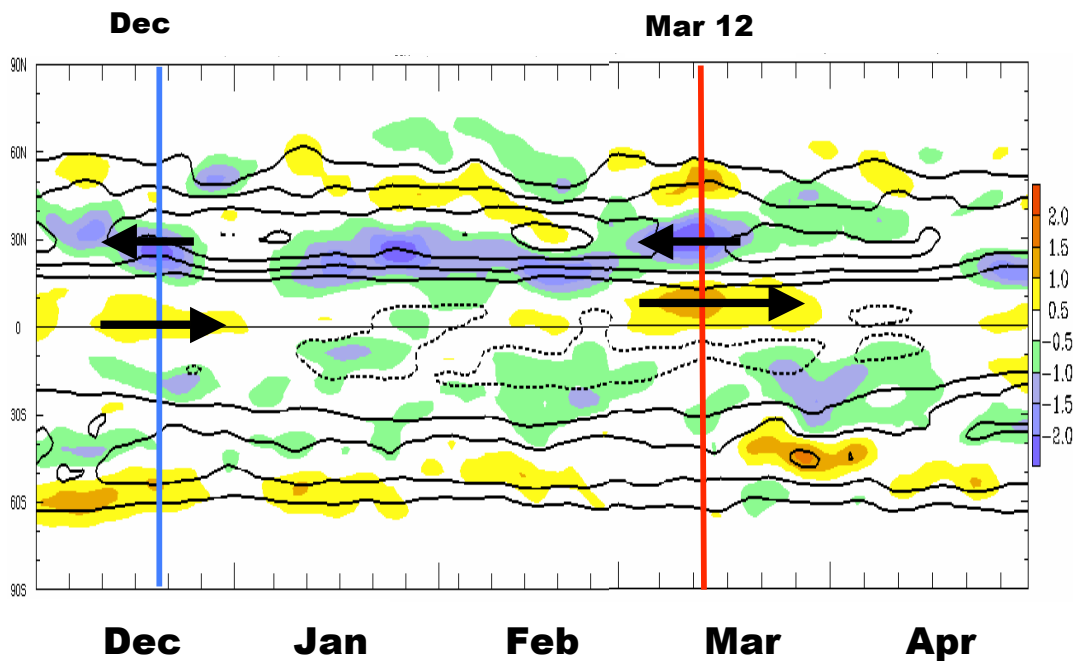


Figure 37. The zonal mean atmospheric angular momentum (AAM) with a 5-day running mean applied. The black arrows show anomalous zonal mean zonal winds that imply cyclonic shear in the northern hemisphere subtropics. The blue and red lines denote the initiation time of the two MJOs described in the text.

stationary wave energy into the tropics. The following weekly averages of the wind at 150 hPa reveal the synoptic structure, basically a residual of 2-3 fast synoptic events.

Figure 38 confirms earlier statements that the twin cyclones over the Pacific were well defined prior to MJO initiation. However, the upstream anticyclones are less extensive and have embedded wavetrains that propagate into and along the tropical eastern hemisphere. A slow downstream energy dispersion across North America from the La Nina North Pacific anticyclone is also clearly evident. These are the week before the MJO initiation as defined using Hovmollers (Figure 36) and phase diagrams (Figure 35).

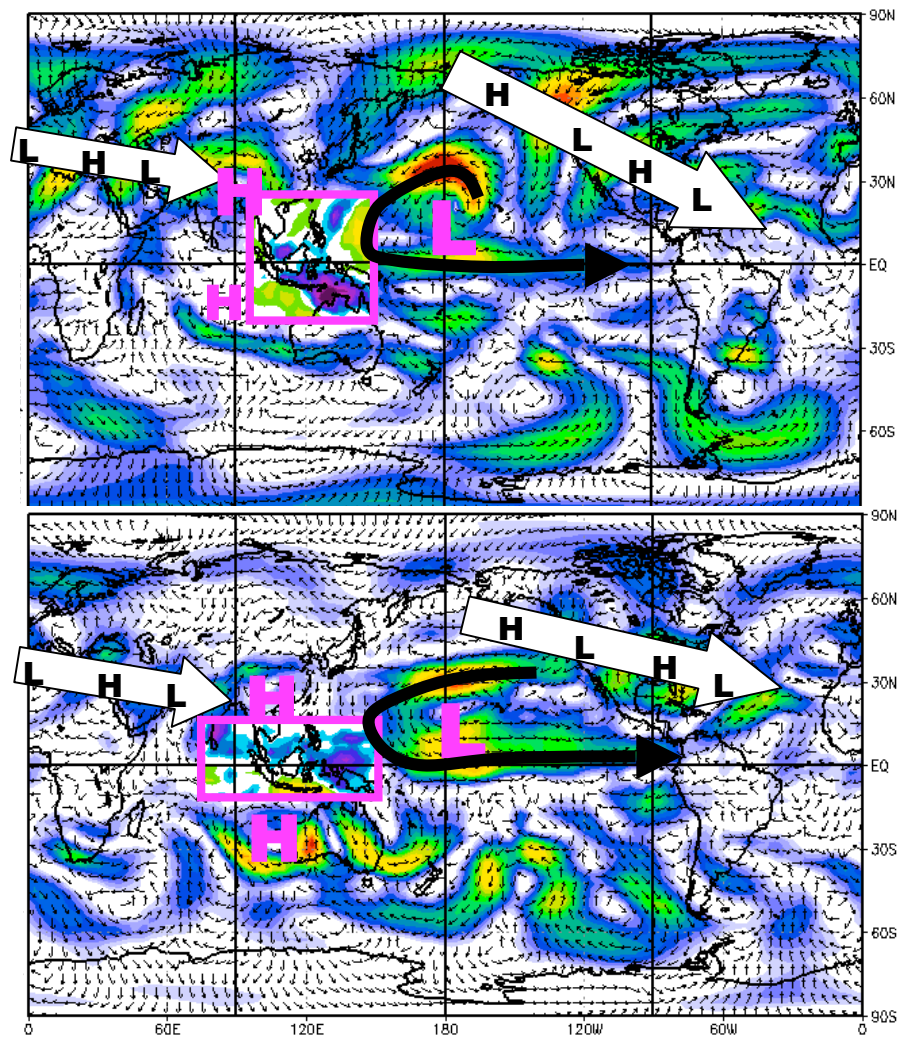


Figure 38. The 150hPa vector wind anomaly showing direction (arrows) and magnitude (color shading: red => 30 m/s; green +. 20 m/s) for the weekly averages just preceding the initiation of the MJOs top: 14-20 Dec 2008; bottom: 6-12 Mar 2009. A “cutout” of the weekly mean OLR anomalies for the same periods have been superimposed over the Maritime Continent region.

3.9.4 Trend toward a warming equatorial Pacific: MAM 2009

Very slow changes of tropical convection and circulation anomalies associated with the ENSO cycle are also occurring during YOTC. Figure 39 suggests a coherent eastward movement of convection from the Indian Ocean in boreal summer 2008 to the west Pacific in boreal spring 2009. The period depicts a slow return eastward of tropical convection following the moderate-large anomalies of the 2007-08 La Nina. A similar signal can be seen in Figure 40 where the WH index is projected on the total OLR and wind anomalies. The Figure 40 trajectories have been color coded as noted in the caption. A pattern can be discerned where, after the May 2008 MJO (red line), the index shows a slow, systematic eastward movement of convective activity that reaches the west Pacific sector at the end of the period. The movement can be visualized by following the centroids of the JJA blue lines (primarily phases 1-3), the SON green lines (primarily phases 3-4), the DJF grey lines (primarily phase 4) and the MAM black lines (primarily in phase 6-7).

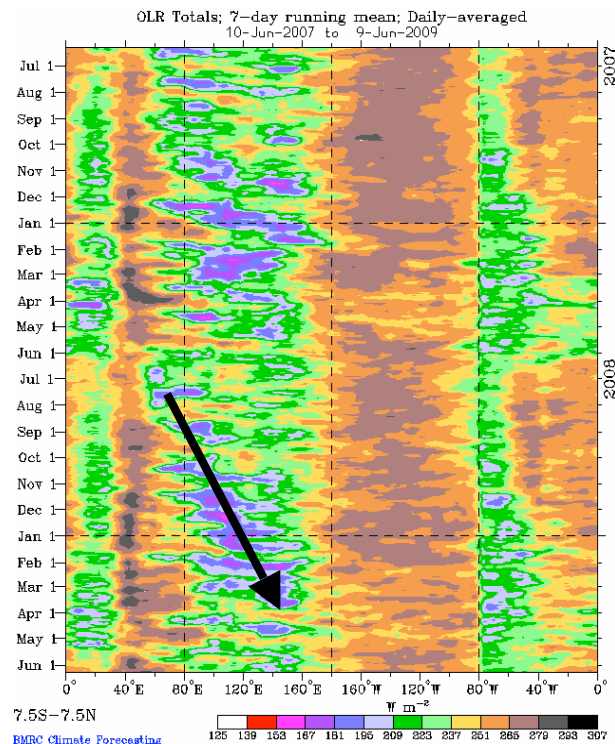


Figure 39. OLR for the last two years averaged along the equator. The arrow illustrates an eastward movement, which can be considered an amplification of the typical movement of convection eastward and into the southern hemisphere during this time.

The movement of convection, which is known to have a seasonal component that also moves from west to east, eventually leads to a rapid weakening of the La Nina signal. This occurs when the seasonal weakening of the zonal mean jet in early March coincides with the presence of persistent tropical convection over the west Pacific Ocean. **Figure 41** shows a comparison of the DJF and MAM 2009 seasonal mean 250 hPa wind field. For the 2008-09 winter, twin anomalous troughs are particularly strong over the Pacific Ocean basin and AAM is low due to strong easterlies in the upper levels of the mid-latitude Pacific and

equatorial Atlantic Oceans. OLR anomalies over the Indo-Pacific are well defined with a prominent NW-SE tilt across the Maritime Continent.

By MAM 2009, 250 hPa wind anomalies have weakened dramatically and shifted westward over the Northern Hemisphere (NH) and perhaps eastward over the Southern Hemisphere. These wavetrains have developed over the Pacific Ocean to North and South America as part of the breakup of the large anomalies seen in DJF 2009. In the NH, the retrogression leads to a trough over central Canada.

Simultaneously, zonal mean westerly flow anomalies moved from the equator to near 15N. Apparently, disturbances in the westerlies penetrated farther south partially in response to the stronger westerly flow at 15N. This change in the large-scale circulation pattern contributed to significant precipitation events across regions of the southern USA that had been experiencing drought. The OLR anomalies for the MAM season weakened considerably over Australia and now extend in a zonal band north of the equator from India to the west Pacific Ocean.

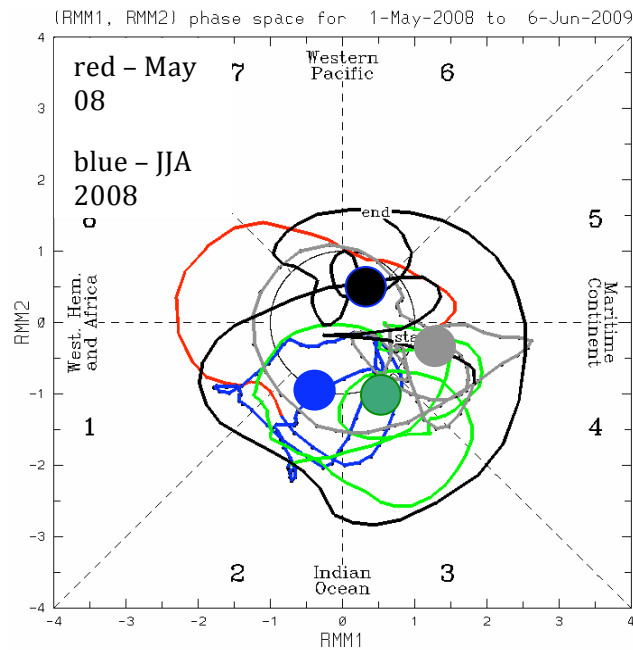


Figure 40. The WH phase plot for the YOTC period (May 1, 2008 to 10 June 2009 [present]) is shown. The seasons are color coded so that blue is the trajectory for JJA 2008, green is for SON 2008, gray is for DJF 2009 and black is MAM 2009. A 5-day running average has been applied to the daily values of the indices. The large dots approximate the center of each season from boreal summer 2008 to boreal spring 2009.

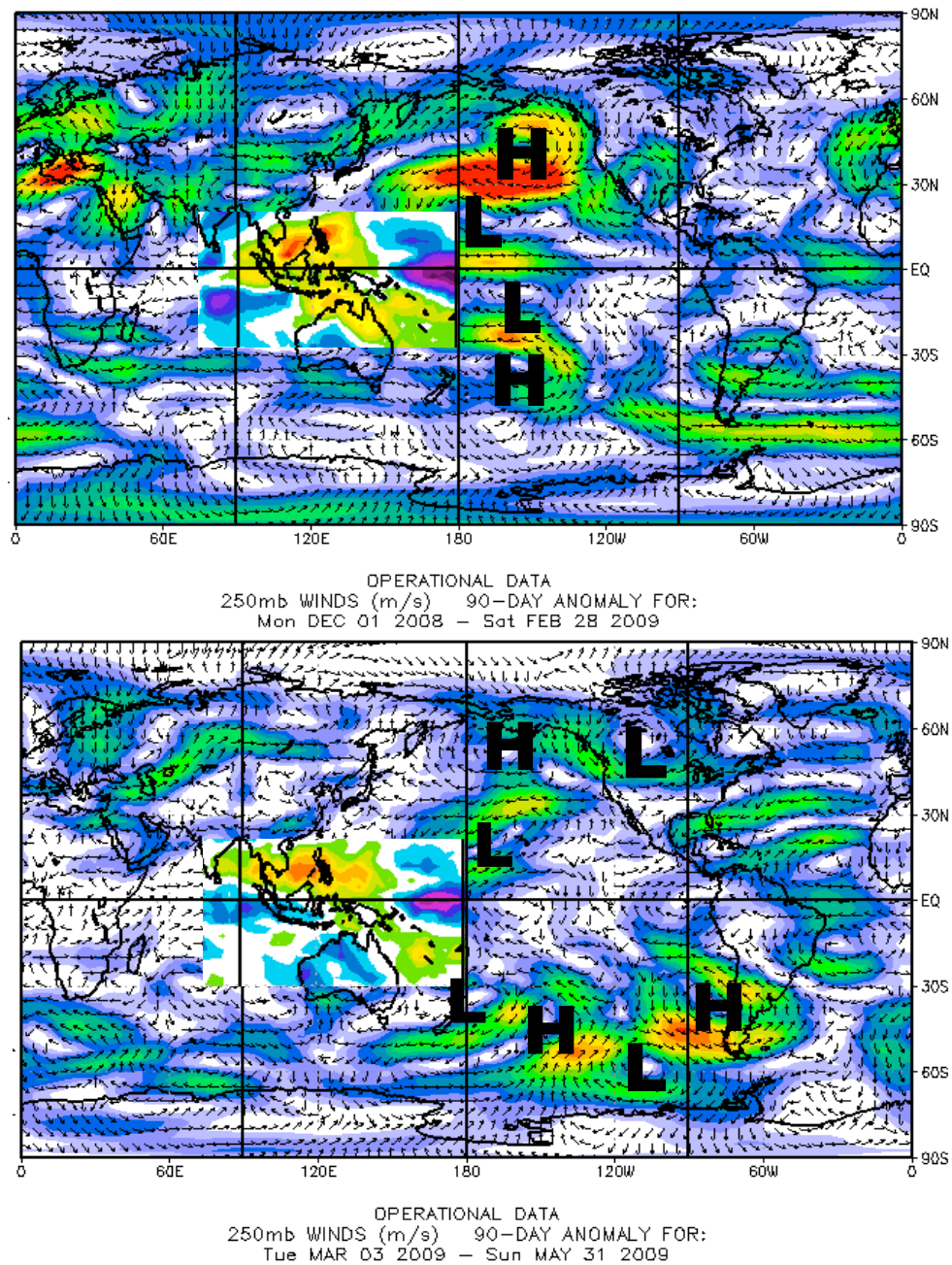


Figure 41. Seasonal mean wind field anomalies are shown for the listed periods. The OLR anomalies for the same period (reds => convection) are shown as insets over the Indo-Pacific Ocean region.

3.10 Overlapping Field Campaigns

3.10.1 THORPEX Pacific Asian Regional Campaign (T-PARC)

3.10.1.1 Introduction

The THORPEX Pacific Asian Regional Campaign (T-PARC) was a multi-national field campaign that addressed the shorter-range dynamics and forecast skill of one region (Eastern Asian and the western North Pacific) and its downstream impact on the medium-range dynamics and forecast skill of another region (in particular, the eastern North Pacific and North America). The field phase of T-PARC (1 August – 3 October 2008) was designed to leverage multi-national efforts to address these two overarching foci. While T-PARC encompasses varying time and space scales, the primary objectives of each region are the same (*i.e., to increase understanding of the mechanisms that will lead to improved predictive skill of high- impact weather events*). This multi-scale approach of T-PARC is desirable as high-impact weather events over these two regions have strong dynamical links. For example, high-impact weather events over the western North Pacific and East Asia, such as persistent deep tropical convection and intense cyclogenesis, can trigger downstream responses over the eastern North Pacific and North America via upper-tropospheric wave packets on the primary Asian wave guides. These wave packets can, in turn, be invigorated by subsequent cyclogenesis events, which make the impacts farther downstream fast-spreading, far-reaching, and associated with reduced predictability. The high-impact weather events over North American driven by these processes include intense extratropical cyclones, orographic precipitation, flooding, severe weather and the hot, dry winds that increase the risk of wild fires and the severity of droughts.

Although many significant weather events occur over eastern Asia and the western North Pacific, the focus of T-PARC is on various aspects of typhoon activity, which include formation, intensification, structure change, motion, and extratropical transition. Because of the significant impact of typhoon activity on the region of eastern Asia and the western North Pacific, T-PARC was affiliated with several programs. These programs and their national sponsor include:

- Tropical Cyclone Structure-2008 (TCS-08) [United States];
- Typhoon Hunter-2008 (TH-08) [Japan];
- Predictability and Observation Experiment (PROBEX) [South Korea];
- Tibetan Plateau Experiment [China];
- The South China Sea Experiment [China];
- Dropsonde Observations for Typhoon Surveillance near the Taiwan Region (DOTSTAR) [Taiwan].

In addition to the above list of field campaigns, a significant international component exists via contribution of specific observation platforms. A high-altitude jet aircraft (FALCON) was operated by the Deutsches Zentrum für Luft- und Raumfahrt (DLR) under a funding consortium that consisted of the following partners:

- DLR;
- U.S. National Science Foundation;
- Japan Meteorological Agency;

- National Institute of Meteorological Research, Korea;
- Institut fuer Meteorologie und Klimaforschung, Universitaet Karlsruhe / Forschungszentrum Karlsruhe, Germany;
- Environment Canada; and
- EUMETNET Composite Observing System, EC EUCOS.

Driftsonde balloon operations were conducted by the Centre National d'Etudes Spatiales (CNES) of France. Although the region of the western North Pacific plays an important and unique role in defining many characteristics of the midlatitude circulation of the Northern Hemisphere, the near-global participation in T-PARC is an indication that the scientific principles being examined with respect to the impacts on downstream weather by significant events upstream are applicable to many regions of the globe.

During T-PARC and its collaborative programs, several aircraft were used to obtain measurements in and around western North Pacific tropical cyclones during formation, intensification, and extratropical transition (Figure 42). In addition to the FALCON aircraft mentioned above, a USAF WC-130J from the 53rd Weather Reconnaissance Squadron and a Navy Research Laboratory (NRL) P-3 participated. A high-flying business class jet (ASTRA) was flown as part of the DOTSTAR program.

The combination of observational platforms and collaborative experiments led to an experimental design for T-PARC addresses three primary components: (1) A tropical measurement strategy designed to examine circulations of the tropical western North Pacific monsoon environment as they relate to enhanced and reduced periods of widespread deep convection, tropical cyclone formation, tropical cyclone intensification, and tropical cyclone structure change. (2) The measurement strategy for the extratropical transition (ET) and downstream impacts was based on the poleward movement of a decaying tropical cyclone and the resulting intense cyclogenesis that results from its interaction with the midlatitude circulation. The ET process illustrates clearly the need for tropical-to-extratropical measurement strategies as the predictability of an ET event depends on the intensity and structure of the tropical cyclone, where and when the tropical cyclone arrives in the middle latitude westerlies, and the characteristics of the middle latitude wave guide that impact the ET cyclogenesis, and the downstream propagation and evolution of the wave packets. (3) The third measurement strategy focused on identification of regions in which extra observations may reduce numerical forecast error growth. In T-PARC, the targeted observations were aimed primarily at reducing errors associated with forecasts of tropical cyclone tracks over the western North Pacific. In particular, this included whether a tropical cyclone will recurve, the longitude of recurvature, and the orientation and speed along the track following recurvature.

During T-PARC and its collaborative programs, several aircraft were used to obtain measurements in and around western North Pacific tropical cyclones during formation, intensification, and extratropical transition (Figure 42). In addition to the FALCON aircraft mentioned above, a USAF WC-130J from the 53rd Weather Reconnaissance Squadron and a Navy Research Laboratory (NRL) P-3 participated. A high-flying business class jet (ASTRA) was flown as part of the DOTSTAR program.

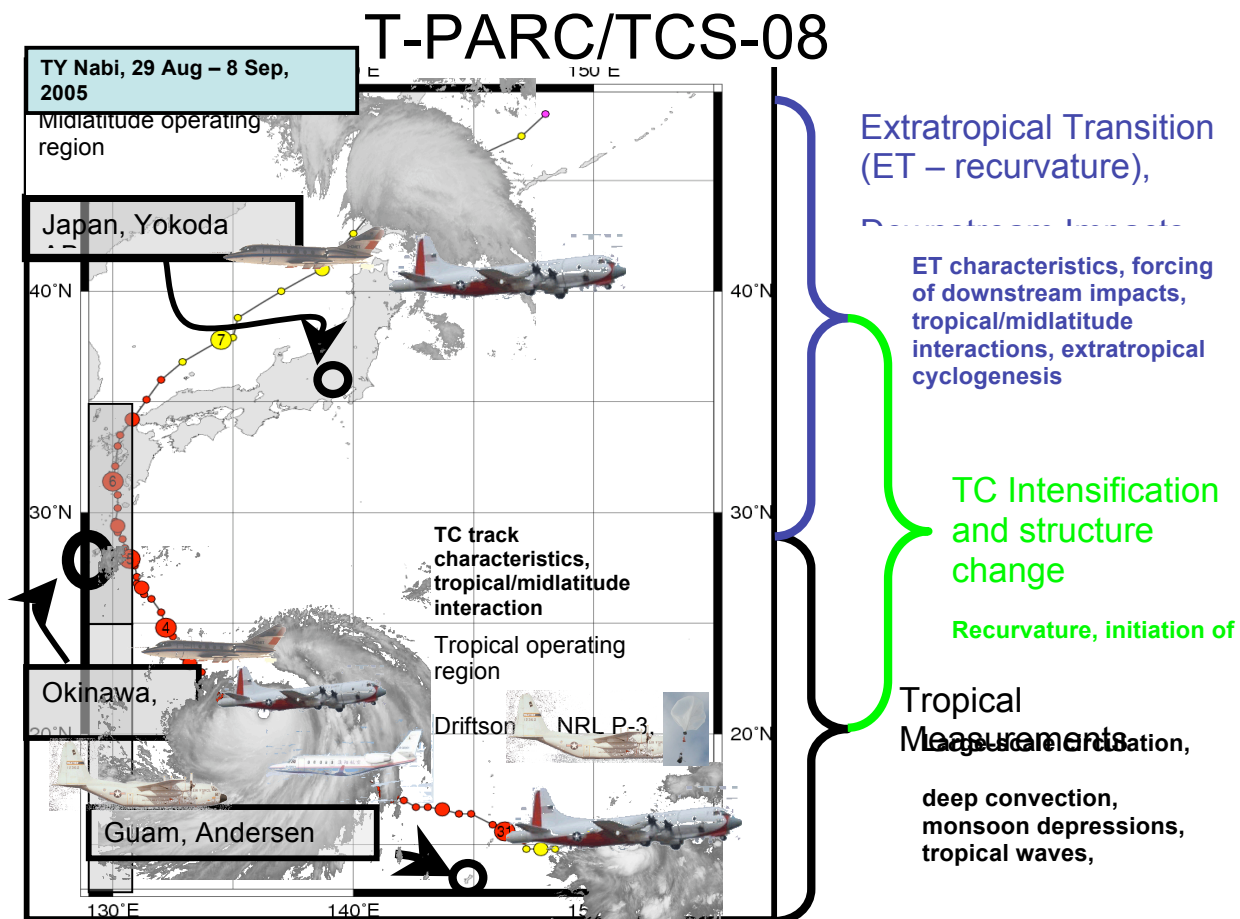


Figure 42. Schematic of the aircraft observation strategy for the combined TCS08 and T-PARC missions using the Typhoon Nabi case from 29 August to 8 September 2005 as the “perfect storm” scenario with the formation stage and structure change being observed from Andersen AFB, Guam, the recurvature and initiation of extratropical transition (ET) being observed from Kadena AB, Okinawa, and the extratropical transition being observed from Yokota AB or Atsugi NAF, Japan. The DOTSTAR missions begin and end in Taiwan. The Driftsonde is a stratospheric-level balloon deployed from Hawaii that will deploy dropwindsondes on command within the area.

3.10.1.2 SCIENCE OBJECTIVES

In general, the science objectives of T-PARC and TCS-08 were associated with increasing predictability of high-impact weather events (i.e., tropical cyclone formation, intensification, motion, and extratropical transition) and the forcing of one region on the forecasts of a downstream region. As such, the specific objectives were divided into three categories.

Tropical Cyclone Formation, Intensification, Structure Change, and Satellite Validation

The key objectives associated with the tropical cyclone component contained in the affiliated TCS-08 program address understanding and predictability of tropical cyclone formation, intensification, and structure change. In particular, outer structure change is a

special focus as changes at outer radii impact interactions between the tropical cyclone and its environment that will affect motion. Specific objectives were:

- Define the factors that impact the large-scale atmospheric and oceanic control on tropical cyclone formation;
- Define the relative roles of mesoscale processes during tropical cyclone formation. Specifically, identify contributions from the organization of low-level vorticity in deep convective towers versus mid-level circulations embedded in stratiform regions of mature mesoscale convective systems. This objective addresses the predictability associated with the location, timing, and rate of tropical cyclone formation over the western North Pacific;
- Define the relative role of environmentally-induced, vortex-generated mechanisms versus cyclogenesis determined initial conditions in determining the outer wind structure of a mature tropical cyclone;
- Define the key structural characteristics that limit the predictability of recurvature and the start of extratropical transition over the western North Pacific;
- Define representative wind distributions and maximum intensities of tropical cyclones from in situ data obtained at times coincident with satellite overpasses. The purpose of this objective is to provide baseline measurements and validation of satellite-based estimates of tropical cyclone intensity and structure.

Data Targeting

To advance forecast skill of high-impact weather events such as tropical cyclones over the western North Pacific and their downstream impacts, it was necessary to address issues associated with such factors such as reducing analysis and forecast errors, observational network design, data calibration, and data assimilation. The use and evaluation of a variety of adaptive sampling strategies for reducing errors in numerical forecasts was an integral part of the T-PARC field program design. The adaptive sampling strategies included *in situ* data as well as remotely-sensed observations. Specific objectives included:

- Define the influence of adaptive sampling based on dropwindsonde measurements from aircraft in the synoptic environment of tropical cyclones over the western North Pacific on the forecast skill of the tropical cyclone track;
- Increase understanding of the significant differences in the prediction of targeting locations produced by different targeting techniques;
- Identify the impact of assimilating additional observations from a variety of platforms, which included in situ aircraft observations and satellite remote sensing; and
- Identify the impact of data on multiple spatial and temporal scales using a variety of data assimilation methods.

Extratropical Transition of Tropical Cyclones and Downstream Impacts

The extratropical transition of a tropical cyclone is a particular tropical-extratropical interaction that often has far-reaching effects on the midlatitude circulation. Furthermore, a large amount of variability exists in the occurrence and amplitude of the downstream impacts. During ET events (Figure 43), forecasts of the downstream circulations tend to have reduced skill and the variability among ensemble members during extratropical

transition events suggests that the predictability associated with these cases is low (Figure 44).

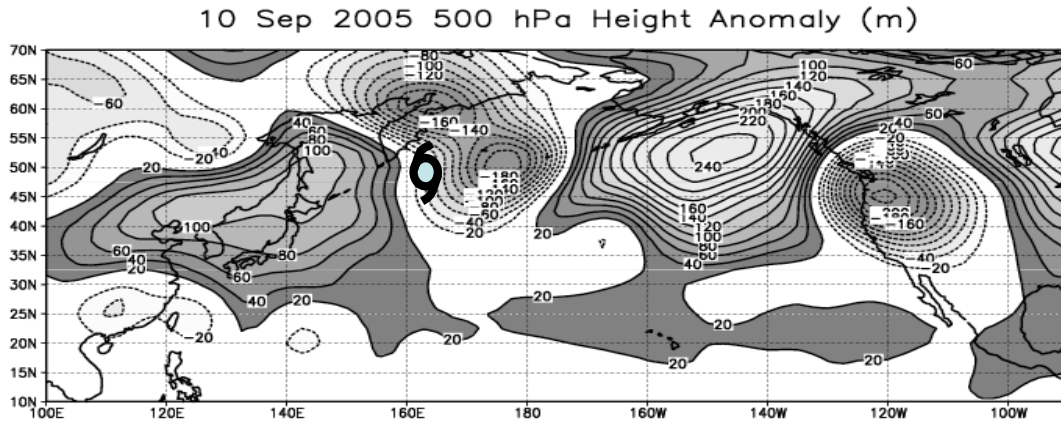


Figure 43. Anomalies of 500 hPa height (m) averaged for 0000-1200 UTC 10 September 2005 during the extratropical transition of TY Nabi and representative of a Rossby-wave like pattern. The tropical cyclone symbol marks the ex-TY Nabi.

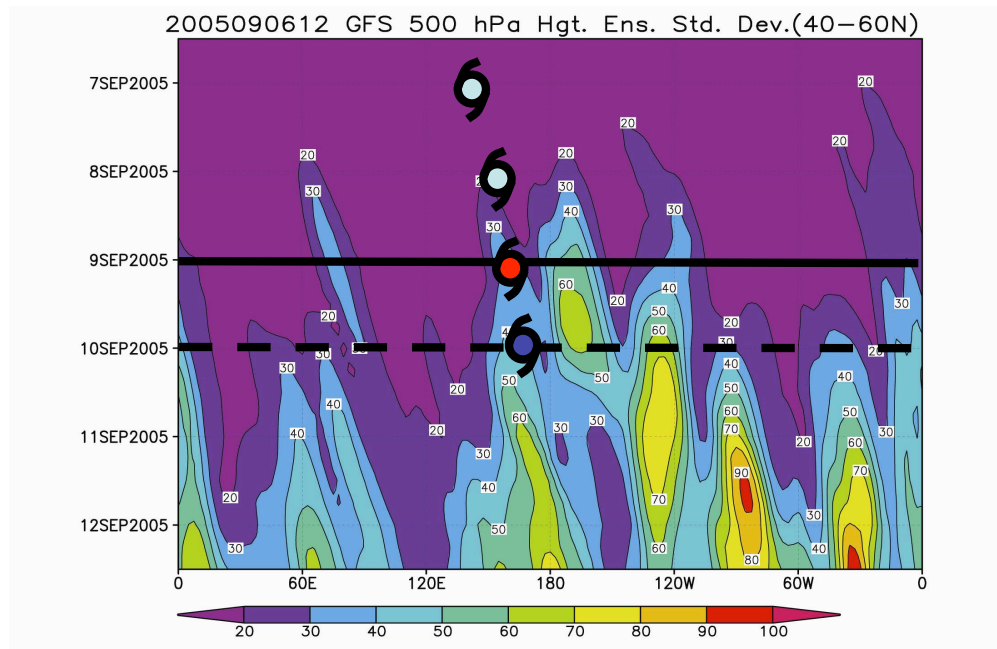


Figure 44. Time-longitude diagram of the standard deviation (m) in ensemble members for 500 hPa heights for the forecasts initiated from 1200 UTC 6 September 2005 with the Global Forecast System model run at the National Centers for Environmental Prediction. The horizontal line at 0000 UTC 9 September marks the time of the ET of TY Nabi. The dashed horizontal line marks the time that the ex-Nabi intensified to a deep extratropical cyclone. The tropical cyclone symbols mark the longitude of Nabi.

Combinations of aircraft, radar, dropwindsonde, and satellite observations were used in conjunction with model simulations to define the interactions between a decaying tropical

cyclone and the midlatitude circulation into which it was moving that then affected the downstream impact. Specific objectives were:

- Document the contributions from various physical processes that impact the development of the deep tropospheric anticyclone immediately downstream of an ET event. Physical mechanisms associated with such features as the poleward movement of heat and moisture along the eastern side of the decaying tropical cyclone, warm frontogenesis, and the interaction of the tropical cyclone outflow and the midlatitude jet stream were examined;
- Examine the temporal evolution of the processes by which the decaying tropical cyclone impacts the midlatitude circulation;
- Define the relative roles of a variety of tropical cyclone and midlatitude circulation characteristics as they influence the variability of downstream impacts during ET;
- Examine the utility of satellite data in defining the important physical characteristics of an ET event;
- Examine the importance of the re-intensification of the decaying tropical cyclone as an extratropical cyclone on maintaining the downstream transport of energy; and
- Examine the impact on forecast accuracy due to improved analysis of key structural characteristics during the ET of a decaying tropical cyclone.

3.10.1.3 FIELD PROGRAM SUMMARY

During the field program period of 1 August – 4 October 2008, four typhoon, four tropical storms, and four tropical depressions occurred over the western North Pacific. In addition to these circulations for which official forecasts were issued by the Regional Specialized Meteorological Center (RSMC, Tokyo), a separate set of 51 tropical circulation systems were identified by the T-PARC/TCS-08 research team. These systems were defined as tropical cloud clusters, low-level waves, or subtropical circulations of interest to the project.

During the period, 500 aircraft mission hours were flown during a total of 76 missions. The missions were flown into 4 typhoons, one tropical depression, and 5 tropical cloud clusters. Overall, 72% of the flight missions were flown into the four typhoons. A significant number of flight hours were dedicated to each objective listed above.

A number of the T-PARC and TCS-08 field mission types and accomplishments had never been done in the region of the western North Pacific or any other tropical cyclone ocean basin. During T-PARC, the first systematic data targeting operation applied to tropical cyclones over the western North Pacific was conducted. This included comparison of several methods from a variety of operational and research organizations. A consistent set of verification regions was used for each product and the displays were produced in a systematic manner. A majority of the products were made available via the Data Targeting System PREVIEW at the European Center for Medium range Weather Forecasts (ECMWF).

Another first-time accomplishment was the four-plane operation in Typhoon (TY) Sinlaku at category four intensity. Also, two missions were conducted to deploy drifting buoys directly in the path of TY Hagupit and TY Jangmi, respectively. At the time of the buoy deployment in TY Jangmi, the storm was at category five intensity. In both cases, the typhoon passed directly over the buoy arrays.

The T-PARC/TCS-08 program was the first operation of the Driftsonde in the equatorial Pacific. The balloons were launched from Hawaii and dropsondes were deployed based on commands given from the operations center in Monterey, CA. Data were retrieved and transmitted to the GTS for use in operational numerical weather forecast models.

Finally, during T-PARC/TCS-08 and affiliated programs, many instruments were deployed for the first time into the environment of a west Pacific tropical cyclone. These included the ELeCTra DOppler RADar (ELDORA) and the Twin Otter Doppler Wind Lidar (TOWDL) on the NRL P-3, the Stepped Frequency Microwave Radiometer on the USAF 53rd Weather Squadron WC-130J, and the DLR Doppler wind lidar and Differential Absorption Lidar (DIAL) water vapor lidar.

Overall, the field phase of the T-PARC/TCS-08 and affiliated programs were conducted with great success. The results of the data collection strategies during the field programs were such that sufficient resources were applied to each objective, which will lead to significant advances in understanding and increase in predictability of high-impact weather over eastern Asia, the western North Pacific, and regions downstream.

3.8.1.4 Relevance to YOTC

The nature of the primary science objectives of T-PARC and YOTC necessitates a linkage between them. The character and variability in tropical convection has a significant influence on tropical cyclone activity over the western North Pacific that ranges over a wide range of spatial and temporal scales. Furthermore, the objective of T-PARC to increase understanding of the role of tropical-extratropical interaction on midlatitude predictability via the poleward movement of a tropical cyclone provides a unique connection to YOTC. Finally, many aspects of the T-PARC analysis will utilize observations and model data that are being collected and made available as part of the YOTC.

3.10.2 Winter THORPEX Pacific Asian Regional Campaign (Winter T-PARC)

Pacific winter storms affect not only the western states directly hit, but also affect weather patterns throughout the North America. Strong winds, heavy rain/snow and extreme flooding, cold temperature can occur in a very short period time as the storms come ashore. Through downstream propagation, storms that form far out over the western Pacific, Asia and Siberia often affect weather patterns across the North America. The direct and indirect human and economic damages of high impact winter storms are comparable to other natural disasters such as earthquakes, tornados and hurricanes. For example, in the March 1993 Superstorm, newspaper “reports” showed damage from \$1 billion to as much as \$6 billion and some 200 to 300 deaths. As coastal populations continue to grow, the impact of major weather events could be more significant than before. Timely and accurate warnings based on accurate forecasts of these storms are needed to emergency managers, private industry and the general public for appropriate safety preparations.

The winter T-PARC (**January 13 2009 to February 28 2009**) aims at improving the high impact winter weather events over the North America and the Arctic by using adaptive observations (dropsondes) taken over the Pacific, AMDAR data over Eastern Asia and additional rawinsondes over Eastern Siberia. The quality of the 3-6 day numerical forecasts

over North America are often related to processes over sensitive regions that are sparsely observed where analysis errors introduced by observation errors can often bust the forecasts at a longer lead time.

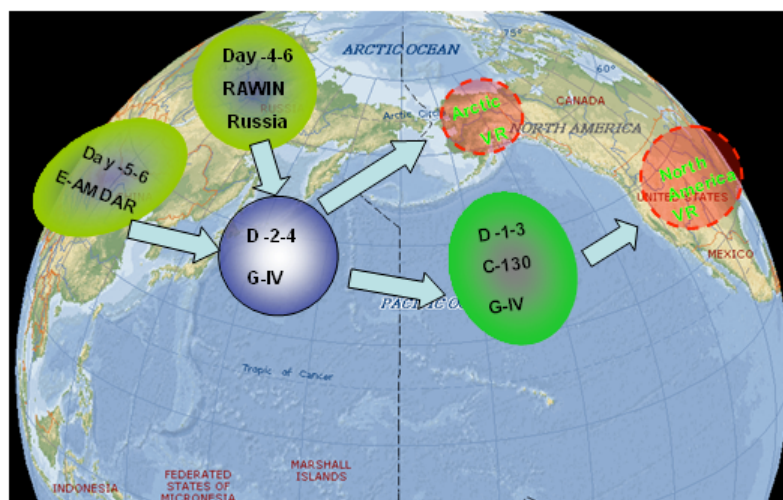


Figure 45. Schematic diagram of winter T-PARC observing platforms.

Several scientific hypotheses are to be tested in the winter T-PARC related to YOTC:

- Rossby-wave propagation plays a major role in the development of high impact weather events over North America and the Arctic on the 3-6 days forecast time scale;
- How are strong convective activities in the tropics related to the extratropical storms?
- Forecast busts are often related to our inability to resolve the vertical structure of the storm in their early stages.
- How important is the moist process playing during the early stages of the storms?

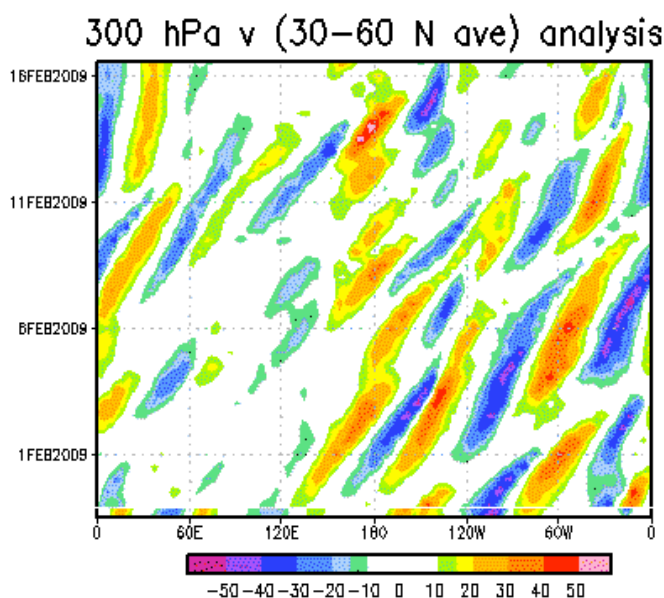
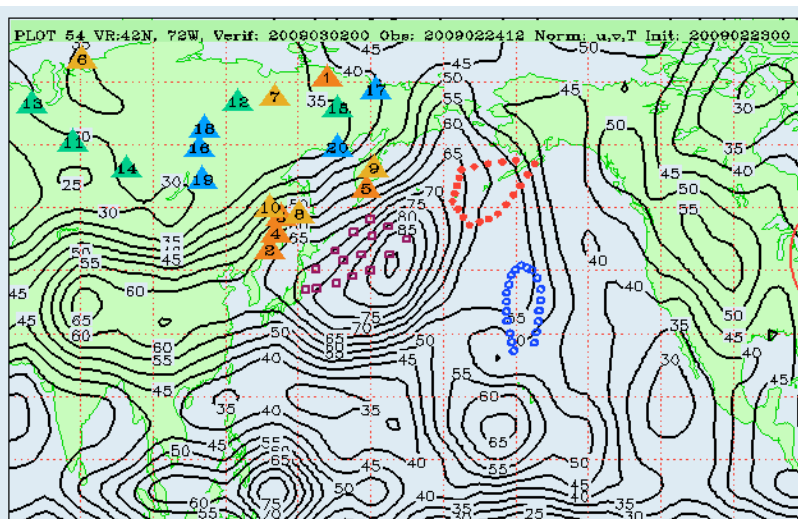


Figure 47. Wave packet analysis done by using 300mb meridional wind component averaged over 30N – 60N in the Northern Hemisphere. It shows strong Rossby wave packet around Jan 31, 12Z propagating downstream from Eastern pacific to the US. How well the numerical forecast model is capturing this is crucial for the 3-6 day forecast.

The vertical structure of the storms in the early stages is crucial for the forecast since the interaction of the storms with the ambient environment decides their direction and speed of migration. A poorly resolved storm can lead to a rapidly deteriorating downstream forecast due to the downstream development of the Rossby waves – which travels at a group velocity by theory. The goal of

the current T-PARC plan is to extend the forecast to beyond 3-6 days for North America and the Arctic. It is therefore necessary for us to look further upstream for accurate observations which can resolve the storm systems at their early stages. The current T-PARC plan approaches the problems by taking direct observation adaptively over regions (such as the tropics) that are important for the early formation of the storms.

Figure 48. Sensitive area calculation based on NCEP/UM Ensemble transformed Kalman Filter (ETKF) technique. Areas with large contour values provide guidance for February 24, 12Z observation plan which could improve the forecast for March 2, 00Z when a strong winter storm hit the US east coast – a 5.5 day lead time forecast. The value is calculated based on an kinetic energy norm derived from wind and temperature. Strong sensitive regions in the tropics are also shown to be related to the east coast storm.



Winter T-PARC marks the *first time* vertical profiling of winter storms has been conducted west of the international dateline with the goal of improving the 3-6 day numerical weather forecasts for North America and the Arctic. It has strong ties with YOTC in terms of the tropical and extratropical interaction. For example, during February, strong MJO over the Eastern Pacific has been observed, strong convective activities modulate the Eastern Asian jet stream system which was crucial for when and where small perturbations coming from the East Asia would grow. In the meantime, perturbations from the tropics were often found to be entrained into extratropical storm system and developed into major storms.

T-PARC represents a major advancement in the science of targeted observations for improving weather forecasting farther than ever attempted. It is expected that the data collected had a significant positive impact on real time forecasts in advance of high impact weather events over North America, while also yielding a historic data set that will be used by researchers to understand physical and dynamical processes of the storm initiation, growth and propagation to further improve the forecast skill in the future.

Contact Information: Yucheng Song and Zoltan Toth, NOAA/NWS/NCEP/EMC,
yucheng.song@noaa.gov, project reference: <http://www.emc.ncep.noaa.gov/gmb/tparc>

3.10.3 AMY

3.10.4 VAMOS Ocean-Cloud-Atmosphere-Land Study (VOCALS)

The Southeast Pacific (SEP) climate is a tightly coupled system involving poorly understood interactions between clouds, aerosols, marine boundary layer (MBL) processes, upper ocean dynamics and thermodynamics, coastal currents and upwelling, large-scale subsidence, and regional diurnal circulations (Figure 3.10-5). This unique system is very sparsely observed, yet its variations have important impacts on the global climate. There are also great economic impacts, with the regional fisheries representing almost one-fifth of the worldwide marine fish catch.

Several fundamental problems are barriers to the understanding of SEP's weather and climate:

- Difficulties in the quantification of the indirect effect of aerosols upon cloud radiative properties (e.g. Lohmann and Feichter 2005);
- The existence of systematic errors in coupled atmosphere-ocean general circulation models (CGCMs), which in the SEP include too warm SSTs and too little cloud cover.
- Our inability to make accurate regional weather predictions in coastal areas dominated by low cloud.

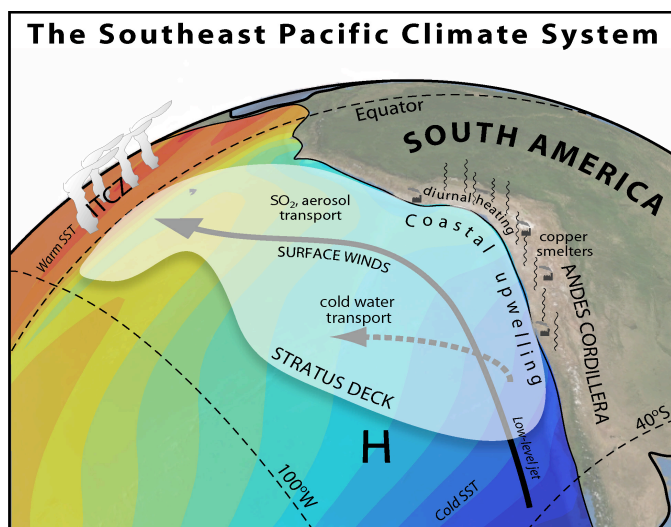


Figure 49. Key features of the SEP climate system.

VOCALS (VAMOS² Ocean-Cloud-Atmosphere-Land Study) is an international CLIVAR program the major goal of which is to develop and promote scientific activities leading to improved understanding of the SEP coupled ocean-atmosphere-land system on diurnal to inter-annual timescales. The principal program objectives are: 1) the improved understanding and regional/global model representation of aerosol indirect effects over the SEP; 2) the elimination of systematic errors in the region of coupled atmospheric-ocean general circulation models, and improved model simulations and predictions of the coupled climate in the SEP and global impacts of the system variability. *Program documents and information can be found at www.eol.ucar.edu/projects/vocals/.*

VOCALS is organized into two tightly coordinated components: 1) a Regional Experiment (VOCALS-REx), and 2) a Modeling Program (VOCALS-Mod). Extended observations (e.g. IMET buoy, satellites, EPIC/PACS cruises) will provide important additional contextual datasets that help to link the field and the modeling components. The coordination through VOCALS of observational and modeling efforts will accelerate the rate at which field data can be used to improve simulations and predictions of the tropical climate variability.

² VAMOS – Variability of the American MONsoon Systems, a CLIVAR sponsored program to study the American monsoons in the context of the global climate. Additional information at <http://www.eol.ucar.edu/projects/vamos/>

VOCALS-Rex will collect datasets required to address a set of hypotheses that are organized into two broad themes: (1) aerosol-cloud-precipitation interactions in the marine boundary layer (MBL) and the physicochemical and spatiotemporal properties of aerosols; (2) chemical and physical couplings between the upper ocean, the land, and the atmosphere. VOCALS-REx will have an intense observing period during **October-November 2008**. The observational platforms during the period will comprise aircraft (chiefly the NSF C-130, the CIRPAS Twin Otter, the DoE G-1, and possibly the UK BAe-146), research ships (the NOAA Ronald H Brown (RHB), and a second ship, most likely the R/V Wecoma or similar), a land site in Chile, and Peruvian and Chilean coastal cruises. Figure 7 shows a map of the VOCALS-REx study region and platforms involved. VOCALS-Rex activities have been carefully designed to complement and enhance a suite of enhanced long-term observations in the SEP. These include an uninterrupted six year record from the IMET instrumented surface buoy (85°W, 20°S), annual buoy maintenance cruises (in 2001 and then in 2003-2006 as part of the EPIC/PACS program), and regionally-subsetted satellite data (coordinated through JOSS), have been used extensively to provide important context for modeling activities and to aid our understanding of the physical processes occurring in the SEP. Figure 51 presents a graphical summary of the field sampling.

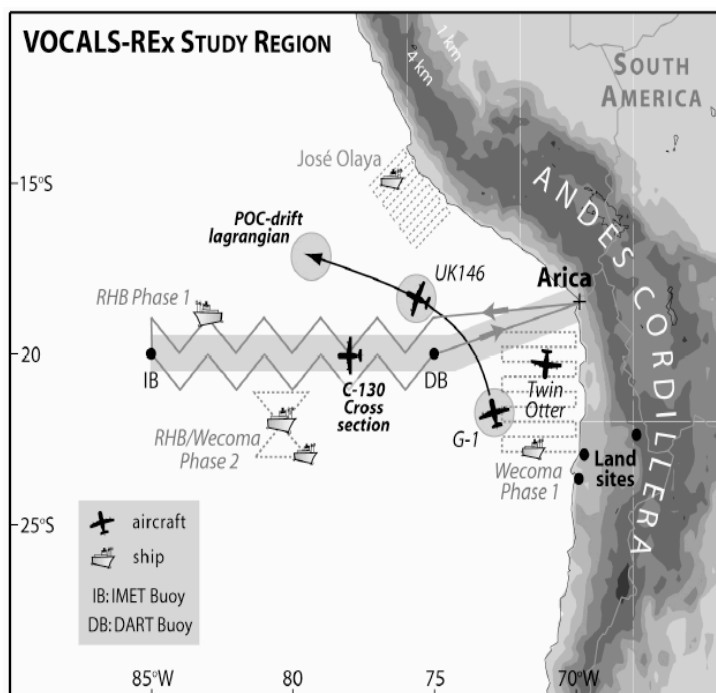
Figure 51. VOCALS-REx study region and key platforms/components.

For Phase 1, the NOAA Ronald H Brown (RHB) will make measurements for 6 days at each of the IMET (20°S, 85°W) and DART (20°S, 75°W) buoys, transiting between the buoys with a concertina pattern to sample mesoscale ocean variability, while the Wecoma carries out a survey of the eddy-genesis region close to the coast.

For phase 2, the Wecoma will survey oceanic mesoscale variability (using SeaSoar) and its effects on the atmosphere around the RHB (one possible pattern is shown).

The NCAR C-130 will make cross-sectional measurements along 20°S out to 85°W, and will also conduct POC-drift and multi-day lagrangian flights (with other aircraft) to study the structure of POCs and the evolution of the MBL. The other aircraft (DoE G-1, CIRPAS Twin Otter, and the UK 146) will work mainly in the near-coastal zone to examine aerosol, cloud and precipitation variability.

The R/V José Olaya coastal cruise will sample oceanic upwelling and the MBL structure. The land sites will be used to examine the chemical and physical properties of air masses advected from Chile over the SEP.



A principal goal of VOCALS is to improve model³ simulations of key climate processes using the SEP as a testbed, particularly in coupled models that are used for climate change projection and ENSO forecasting. VOCALS-Mod, therefore, provides the context for VOCALS

³ The numerical models to be used include 1) Large-Eddy Simulation Models (LESs), 2) Regional Atmospheric Models (RAMs), 3) Regional Ocean Models (ROMs), 4) Coupled ROM-RAM Models (ROAMs), 5) Atmospheric General Circulation Models (AGCM), 5) Oceanic General Circulation Models (OGCMs), 6) Coupled Atmosphere-Ocean General Circulation Models (CGCM), and 7) Single Column Models (SCM) for clouds and aerosols.

and will directly benefit from the observations collected in the field campaign. The goals of VOCALS-Mod reflect the two overlapping themes of VOCALS, coupled ocean-atmosphere-land interaction and cloud-aerosol-drizzle interactions. These goals are:

- (1) Understanding and reducing the warm SEP SST bias near the coast and excessive inter-hemispheric symmetry in the eastern tropical Pacific present in most CGCMs.*
- (2) Using the SEP as a testbed for better simulation of boundary-layer cloud processes and aerosol-cloud interaction, including the relative roles of natural and anthropogenic aerosol sources and their impact on cloud optical properties (coverage, thickness, and droplet size).*
- (3) Improving the understanding and simulation of oceanic budgets of heat, salinity, and nutrients in the SEP and their feedbacks on the regional climate.*
- (4) Elucidating interactions between the SEP and other parts of the earth's climate system, including the South American continent, the Pacific circulation and ENSO.*

The VOCALS modeling vision is based on the concept of a multi-scale hierarchy of models. This is motivated by the multiscale nature of processes in the SEP and the multiscale hierarchy of VOCALS observations, including REx, extended in-situ and satellite data. To implement this vision, VOCALS-Mod will coordinate activities carried out at operational centers (NCEP), research laboratories (NCAR, GFDL) and universities, using VOCALS observational datasets both to evaluate model performance and to inform physical parameterization development. Use of the operational modeling systems will provide insight into the time evolution of errors and their dependency on the analysis employed for initialization; use of research modeling systems will facilitate hypothesis-testing experiments. The following are the main modeling components associated with each of the two main VOCALS themes.

Cloud-Aerosol-Precipitation Themes

- 1. Chemical and aerosol transport modeling*
- 2. Improving parameterizations of boundary layer clouds*
- 3. LES of aerosol-drizzle-cloud interaction and POCs*

Coupled Ocean-Atmosphere-Land Themes

- 1. Simulation and data assimilation of SEP ocean mesoscale structure from 0-2000 km offshore*
- 2. Multiscale assessment of SEP ocean eddy transport, heat budgets, and SST biases in CGCMs*
- 3. Diagnostic studies of the SEP regional climate system (coupled patterns of variability)*
- 4. Modeling feedbacks between SEP and global-scale climate biases (incl. ENSO).*

VOCALS-Mod will coordinate an assessment of how well atmospheric models can simulate and interpret the time-varying regional structure of clouds, winds, and aerosols during the REx period. Global reanalysis data will be used as forcings for RAMs and ROAMs. The model data will be compared directly with VOCALS-REx and VOCALS extended observations (e.g. mesoscale ocean eddies, satellite and ship-observed clouds). A pilot for this study, the Preliminary VOCALS Assessment (PreVOCA), is being carried out within the VOCALS modeling community. VOCALS-Mod participants will also participate in organized modeling activities, such as community-wide tropical bias workshops, the GCSS/WGNE Pacific Cross-section Intercomparison (GPCI) project, and the GEWEX Cloud System Study (GCSS).

Contact Information: Robert Wood, U. of Washington, robwood@atmos.washington.edu

4 Modeling Resources and Research Tasks

4.1 Overview

Figure 52 illustrates the three primary components of the YOTC project: high-resolution operational deterministic prediction systems (i.e., ECMWF, NASA, NOAA), integrated observations (i.e., satellite, field-campaign, *in situ*) and research-oriented modeling and analysis of various kinds. This integrative approach is a framework for addressing the multiscale organization of tropical convection and its interaction with the global circulation. In the long-terms it is also a contribution to strategic aspects, such as the role of the Tropics in seamless weather-climate prediction and the physical basis of climate at large.

There are several advantages for a YOTC focus on multiscale convective organization. One compelling reason is that representing organized tropical convection in global models has long been recognized but inadequately addressed (Houze and Betts (1981). Historically, convective parameterization was the only way the global effects of precipitating convection could be assessed. Advances in this area can be anticipated.. Firstly, the spatial resolution of operational global prediction systems is now adequate to assess the impacts of large-scale convective organization. Secondly, research models explicitly simulate multiscale convective organization and its scale interactions. The focus on time scales up to seasonal can fully exploit high-resolution simulations.

The YOTC project will target the phenomena detailed in the YOTC Science Plan (2008); namely the monsoon systems, intraseasonal variability, the InterTropical Convergence Zone (ITCZ), and easterly waves and tropical cyclones. The diurnal cycle is involved in all these phenomena.

4.1 Global analysis and prediction

- High-resolution operational global prediction systems utilizing data-assimilation are an important part of the YOTC project. Attribution studies will evaluate the successes and failures of these advanced deterministic prediction systems;
- Hind-cast experiments of targeted meteorological phenomena of importance to seamless prediction on time scales up to seasonal, including interactions between the tropics and extratropics involving multiscale convection;
- Hind-cast prediction experiments of selected events during summer and winter phases of the THORPEX Pacific Area Regional Campaign (TPARC) and Tropical Cyclone Structure (TCS08);

- High-resolution short-range (< 48 hr) numerical weather prediction experiments utilizing explicit convection to quantify aspects including the effects of convective organization on the tropical atmospheric circulation;
- Lateral boundary conditions and initial conditions for cloud-system resolving model (CRM) simulations;
- Meridional boundary conditions and initial conditions for interactively-nested tropical channel models to investigate the effects of extra-tropical forcing on tropical convection and *vice versa*, and the upscale evolution of precipitating convection into multi-scale organized cloud systems.
- Comparisons of the above models with simple theoretical-dynamical model.

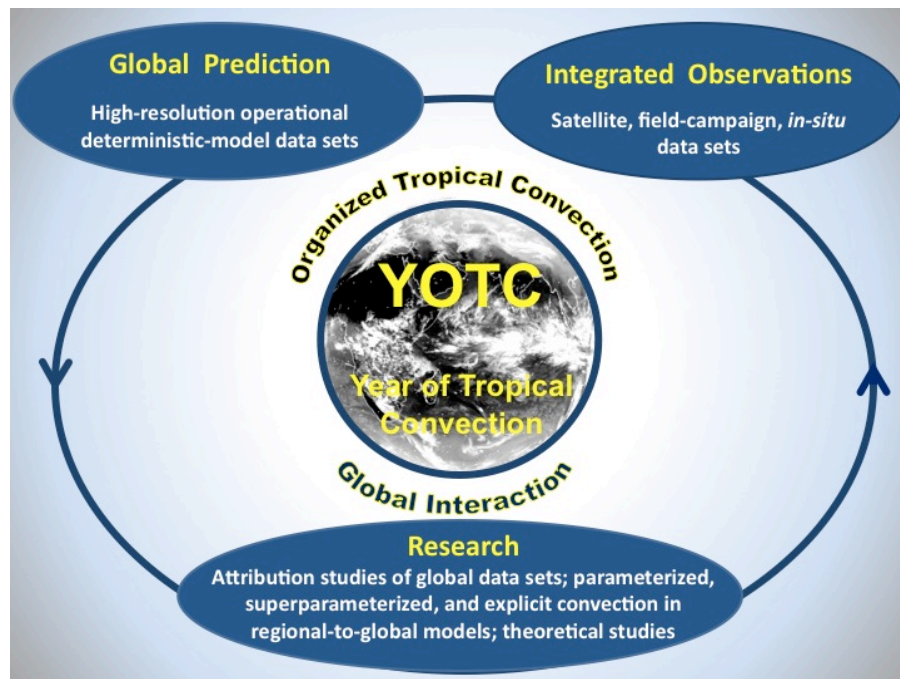


Figure 52. Anatomy of the YOTC project.

4.2 Multiscale cloud-system simulation and modeling

Cloud system simulation and dynamical modeling is a comprehensive explicit resource: i) cloud-system resolving models (CRMs); ii) the application of CRMs to superparameterization in place of conventional parameterizations of convection and the planetary boundary-layer; iii) global CRMs; iv) nested regional climate models (NRCM) which includes tropical channel models; and v) theoretical-dynamical models.

These explicit approaches do not obviate the need for convective parameterizations but they are important resources for improving parameterizations.

4.2.1 Cloud-system resolving models

CRM are a key element of the YOTC project, especially CRMs with computational domains large enough to represent meso-to-regional interactions and hence address multiscale convective organization and the accompanying upscale cascade of energy and momentum. By coupling mesoscale dynamics to the parameterized small-scale processes (e.g., cloud-microphysics, turbulence, and surface exchange), CRMs bridge these important aspects of atmospheric physics. The CRMs also explicitly represent the interaction of convection with the underlying surface (e.g., downdraft-generated cold pools or density currents) as well as convectively generated inertial-gravity waves that are a key element of *scale-selection in the tropics*. *Tao and Moncrieff (2009) reviews the extensive framework and application of CRMs to atmospheric science.*

4.2.2 Superparameterization

Superparameterization sidesteps many issues of conventional parameterization by placing two-dimensional CRMs in each grid-column of a global circulation model (GCM) instead of conventional parameterization of convection (Grabowski and Smolarkiewicz 1999; Grabowski 2001; Khairoutdinov and Randall 2001; Randall et al., 2003b). This approach is called the Multiscale Modeling Framework (MMF). The GCM provides global coverage while the CRMs simulate mesoscale dynamics, cloud-overlap, cloud-radiation interaction, interaction between convective downdrafts and surface fluxes. The time-dependent two-way interaction between the CRMs and the parent GCM explicitly bridges the scale-gap assumed in contemporary parameterizations. However, the scales transferred within the CRM are not directly transferred to the larger scale since they are represented by a true high-resolution model. Whilst the few-km grid-spacing typical of the CRMs applied in MMF resolve the mesoscale circulations associated with precipitating cloud system, neither cumulus convection nor the boundary-layer turbulence are properly resolved (this requires a resolution of $\sim 100\text{m}$, Skamarock 2004). How to represent small-scale processes in CRMs is an important research issue. Despite such caveats, several aspects of MMFs are demonstrably superior to contemporary climate models as described later.

4.2.3 Nested Regional Climate Models/Tropical Channel Models

Nested Regional Climate Models (NCRM) provides an efficient way to quantify large-scale phenomena such as the MJO and convectively-coupled Kelvin waves with inherently multiscale properties (e.g., synoptic-scale superclusters and mesoscale clusters) that can be simulated at suitably high resolution. Tropical channel models (TCM) are a particular type of NRCM -- zonally global but meridionally bounded. Computationally more efficient and “controllable” than full global CRMs. They also have higher resolution and sophisticated physics compared to the GCMs. The main advantage of a TCM over a regular regional model is the fact that the TCM can isolate the boundary effects that arrive solely from the extratropics. Thus, a TCM can effectively quantify extratropical effects such as Rossby waves and wintertime surges on large-scale organization, as well as the upscale cascade of energy and momentum within the tropics. Ray et al. (2009a) used a TCM based on the NCAR Mesoscale Model Version 5 (MM5) to isolate and identify the forcing responsible for the MJO initiation. The exact mechanism through which the extratropics influences the MJO initiation was further explored by Ray and Zhang (2009). These results

point to a new possible practice in MJO prediction: a high-resolution domain of the tropics nested in a coarse-resolution global model. The latter is known to suffer less from deficiencies in cumulus parameterization in the extratropics because of strong dynamical control there. The NCAR TCM, which is based on the Weather Research and Forecasting (WRF) model, has been run for 10 years at 36 km grid-spacing, and nested sub-domain simulations for periods of months. Analysis of these simulations is underway (e.g., Caron 2009; Done et al. 2009; Ray et al. 2009; Tulich and Kiladis 2009).

4.2.4 Global cloud-system resolving models

Global CRMs are being developed in several establishments around the world. The nonhydrostatic icosahedral-grid atmospheric model (NICAM) developed in Japan run on the Earth Simulator is the only global CRM in action (Satoh et al., 2008). The UK Met Office Unified Model is formally a global CRM since it has a nonhydrostatic dynamical core although it is not run as such. It is essential that high-resolution (convection permitting and parameterized) models be analyzed in full in order to assess the fidelity of simulated convective organization, the sensitivity to model configuration, and why some global models applying convective parameterization generate more realistic MJOs than others (Sperber et al., 2008). One inherent difficulty in the analysis and validation of CRMs is unavailability of observed/analysed datasets of similar resolution. The approach to reconcile such problem is also a necessary part of the YOTC activity.

4.2.5 Idealized models

Comprehending multiscale convective organization and its global effects at a fundamental level is essential for setting modeling, prediction, and observational analysis on a firm physical basis. Idealized models have already achieved substantial success in this area. For example, two-dimensional idealized global-scale CRM simulations show that multi-scale convective organization can evolve out of horizontally uniform initial conditions (e.g., Grabowski and Moncrieff 2001) and the organization is explainable by theoretical-dynamical models (e.g., Moncrieff 1992; Moncrieff 2004; Biello et al. 2007; Majda and Stechmann 2009). Superparameterization came about as a natural evolution of the cloud-system studies using CRMs (Grabowski and Smolarkiewicz 1999; Grabowski 2001). The effects of simplified convective parameterization have on multiscale convective organization has been quantified using idealized models (e.g., Yano et al., 1996; Khouider and Majda 2007). There are also applications in the stochastic-dynamics context (e.g., Shutts, 2004; Craig et al. 2005; Tompkins 2005; Teixeira and Reynolds 2008; Berner et al. 2005).

4.3 Key Elements

Making substantial progress on answering the following questions (among other difficult questions) lie at the heart of YOTC research goals (YOTC Science Plan 2008):

- What are the global and regional characteristics of tropical convection over both land and ocean, including variability on diurnal to seasonal time scales?
- What are the characteristics and relative roles of processes occurring: i) within the large-scale circulation, ii) on the mesoscale, and iii) internally on the storm scale

that influence the development, organization, and maintenance of tropical convection?

- Under what circumstances and via what mechanisms is water vapor, energy, and momentum transferred across scales ranging from the mesoscale to the planetary scale?
- How does organized tropical convection interact with the extra-tropical circulation?

It will also be a contribution to strategic elements such as the role of the Tropics in seamless weather-climate prediction and establishing a reliable physical basis for climate-change and the role of moist physics in future Earth-system models. The following are a few of many general tasks involved in the YOTC project.

4.3.1 *Improving convective parameterization*

Moist convection will need to be parameterized in certain classes of global model for the foreseeable future, e.g., operational global prediction systems especially the probabilistic ensemble approach; climate models run for centuries; and future Earth System models. In such applications, especially the latter, computational facilities are deployed for purposes other than resolution, e.g., representing atmospheric chemistry, carbon and nitrogen cycles, and land and ocean biogeochemistry.

The parameterization of convective organization confronts a key assumption of convective parameterization: existence of a scale-gap between cumulus and the grid-scale that mesoscale convective organization directly invalidates. The explicit representation of mesoscale convective systems (MCS, spatial scale ~ 100 s km) requires at the very least 10-km grid-spacing (Moncrieff and Liu 2006). Within a decade global NWP models will have this resolution but likely not ~ 1 km spacing necessary to fully represent MCS. This aspect involves the fairly new aspect of hybrid convective parameterization (i.e., explicit + parameterized convection).

One primary reason that mesoscale convective organization remains to be parameterized in global models is that contemporary parameterization approaches were not designed to represent dynamical aspects which are central in the organized convection context. Efforts to represent convective organization are needed but unfortunately few. Exceptions are Moncrieff and Liu (2006) and Kuell et al. (2007).

Hybrid parameterization is a relatively new issue for high-resolution NWP models where cumulus parameterization operates side-by-side with explicit grid-scale circulations. While such parameterizations under-resolve convective organization, they are nevertheless a vast improvement over contemporary parameterization. Moncrieff and Klinker (1997) showed that grid-scale circulations represent large tropical superclusters (spatial scale ~ 1000 km) in the ECMWF model at T213 spectral truncation (about 80 km grid-spacing). Houze (2004) pointed out that this very large convective circulation is consistent with the scale and structure of superclusters observed during TOGA COARE, indicating the untapped potential of the hybrid approach. This is important because for computational reasons 10-km-grid climate models will likely be operative for climate studies long before global CRMs, unless decisions are made not to run at this resolution for climate.

Improved convective parameterizations have been shown to improve large-scale convective organization on climate timescales, such as the MJO intraseasonal variability on interannual variability of the El Niño-Southern Oscillation (ENSO). Wu et al. (2007) showed that the genesis, evolution and termination of 1997/98 El Niño event as a result of atmosphere-ocean interaction are improved. Moist convection occurs less frequently, is better organized, and is closer to TRMM satellite observations (Fig. 4.2).

Stochastic parameterization requires further investigation for the obvious reason that atmospheric convection has very limited predictability compared to the large-scale state. Shutts and Palmer (2007) provided probability distribution functions for stochastic parameterizations using CRM simulations to evaluate the extent to which deterministic convective parameterizations fail to capture statistical fluctuations.

4.3.2 Modeling in support of field campaigns

The development of CRMs was accelerated through involvement with field-experiments such as a TOGA COARE (e.g., Wu et al. 1998), TRMM (Tao et al. 1993), and in association with organized activities such as the GEWEX Cloud System Study (GCSS; Moncrieff et al. 1997; Randall et al. 2003). The computer capacity in the late 1990s, two decades after the GATE field campaign, finally permitted regimes of convective organization and transitions between regimes in African easterly waves observed in GATE to be simulated by three-dimensional CRMs (Grabowski et al. 1998).

Operational prediction models will be used for hind-cast experiments of selected events during field campaigns. Examples are: i) summer and winter phases of the THORPEX Pacific Area Regional Campaign (TPARC) and the Tropical Cyclone Structure (TCS08); ii) field campaigns associated with the Asian Monsoon Years (AMY) will provide opportunities to examine the monsoons, intraseasonal variability of the monsoon, and the role of organized convection.

There are also field campaigns in the planning stage relevant to YOTC, e.g., Dynamics of the MJO (DYNAMO) with emphasis on the initiation of the MJO is proposed for the Maldives locale of the Indian Ocean during the boreal winter of 2010. Both NSF and NASA will have field campaigns in the Atlantic, and ONR will have one in the Pacific.

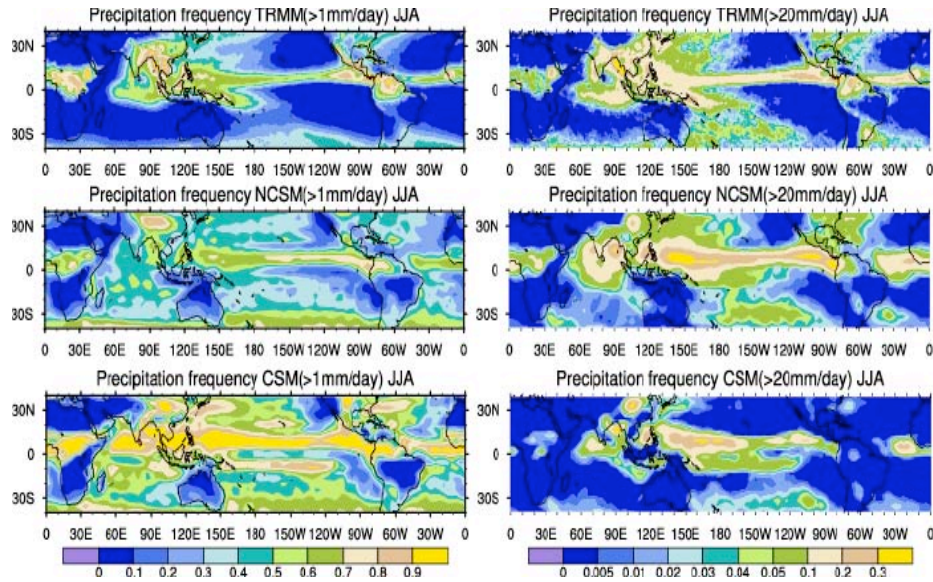


Figure 53. June, July and August (JJA) daily precipitation (>1 mm/day, left; >20 mm/day, right) frequencies (%) from TRMM 3B42 satellite observations (1998-2003, top), the GCM with improved convection scheme (NCSM, years 80-89, middle), and the standard GCM (CSM, years 80-89, bottom). NCSM rains much less frequently compared with the standard CSM over the Indian Ocean, the Pacific and the Atlantic (left panel), while NCSM produces more heavy precipitation than CSM over North, Central and South America, the Indian Ocean and the Western Pacific (right panel). [Courtesy: Wu et al. 2007].

4.3.3 Weather as an initial-value problem for climate

The focus of YOTC on time scales up to seasonal is an opportunity to examine critical issues associated with seamless prediction. A critical issue is the global distribution of precipitation which is proxy for the moist part of the global circulation. Climate models certainly have problems with large-scale convective organization, e.g., ITCZ and MJO. Interestingly, short-term initial-value (weather) experiments with climate models feature similar precipitation biases (Fig. 4.3). Climate models run in weather mode are in place (e.g., Boyle et al. 2008). This aspect is as part of the YOTC project as well.

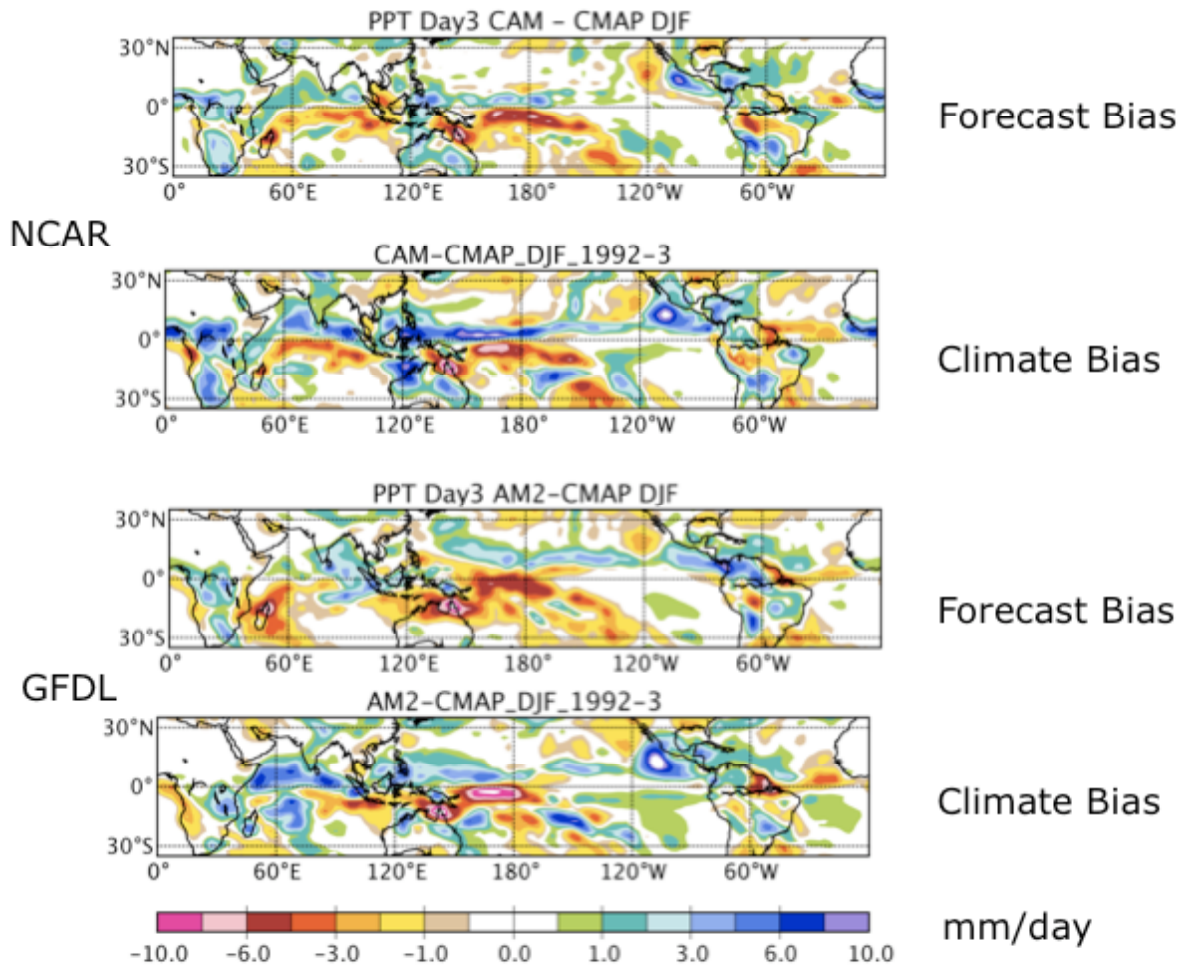


Figure 54. Comparison of weather-climate bias in terms of precipitation rate (mm/day) for two modeling systems, GFDL and NCAR. Weather bias is the difference between predicted and observed precipitation rate for composited 3-day forecasts for December, January and February (DJF), 1992-1993. Climate bias is from a single integration of these modeling systems with prescribed SSTs (AMIP mode) for DJF 1992-1993. [Courtesy: Boyle et al., 2008.]

The role of the ocean and how it responds to the atmosphere as we move from short range forecasting, through monthly and seasonal, to climate scales is a major uncertainty. Atmosphere-ocean feedback effect on atmospheric variability needs to be thoroughly researched, since there are contradictions as indicated below. MJO-like systems can occur for constant SST (e.g., Grabowski and Moncrieff 2001; Grabowski 2001). The amplitude and variability of the MJO in the Indian Ocean/Tropical Western Pacific is likely associated with ocean variability. The upper-ocean has an impact even at diurnal time scales by convective downdrafts disrupting the diurnal cycle of solar heating on SST.

An aquaplanet CRM coupled to a mixed-layer ocean model (Grabowski 2006) used a slab-ocean model to examine differences arising from the prescribed depth of the oceanic

mixed-layer. The spatial distribution and the amplitude of the surface heat fluxes, precipitation, shortwave and longwave radiative fluxes, and the large-scale flow associated with MJO-like systems in Grabowski (2006) compare favorably with TOGA COARE measurements. The development of large-scale organization was *impeded* by negative feedback between the large-scale organization of convection and SST which increased/decreased in regions of suppressed/enhanced convection. Mature MJO-like systems were little impacted. This convection–SST negative feedback contradicts traditional general circulation model results where an enhancement of the intraseasonal signal usually occurs compared to prescribed-SST. This contradicts speculations that the MJO is a fundamental coupled mode of climate variability (Sperber et al. 1997; Stephens et al. 2004). Also, climate studies using parameterized convection show enhanced intraseasonal signal when coupled to the ocean.

The importance of high-frequency SST variability on the intraseasonal variability of Indian summer monsoon rainfall have been shown in coupled simulations using a fine-resolution mixed-layer ocean model (Klingaman et al., 2008). The relevance of the CRM approach is indicated by the quotation from Klingaman et al. (2009), namely “atmosphere-to-ocean feedbacks are of little value if the atmospheric models cannot diagnose fluxes of the magnitude required to substantially modify the SSTs”. CRMs simulate explicit convective downdrafts and explicit surface momentum fluxes provide more realistic surface fluxes than convective parameterizations in traditional GCMs.

4.4 Research tasks

[Incomplete - discussion at YOTC Implementation Workshop]

The research tasks are consistent with the five targeted phenomena identified in the YOTC Science Plan.

4.4.1 GCSS Pacific Cross-section Intercomparison (GPCI)

The main goal of the GCSS Pacific Cross-section Intercomparison (GPCI) is to evaluate and improve the representation of tropical and sub-tropical cloud and precipitation processes in weather and climate prediction models. GPCI is a working group of the GEWEX Cloud System Study (GCSS). Despite its successes, the current GCSS strategy of using one-dimensional subsets of weather and climate prediction models does not fully address the fundamental role of clouds in climate, since it does not allow for feedback to the large-scale dynamics.

In GPCI an approach is proposed where weather and climate prediction models are analyzed along a Pacific Ocean cross-section, from the stratocumulus regions off California, across the shallow convection trade-wind areas, to the deep convection regions of the ITCZ (see Figure 55). This approach aims at complementing GCSS by providing a simple framework for 3D model evaluation that includes several important cloud regimes such as stratocumulus, shallow and deep cumulus, as well as the transitions between them. The

fact that data is only needed along a cross-section allows for a technically easier intercomparison.

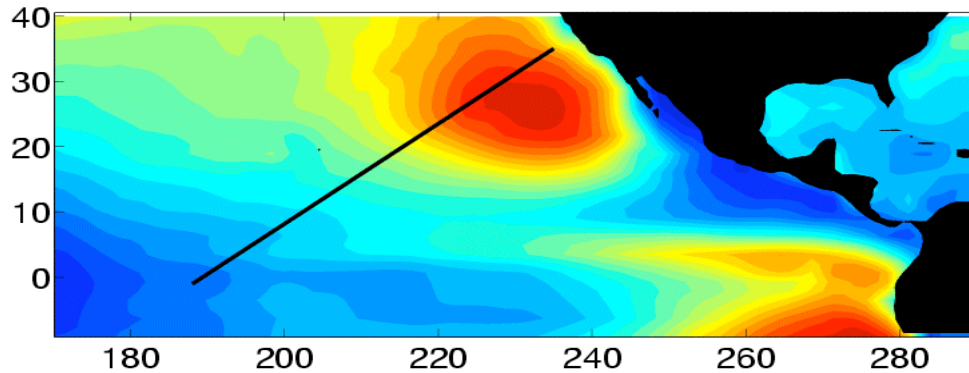


Figure 55. GPCI cross-section (black line) and the ISCCP annual mean low cloud cover.

During the first GPCI exercise, 23 weather and climate prediction organizations participated, including: NCAR, NASA/GISS, GFDL, NCEP, ECMWF, UKMO (United Kingdom), MeteoFrance (France), JMA (Japan) and ECHAM (Germany). Instantaneous model output was collected every 3 hours for the periods of June-July-August 1998 and 2003.

The plans for a GPCI contribution to YOTC include:

- Climate and weather prediction model submission for at least the period of June-July-August 2008 (output every 3 hours).
- Model evaluation along GPCI against observations organized in the context of YOTC, in particular NASA A-Train measurements along GPCI cross-section.

As an example, for the first GPCI exercise the AIRS temperature and humidity observations were used to evaluate models along the GPCI transect. Figure 56 shows two relative humidity cross-sections along the GPCI transect from AIRS and the NCAR climate model for June-July-August (JJA) 2003. These two figures show several important differences. For example, it is clear that compared to AIRS the NCAR model produces a boundary layer that is unrealistically shallow. This is a result that has been confirmed by other sources. Major differences above the boundary layer may also be due to sampling issues related to the AIRS data.

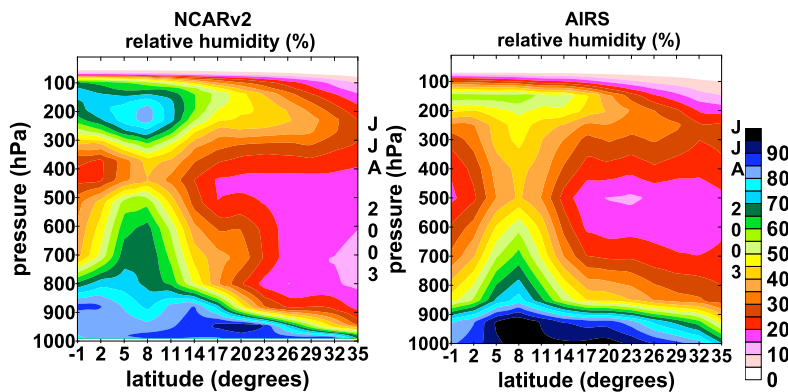


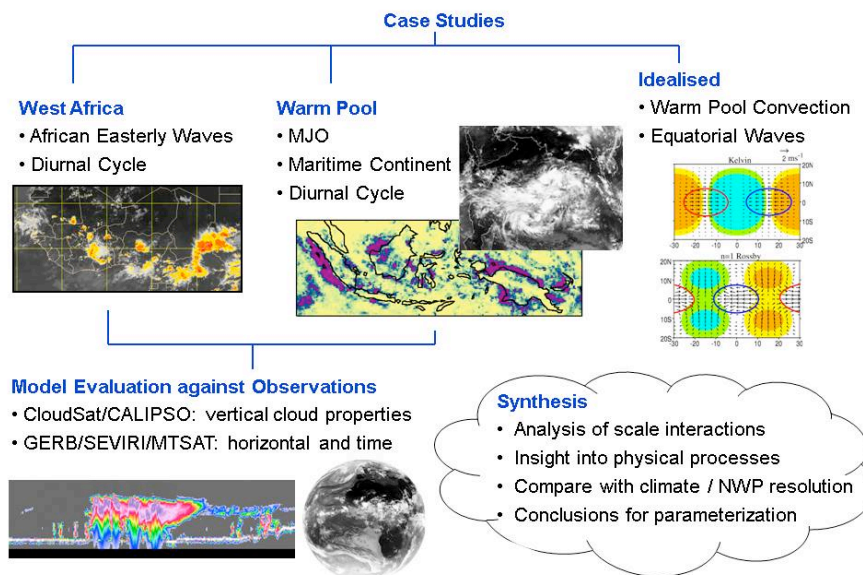
Figure 56. Relative humidity cross-section along the GPCI transect from the NCAR model and AIRS for JJA 2003.

The model results for GPCI have been assembled and organized on the DIME website: <http://gcss-dime.giss.nasa.gov/index.html>. The results for GPCI are at: http://gcss-dime.giss.nasa.gov/gpci/modsim_gpci.html. In the spirit of the DIME site, the GPCI/DIME webpage is a dynamical website as it allows dynamical comparisons between the individual models, the observations and other models for each field. In addition to the climate/weather models and the satellite observations, some groups will try to use Large Eddy Simulation (LES) modeling for boundary layer clouds and Cloud Resolving Models (CRMs) for deep convection in the region of the GPCI transect.

4.4.2 Madden-Julian Oscillation and Convectively-Coupled Equatorial Waves

a) Cascade

The objective of the UK *Cascade*⁴ project is to use CRMs with large domains to improve understanding of scale-interactions in tropical weather and climate, with the aim of improving our representation of convection in climate and NWP models. The project is divided into 5 work packages: i) development and testing of the high resolution modeling framework; ii) convection over West Africa (African Easterly Waves, AEWs and the diurnal cycle); ii) convection over the Indian Ocean and West Pacific Warm Pool (MJO, CCEW, diurnal cycle over Maritime Continent, including idealized studies of oceanic convection); iv) satellite observations (e.g. geostationary satellites, TRMM, CloudSat) to evaluate the high-resolution representation of the convective processes; and v) synthesis to improve the representation of convective processes in global NWP and climate models (Fig 4.4).



⁴ Natural Environment Research Council (NERC)-funded project involving University of Reading, University of Leeds, University of East Anglia, and the Met Office provides approximately 21 FTE-years of postdoctoral scientists.

Figure 57. *Summary of focus areas of the UK Cascade study.*

Cascade plans to perform case studies of particular events at resolutions ranging from about 1km to those typical of NWP and climate models using the Met Office Unified Model. The plan is to perform simulations at 40km, 12km, 4km and 1.5km grid-spacing, resolutions used operationally within the Met Office. The 40km and 12km models have 38 vertical levels and the 4km and 1.5km models 70 levels. The model includes options for 3 component (cloud liquid, rain and ice/snow) or 5 component (cloud liquid, rain, ice, snow, graupel) microphysics schemes. Convection parameterization operates in the 4km resolution integrations with the standard CAPE closure scheme modified to make the closure timescale a function of CAPE (Roberts, 2003). This limits the cloud base mass flux in high CAPE situations and allows the resolved circulation to take over.

Indian Ocean – West Pacific Warm Pool Studies will be focused on the MJO, CCEW and the diurnal cycle over the Maritime Continent and were chosen to lie within the YOTC timeframe. We have performed preliminary integrations at the 40km and 12km resolution and have done some analysis of the diurnal cycle at these resolutions. Detailed below are the integrations we plan to do as part of the project:

- One 6-month integration at 40km and 12km resolution forced by lateral boundary conditions from ECMWF starting about 15th October 2008 (to initialize the model near the beginning of the October MJO) with the model reinitialized approximately every month over a domain of 40E-183E, 22S-22N.
- Two ~1 month integrations forced by lateral boundary conditions from the 12km model starting around the 15th October 2008 to catch the October MJO event and around 5 April 2009 to catch the April 2009 MJO event (note the reinitialization of the 12km/40km model integrations will likely be chosen to coincide with this start date). The domain will be slightly smaller than the 12km integrations (about 2 degrees in each direction to allow the forcing to be determined from the 12km model (*This year*)).
- One ~1 month integration of one of the above events at 1.5km resolution forced by lateral boundary conditions from the 4km model (*Spring 2010*).

b) Tropical Channel Modeling

Forced at the meridional boundaries by NCEP/NCAR reanalysis and with specified SST the NCAR WRF-based NRCM has been run for 10 years at 36 km grid-spacing. Nested within the parent model are sub-domains at 12 km and 4 km grid-spacing run for shorter periods to provide information on convective organization. Figure 4.5, a snapshot of the total precipitable water for the 36 km grid during the 1998 El Nino event, shows the large-scale and synoptic-scale organization of atmospheric water, rivers of moisture flowing from the tropics to midlatitudes, and tropical cyclones. Evaluation of this multiscale simulation is in progress. It was anticipated that the multi-year simulations would reproduce reasonable MJO statistics under the influence of prescribed lateral boundary conditions derived from the global reanalyses.

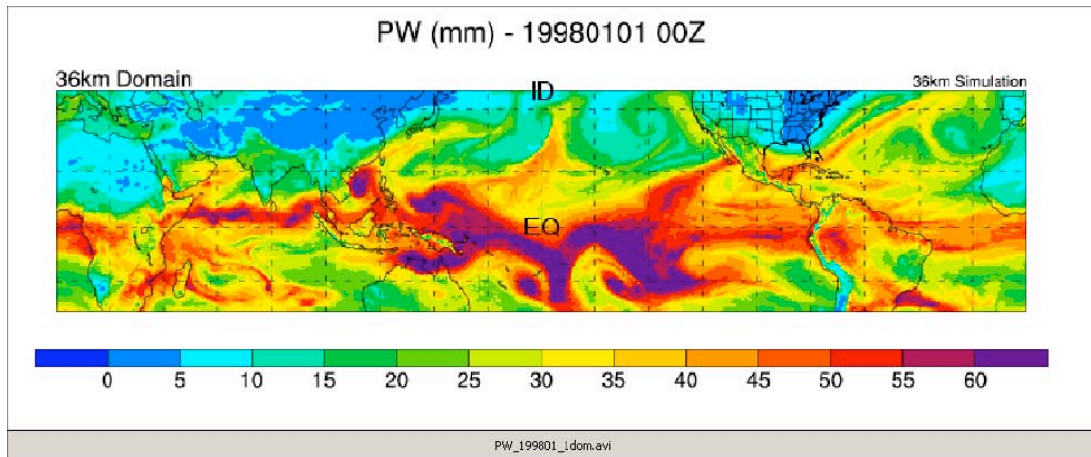


Figure 58. Snapshot of total precipitable water in the NCAR Tropical Channel Model (36-km grid).

As reported in Ray et al. (2009b), MJO statistics in the TCM are similar to those from

global climate models. The error in the mean state was identified as a reason for the poor performance. However, even with a large bias in the mean state, the multi-year simulation did capture two MJO events previously shown to be initiated by extratropical influences. The model did not reproduce a third event, whose initiation was not directly influenced by the extratropics. This indicates that in the absence of dynamical connections between the MJO and the lateral boundary conditions, the error in the mean state is sufficient to prevent MJO onset. Sensitivity tests showed that the simulation of this MJO event was not critically influenced by horizontal resolution, cumulus parameterization, sea surface temperature, and initial conditions. It took less than ten days for the error in the simulated mean state to reach its climate bias.

These results raise a number of questions:

- By what mechanism(s) do errors due to cumulus parametrization schemes in the parent domain affect the cloud-system resolving domains?
- What nature of error in the mean state is sufficient to destroy the MJO? Is it event dependent? A systematic study of multiple MJO events including “primary” events (no prior MJO) and “successive” (with prior MJO events), following the classification of Matthews (2007), may quantify this aspect.
- Is it possible for the NCRM to simulate MJOs not forced by extratropical excitation, i.e., validity of the upscale hypothesis obtained from theoretical studies?
- What are the implications for ENSO prediction? The May 1997 MJO event of Ray et al. (2009) which was poorly represented was followed shortly after by a very strong ENSO event in the summer (McPhaden 1999). The precipitation associated with 1997-98 ENSO event was disorganized in the NRCM simulation compared to observations despite being forced by observed SST. If such MJO events cannot be predicted beyond its believed predictability limit, do model errors affect the amplitude of the predicted ENSO?

c) Theoretical and idealized numerical modeling

Excellent progress has been made with theoretical and idealized modeling studies of multiscale convective organization. *This identifies untapped potential for making progress with the strategic problem of representing convective organization in global models.*

The upscale effects of organized precipitating convection has been demonstrated by dynamical models with emphasis on slantwise overturning and convective momentum transport (Moncrieff 1992; Moncrieff 2004; Biello et al. 2007, Majda and Stechmann 2009), by idealized global multiscale models configured on aquaplanets (Grabowski and Moncrieff 2001), and by superparameterized models (Grabowski 2001; Khairoutdinov et al. 2005). A spectrum of clouds is involved: deep convection, stratiform cloud, and cumulus congestus.

Another idealized approach has a dynamically passive boundary layer (heat and moisture reservoir), simplified parameterizations of convection, surface heat exchange, and radiative cooling, reduced dynamics: horizontally long and vertically grave (first- and second-baroclinic) gravity wave modes. While multi-scale convective organization occurs with the first-baroclinic mode (Yano *et al.* 1995), the second-baroclinic mode provides more realistic MJO systems (Khouider and Majda, 2006). Grabowski and Moncrieff (2001) simulated multi-scale systems in a two-dimensional global-scale CRM starting from a initially motionless and uniform base state. Westward-propagating MCSs developed spontaneously within an eastward-propagating large-scale envelope similar to observed MJOs. The vertical redistribution of horizontal momentum generates shear that sustains MCS, i.e., positive feedback.

Satoh et al. (2008) three-dimensional global CRM simulates westward-propagating systems embedded in the eastward-propagating cloud envelope suggests that these upscale effects may not be a two-dimensional artifact. The large-scale convective organization in Satoh et al. (2008) was Kelvin-like rather than MJO-like in terms of the fast eastward propagation speed (17 m/s).

The above studies raise the following question:

- Can the theoretical/idealized modeling results on upscale effects and the mode of large-scale organization be realized in full-physics prediction models?
- Is the correct representation of convective organization in the NRCM largely a resolution issue? Do difficulties global models experience with MJO stem from an inadequate representation of convective organization?
- Why does the NRCM generate too much Kelvin-like large-scale convective organization in preference to MJO-like organization?

The *Cascade* project plans to conduct idealized studies. These involve two long (~1-2month) large-domain (8000 x 4000km) radiative convective equilibrium type of numerical experiments at 4km resolution. The aim is to study the spontaneous organization of convection in a large tropical 3D domain. One experiment will be on an equatorial f-plane to examine the organization of convection in the absence of equatorial

wave dynamics. This experiment will also allow us to assess the sensitivity of the results of Bretherton et al. (2005) and Stephens et al. (2008) to dimensionality and domain size. The second experiment will include the full rotational effects on a similar domain to examine the impact of equatorial wave modes on the organization of convection.

c) MMF/superparameterization

Two-dimensional CRMs applied in as a superparameterization in the NCAR Community Atmospheric models (SP-CAM) by Khairoutdinov et al. (2005) generate strong mesoscale convective system (MCS) and robust MJOs. Figure 4.6 is a snapshot of the MCS-like systems simulated by the CRMs in SP-CAM. The MCS propagate eastward with the characteristic backward-tilt. The role of the MCS-like systems in generating MJOs is consistent with the role of upscale effects in mesoscale convection in generating large-scale tropical convective organization.

- Why do superparameterized global models produce overly-strong MJOs? Is this an artifact of the two-dimensional CRMs applied in superparameterization?
- Given that theoretical studies stress the importance of convective momentum transport, should the momentum tendencies be passed from the CRMs onto the global model grid in superparameterization/MMF?

d) Global CRMs

An aquaplanet version of NICAM with grid-spacing of 7 km and 3.5 km simulates large-scale tropical convective organization (Tomita et al., 2005, Miura et al., 2005). Nasuno et al (2007) analyzed the multiscale convective organization in the 40-day 7-km mesh and 10-day 3.5 km mesh of the Satoh et al. (2008) simulation. Cold-pool triggering of new convective activity occurred producing organized squall-type MCS in regions of stronger vertical shear. The westward-propagating MCS had the characteristic properties of the observed systems. In terms of propagation, the fast travel speed (about 15 m/s) of the large-scale organization resembles a convectively-coupled Kelvin wave rather than a MJO.

The above raises the questions:

- What is the initiation mechanism for MJOs in global CRMs?
- What are the relative roles of extratropical excitation in global CRMs compared to upscale evolution within the tropics?

e) Other contributions

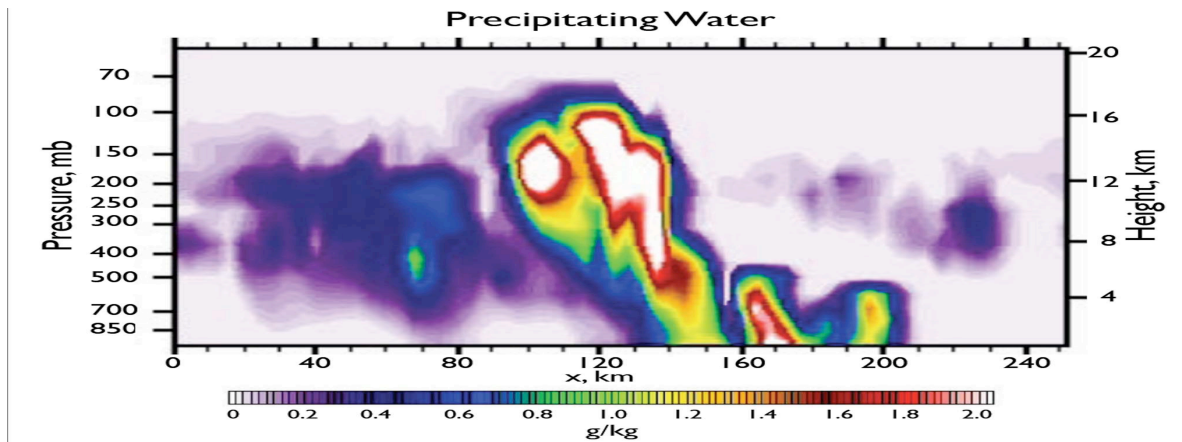


Figure 4.6: Snapshot of MCS-like convective organization in SP-CAM shown in terms of water content. [Courtesy: Marat Khairoutdinov, SUNY-Stony Brook.]

4.4.3 Easterly Waves and Tropical Cyclones

West African case studies are part of Cascade project. They address the AMMA period for the summer of 2006. Although the following 3 cases do not fall within the YOTC timeframe it is anticipated that the findings will be able to contribute our understanding of convective weather systems in this region. The focus of these studies will be the interactions between the diurnal cycle, mesoscale weather systems, African easterly waves (AEWs) and control by surface features. The cases are summarized below:

- **Case 1:** 26-28 July 2006 – Significant but “unusual” AEW with a range of significant scales.
- **Case 2:** 31 July – 5 Aug 2006 (or some time in that interval) – weak AEW activity but several strong storms, good examples of diurnal cycle, secondary initiation etc.
- **Case 3:** around 10 September 2006 – A “textbook” AEW that subsequently initiates an Atlantic hurricane.

[Further input: discussion at YOTC IP Workshop, e.g., Summer TPARC]

4.4.4 Diurnal Cycle

Superparameterization has been shown to improve the diurnal cycle. Figure 4.7 shows the geographical distribution of the local solar time (LST) of the non-drizzle precipitation frequency maximum in winter and summer of 1998 as simulated by a GCM, and two different MMFs: NASA Goddard and CSU (Tao et al. 2008). Both MMFs are superior to the standard GCM in regard to the late-afternoon precipitation maximum over land and the early-morning precipitation maximum over the oceans. The GCM produces a dominant morning maximum rain frequency over continents.

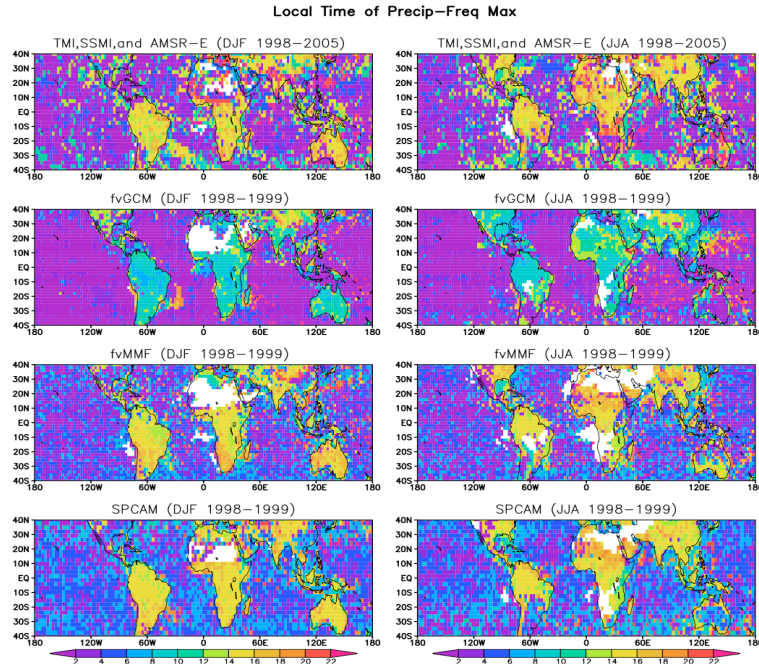


Figure 59. Distribution of the local solar time (LST) for the non-drizzle precipitation frequency maximum in winter (left panels) and summer (right panels) as observed by satellite from 1998-2005 (upper panels) and as simulated for two years (1998-1999) with the Goddard fvGCM (middle-upper panels), Goddard MMF (middle-lower panels) and CSU MMF (bottom panels). Blank regions indicate no precipitation. [Adapted from Tao et al. (2008).]

The evaluation of MMFs against observations, the treatment of orography in the CRMs, the implications of two-dimensionality, and improved MMFs models are active areas of research. The MMF-simulated diurnal variation of precipitation shows good agreement with merged microwave observations. For example, the MMF-simulated frequency maximum was in the late afternoon (1400-1800 LST) over land and in the early morning (0500-0700 LST) over the oceans. The fvGCM-simulated frequency maximum was too early for both oceans and land. The MMF results are based on detailed 2D GCE model-simulated hourly rainfall output. Satellite retrieved rainfall is based on a 5-satellite constellation including the TRMM Microwave Imager (TMI), Special Sensor Microwave Imager (SSMI) from the Defense Meteorological Satellite Program (DMSP) F13, F14 and F15, and the Advanced Microwave Scanning Radiometer – Earth Observing System (AMSR-E) onboard the Aqua satellite.

4.4.5 Tropical-Extratropical Interaction

Thomas Jung (ECMWF) is rerunning, at T255 resolution, the Ferranti et al. (1990) forecast relaxation experiments which were conducted at T42 resolution: i) a control forecast without relaxation to the tropical analysis; ii) a forecast with tropical relaxation in the 20S-20N region; iii) a forecast with relaxation over the North Pacific (10N-60N, 90E-220E). Ferranti found that in the extratropics, skill scores in the range of 11-20 days were noticeably improved, particularly over the Pacific/North American region.

[Incomplete: Input from YOTC IP Workshop and Winter TPARC]

4.4.6 Monsoons

[Discussion at the Implementation Workshop. indentify collaboration with Asian Monsoon Years (AMY)]

4.4.7 References

- Berner, J., G. Shutts, and T. Palmer, 2005: *Proceedings of the ECMWF Workshop on Representation of Sub-grid Processes using Stochastic-Dynamic Models*, 6-8 June, 2005, 129-139.
- Biello, J., A. J. Majda, and M. W. Moncrieff, 2007: Meridional momentum flux and super-rotation in the multiscale IPESD MJO model. *J. Atmos. Sci.*, **64**, 1636-1651.
- Boyle, J., S. Klein, G. Zhang, S. Xie, and X. Wei, 2008: Climate model forecast experiments for TOGA COARE. *Mon. Wea. Rev.*, **136**, 808-832.
- Bretherton, C.S., P.N. Blossey, and M. Khairoutdinov, 2005: An Energy-Balance Analysis of Deep Convective Self-Aggregation abover Uniform SST. *J. Atmos. Sci.*, **62**, 4273-4922.
- Caron, J.M., 2009: The Madden-Julian Oscillation in the nested regional climate model. *Clim. Dyn. (Special issue)*, submitted.
- Craig, G.C., B.G. Cohen, and R.S. Plant, 2005: Statistical mechanics and stochastic convective parameterization. *Proceedings of the ECMWF Workshop on Representation of Sub-grid Processes using Stochastic-Dynamic Models*, 6-8 June, 2005, 107-114.
- Done, J., G. Holland, A. Suzuki-Parker, and P. J. Webster, 2009: The role of wave energy accumulation in tropical cyclone genesis over the tropical North Atlantic. *Clim. Dyn. (Special Issue)*, submitted.
- Grabowski, W. W., 2001: Coupling cloud processes with the large-scale dynamics using the Cloud-resolving Convection parameterization (CRCP). *J. Atmos. Sci.*, **58**, 978-997.
- Grabowski, W.W., 2006: Impact of explicit atmosphere-ocean coupling on MJO-like coherent structures in idealized aquaplanet simulations. *J. Atmos. Sci.*, **63**, 2289-2306.
- Grabowski, W. W., X. Wu, M. W. Moncrieff, and W. D. Hall, 1998: Cloud-resolving modeling of cloud systems during Phase III of GATE. Part II: Effects of resolution and the third spatial dimension. *J. Atmos. Sci.*, **55**, 3264-3282.
- Grabowski, W. W., and P. K. Smolarkiewicz, 1999: CRCP: A cloud resolving convection parameterization for modeling the tropical convective atmosphere. *Physica*, **133**, 171-178.
- Houze, R. A., Jr., 2004: Mesoscale convective systems. *Rev. Geophys.*, **42**, RG4003, doi:10.1029/2004RG000150.
- Houze, R.A., Jr., and A.K. Betts, 1981: Convection in GATE. *Rev. Geophys. Space. Phys.*, **19**, 541-576.

- Khairoutdinov, M. F., and D. A. Randall, 2001: A cloud resolving model as a cloud parameterization in the NCAR community climate system model: Preliminary results. *Geophys. Res. Lett.*, **28**, 3617-3620.
- Khairoutdinov, M.F., D. Randall, and C. DeMott, 2005: Simulations of the Atmospheric General Circulation Using a Cloud-Resolving Model as a Superparameterization of Physical Processes. *J. Atmos. Sci.*, **62**, 2136-2154.
- Khairoutdinov, M., C. DeMott, and D. Randall, 2008: Evaluation of the Simulated Interannual and Subseasonal Variability in an AMIP-Style Simulation Using the CSU Multiscale Modeling Framework *J. Climate*, **21**, 413-431
- Khouider, B., and A. J. Majda, 2007: A simple multicloud parameterization for convectively coupled tropical waves. Part II: Nonlinear simulations. *J. Atmos. Sci.*, **64**, 381-400.
- Klingaman, N. P., P. M. Inness, H. Weller, and J. M. Slingo, 2008: The Importance of High-Frequency Sea Surface Temperature Variability to the Intraseasonal Oscillation of Indian Monsoon Rainfall. *J. Climate*, **21**, 6119-6140.
- Klingaman, N.P., H. Weller, S.J. Woolnough, P. M. Inness and J.M. Slingo, 2009: Coupled simulations of the Indian monsoon intraseasonal oscillation with a fine-resolution mixed-layer model. *Proc. ECMWF Workshop on Ocean-Atmosphere Interaction*, 10-12 November 2008, 195-205.
- Kuell, V., A. Gassmann, and A. Bott, 2007: Towards a new hybrid cumulus parametrization scheme for use in non-hydrostatic weather prediction models. *Quart. J. Roy. Meteor. Soc.*, **133**, 479-490.
- Majda, A.J., and S. N. Stechmann, 2009: A simple dynamical model with features of convective momentum transport *J. Atmos. Sci.*, **66**, 373-392.
- Matthews, A.J., 2007: Primary and successive events in the Madden-Julian Oscillation, *Quart. J. Roy. Meteor. Soc.*, **134**, 439-453.
- Miura, H., H. Tomita, T. Nasuno, S. Iga, M. Satoh, and T. Matsuno, 2005: A climate sensitively test using a global cloud resolving model under an aqua planet condition. *Geophys. Res. Lett.*, **32**, L19717, doi:1029/2005GL023672.
- Moncrieff, M. W., 2004: Analytic representation of the large-scale organization of tropical convection. *J. Atmos. Sci.*, **61**, 1521-1538.
- Moncrieff, M. W., and E. Klinker, 1997: Mesoscale cloud systems in the Tropical Western Pacific as a process in general circulation models. *Quart. J. Roy. Meteorol. Soc.*, **123**, 805-827.
- Moncrieff, M. W., S. K. Krueger, D. Gregory, J.-L. Redelsperger, and W.-K. Tao, 1997: GEWEX Cloud System Study (GCSS) Working Group 4: Precipitating convective cloud systems. *Bull. Amer. Meteor. Soc.*, **78**, 831-845.
- Moncrieff, M. W., and C. Liu, 2006: Representing convective organization in prediction models by a hybrid strategy. *J. Atmos. Sci.*, **63**, 3404-3420.
- Moncrieff, M. W., M. Shapiro, J. Slingo, and F. Molteni, 2007: Collaborative research at the intersection of weather and climate. *WMO Bulletin*, **56**, 204-211.
- Nasuno, T., H. Tomita, S. Iga, and H. Miura, 2007: Multiscale organization of convection simulated with explicit cloud processes on an aquaplanet. *J. Atmos. Sci.*, **64**, 1902-1921.
- Randall, D. A., J. Curry, P. Duynkerke, S. K. Krueger, M. W. Moncrieff, B. Ryan, D. O. Starr, M. Miller, W. Rossow, G. Tseliudis, and B. A. Wielicki, 2003a: Confronting models with data, The GEWEX cloud system study. *Bull. Amer. Meteor. Soc.*, **84**, 455-469.
- Randall, D. A., M. Khairoutdinov, A. Arakawa, and W. W. Grabowski, 2003b: Breaking the cloud parameterization deadlock. *Bull. Amer. Meteor. Soc.*, **84**, 1547-1564.
- Ray, P., C. Zhang, J. Dudhia, and S. S. Chen (2008), A numerical case study on the initiation of the Madden-Julian Oscillation, *J. Atmos. Sci.*, **66**, 310-331.
- Ray, P., C. Zhang, M. W. Moncrieff, J. Dudhia, J. M. Caron, L. R. Leung and C. Bruyere, 2009: The role of the mean state on the initiation of the Madden-Julian Oscillation. *Clim. Dyn. (Special Issue)*, submitted.

- Ray, P., C. Zhang, A case study on the mechanics of extratropical influences on the initiation of the Madden-Julian Oscillation, *J. Atmos. Sci.*, (accepted).
- Roberts N. M., 2003: The impact of a change to the use of the convection scheme in high-resolution simulations of convective events. *Met Office Forecasting Research Tech. Rep. 407*, 30 pp.
- Satoh, M., T. Matsuno, H. Tomita, H. Miura, T. Nasuno, and S. Iga, 2008: Nonhydrostatic icosahedral atmospheric model (NICAM) for global cloud resolving simulations. *J. Comp. Phys.*, **227**, 3486-3514.
- Shutts, G.J., and T. N. Palmer, 2007: Convective forcing fluctuations in a cloud-resolving model: Relevance to the stochastic parameterization problem. *J. Climate*, **20**, 187-202.
- Skamarock, W.C. , (2004), Evaluating mesoscale NWP models using kinetic energy spectra. *Mon. Wea. Rev.*, **132**, 3019-3032.
- Sperber K. R., J. M. Slingo, P. M. Innes, and W. K.-M. Lau, 1997: On the maintenance and initiation of the intraseasonal oscillation in the NCEP/NCAR reanalysis and in the GLA and UKMO AMIP simulations. *Climate Dyn.*, **13**, 769-795.
- Sperber, K. R., J. M. Slingo, D. E. Waliser, and P. M. Inness, 2008: Coarse-resolution models only partly cloudy (Comment on "A Madden-Julian oscillation event simulated by a global cloud-resolving model" by Miura et al.), *Science*, **320**, 612.
- Stephens G. L., P. J. Webster, R. H. Johnson, R. Engelen, and T. L'Ecuyer, 2004: Observational evidence for the mutual regulation of the tropical hydrological cycle and tropical sea surface temperatures. *J. Climate*, **17**, 2213-2224.
- Stephens, G.L., S. van den Heever, and L. Pakula, 2008: Radiative-Convective Feedbacks in Idealized States of Radiative-Convective Equilibrium. *J. Atmos. Sci.*, **65**, 2899-3916.
- Tao, W.-K., and J. Simpson, 1993: The Goddard Cumulus Ensemble Model. Part I: Model description. *Terrestrial, Atmospheric and Oceanic Sciences*, **4**, 19-54.
- Tao, W.-K., and M. W. Moncrieff, 2009: Multiscale Cloud-System Modeling. *Rev. Geophys.*, in press.
- Tao, W.-K., J.-D. Chern, R. Atlas, D. Randall, M. Khairoutdinov, J.-L. Li, D. E. Waliser, A. Hou, X. Lin, C. Peters-Lidard, W. Lau, J. Jiang, and J. Simpson, 2009: A multi-scale modeling system: Developments, applications and critical Issues. *Bull. Amer. Meteor. Soc.*, **90**, 515-534.
- Teixeira, J., and C.N. Reynolds, 2008: Stochastic nature of physical parameterizations in ensemble prediction: A stochastic convection approach. *Mon. Wea. Rev.*, **136**, 483-496.
- Teixeira, J., S. Cardoso, A. P. Siebesma, and the GPCI Team, 2008: Results from the first 2 years of the GCSS Pacific Cross-section Intercomparison. *GEWEX NEWS*. **18-4**, 1-4.
- Teixeira, J., and co-authors, 2009: Tropical and sub-tropical cloud transitions in weather and climate prediction models: the GCSS/WGNE Pacific Cross-section Intercomparison (GPCI). *Journal of Climate*, internal reviews before submission.
- Tomita, H., H. Miura, H. Iga, T. Nasuno, and M. Satoh, 2005: A global cloud-resolving simulation: Preliminary results from an aqua planet experiment. *Geophys. Res. Lett.*, **32**, L08805, doi:10.1029/2005GL022459.
- Tompkins, A., Stochastic convective input based on subgrid humidity distributions, 2005: *Proceedings of the ECMWF Workshop on Representation of Sub-grid Processes using Stochastic-Dynamic Models*, 6-8 June, 2005, 15-128.
- Tulich, S.N., and G.N. Kiladis, 2009: Convectively-coupled Kelvin and easterly waves in a nested regional climate model. *Clim. Dyn. (Special Issue)*, submitted
- Wu, X., and M. W. Moncrieff, 1996: Collective effects of organized convection and their approximation in general circulation models. *J. Atmos. Sci.*, **53**, 1477-1495.
- Wu, X., W. W. Grabowski, and M.W. Moncrieff, 1998: Long-term behavior of cloud systems in TOGA COARE and their interactions with radiative and surface processes. Part I: Two-dimensional modeling study. *J. Atmos. Sci.*, **55**, 2693-2714.
- Wu, X., L. Deng, X. Song, G. Vettoretti, W. R. Peltier, and G. J. Zhang, 2007: Impact of a modified convective scheme on the Madden-Julian Oscillation and El Niño-Southern Oscillation in a

coupled climate model. *Geophys. Res. Lett.*, **34**, L16823, doi:10.1029/2007GL030637.
Yano, J. I., J. C. McWilliams, M. W. Moncrieff, and K. A. Emanuel, 1995: Hierarchical tropical cloud systems in an analog shallow-water model. *J. Atmos. Sci.*, **52**, 1724-1742.
YOTC Science Plan, 2008: WMO TD **1452**, WCRP TD **130**, WWRP/THORPEX, TD **9**, 26 pp.

5 Analysis Framework

6 Appendices

6.1 ECMWF Variables

6.1.1 Two – Dimensional Analysis Fields

10 metre U wind component	10 metre V wind component
2 metre dewpoint temperature	2 metre temperature
Albedo	Angle of sub-gridscale orography
Anisotropy of sub-gridscale orography	Budget values
Charnock	Geopotential
High cloud cover	High vegetation cover
Ice surface temperature layer 1	Ice surface temperature layer 2
Ice surface temperature layer 3	Ice surface temperature layer 4
Land-sea mask	Logarithm of surface roughness length for heat
Low cloud cover	Low vegetation cover
Mean sea level pressure	Medium cloud cover
Near IR albedo for diffuse radiation	Near IR albedo for direct radiation
Sea surface temperature	Sea-ice cover
Skin reservoir content	Skin temperature
Slope of sub-gridscale orography	Snow albedo
Snow density	Snow depth
Soil temperature level 1	Soil temperature level 2
Soil temperature level 3	Soil temperature level 4
Soil type	Standard deviation of filtered subgrid orography
Standard deviation of orography	Surface pressure
Surface roughness	Temperature of snow layer
Total cloud cover	Total column ozone
Total column water	Total column water vapour
Type of high vegetation	Type of low vegetation
UV visible albedo for diffuse radiation	UV visible albedo for direct radiation
Volumetric soil water layer 1	Volumetric soil water layer 2
Volumetric soil water layer 3	Volumetric soil water layer 4

6.1.2 Three – Dimensional Pressure-Level Analysis Fields

Divergence
Geopotential
Ozone mass mixing ratio
Potential vorticity
Relative humidity
Specific humidity
Temperature

U velocity
V velocity
Vertical velocity
Vorticity (relative)

Provided on Pressure Levels:

1000	950	925	900	850	800	700	600	500	400	300	250	200
	150	100	70	50	30	20	10	7	5	3	2	1

6.1.3 Two – Dimensional Forecast Fields

10 metre U wind component	10 metre V wind component
10 metre wind gust	10 metre wind gust in the past 6 hours
2 metre dewpoint temperature	2 metre temperature
Boundary layer dissipation	Boundary layer height
Budget values	Charnock
Convective available potential energy	Convective precipitation
Downward UV radiation at the surface	East-West surface stress
Evaporation	Forecast albedo
Forecast logarithm of surface roughness for heat	Forecast surface roughness
Friction velocity	Geopotential
Gravity wave dissipation	High cloud cover
Ice surface temperature layer 1	Ice surface temperature layer 2
Ice surface temperature layer 3	Ice surface temperature layer 4
Instantaneous X surface stress	Instantaneous Y surface stress
Instantaneous moisture flux	Instantaneous surface heat flux
Land-sea mask	Large-scale precipitation fraction
Latitudinal component of gravity wave stress	Low cloud cover
Maximum temperature at 2 metres since last 6 hours	Maximum temperature at 2 metres since previous post-processing
Mean sea level pressure	Medium cloud cover
Meridional component of gravity wave stress	Minimum temperature at 2 metres since last 6 hours
Minimum temperature at 2 metres since previous post-processing	Neutral wind at 10 m x-component
Neutral wind at 10 m y-component	North-South surface stress
Photosynthetically active radiation at the surface	Runoff
Sea surface temperature	Sea-ice cover
Skin reservoir content	Skin temperature
Snow albedo	Snow density
Snow depth	Snow evaporation
Snowfall	Snowmelt
Soil temperature level 1	Soil temperature level 2
Soil temperature level 3	Soil temperature level 4
Stratiform precipitation (Large-scale precipitation)	Sunshine duration
Surface latent heat flux	Surface net solar radiation, clear sky
Surface net thermal radiation, clear sky	Surface pressure
Surface sensible heat flux	Surface solar radiation
Surface solar radiation downwards	Surface thermal radiation
Surface thermal radiation downwards	TOA incident solar radiation
Temperature of snow layer	Top net solar radiation, clear sky

Top net thermal radiation, clear sky	Top solar radiation
Top thermal radiation	Total cloud cover
Total column ice water	Total column liquid water
Total column ozone	Total column water
Total column water vapour	Total precipitation
Vertically integrated moisture divergence	Volumetric soil water layer 1
Volumetric soil water layer 2	Volumetric soil water layer 3
Volumetric soil water layer 4	

6.1.4 Three – Dimensional Pressure-Level Forecast Fields

Divergence
Geopotential
Ozone mass mixing ratio
Potential vorticity
Relative humidity
Specific humidity
Temperature
U velocity
V velocity
Vertical velocity
Vorticity (relative)

Provided on Pressure Levels:

1000	950	925	900	850	800	700	600	500	400	300	250	200
	150	100	70	50	30	20	10	7	5	3	2	1

6.1.5 Three – Dimensional Model-Level Forecast Fields

Cloud cover
Cloud ice water content
Cloud liquid water content
Divergence
Geopotential
Logarithm of surface pressure
Ozone mass mixing ratio
Specific humidity
Temperature
U velocity
V velocity
Vertical velocity
Vertical velocity in the hybrid eta vertical coordinate system
Vorticity (relative)

Provided on 91-Model Levels.

6.1.6 Three – Dimensional Pressure-Level Physics Forecast Fields

Note that these fields are provided every 3 hours out to 36 hours.

Cloud cover
Cloud ice water content
Cloud liquid water content
Ice precip Conv
Ice precip Strat
Liq precip Conv
Liq precip Strat
Mflux-down Conv
Mflux-up Conv
T-tend Clouds
T-tend Conv
T-tend Dyn
T-tend Rad
T-tend SO
T-tend SW Rad
T-tend Shal Conv
T-tend Turb+SO
U-tend Conv
U-tend Dyn
U-tend SO
U-tend Shal Conv
U-tend Turb+SO
V-tend Conv
V-tend Dyn
V-tend SO
V-tend Shal Conv
V-tend Turb+SO
q-tend Clouds
q-tend Conv
q-tend Dyn
q-tend Shal Conv
q-tend Turb
qi-tend Clouds
ql-tend Clouds

Provided on Pressure Levels:

1000	950	925	900	850	800	700	600	500	400	300	250	200
	150	100	70	50	30	20	10	7	5	3	2	1

6.1.7 Two – Dimensional Physics Forecast Fields

Note that these fields are provided out to only 36 hours.

Total Column Rain
Total Column Snow

6.2 GMAO Variables

6.2.1 Two-Dimensional, Hourly, Time-averaged Assimilation and Forecast Fields – Single Level Diagnostics Collection

Sea level pressure	Northward wind at 2 m above displacement height
Time-averaged surface pressure	Northward wind at 50 m above surface
Eastward wind at 850 hPa, 500 hPa, 250 hPa	Temperature at 10 m above displacement height
Northward wind at 850 hPa, 500 hPa, 250 hPa	Temperature at 2 m above displacement height
Temperature at 850 hPa, 500 hPa, 250 hPa	Specific humidity at 10 m above displacement height
Specific humidity at 850 hPa, 500 hPa, 250 hPa	Specific humidity at 2 m above displacement height
Height at 1000 hPa, 850 hPa, 500 hPa, 250 hPa	Radiative skin temperature
Vertical pressure velocity at 500 hPa	Displacement height
Eastward wind at 10 m above displacement height	Tropopause pressure
Eastward wind at 2 m above displacement height	Tropopause specific humidity
Eastward wind at 50 m above surface	Tropopause temperature
Northward wind at 10 m above displacement height	Cloud-top pressure
Northward wind at 2 m above displacement height	Cloud-top temperature

6.2.2 Two-Dimensional, Hourly, Time-averaged Assimilation and Forecast Fields – Turbulence Collection

Latent heat flux	Eastward wind of lowest model layer
Surface evaporation	Northward wind of lowest model layer
Sensible heat flux	Surface air density
Eastward surface wind stress	Effective surface wind speed
Northward surface wind stress	Surface exchange coefficient for heat
Eastward gravity wave surface stress	Surface exchange coefficient for moisture
Northward gravity wave surface stress	Surface exchange coefficient for momentum
Planetary boundary layer height	Surface neutral drag coefficient
Surface buoyancy scale	Effective turbulence skin temperature
Surface velocity scale	Effective turbulence skin humidity
Surface temperature scale	Sea-ice fraction
Surface humidity scale	Surface precipitation flux from anvils
Surface Richardson number	Surface precipitation flux from convection
Roughness length, sensible heat	Surface precipitation flux from large-scale
Roughness length, momentum	Surface snowfall flux
Height of center of lowest model layer	Total surface precipitation flux
Temperature of lowest model layer	Total generation of precipitation
Specific humidity of lowest model layer	Total re-evaporation of precipitation

6.2.3 Two-Dimensional, Hourly, Time-averaged Assimilation and Forecast Fields – Radiation Collection

Surface skin temperature	Absorbed longwave at the surface with no clouds
Surface albedo	Absorbed longwave at the surface with no clouds or aerosols
Diffuse beam NIR surface albedo	Net downward longwave flux at the surface
Direct beam NIR surface albedo	Net downward longwave flux at the surface for cloud-free sky
Diffuse beam VIS-UV surface albedo	Net downward longwave flux at the surface for clear sky
Direct beam VIS-UV surface albedos	Upward longwave flux at top of atmosphere
Emitted longwave at the surface	Upward longwave flux at TOA assuming clear sky

Absorbed longwave at the surface	Upward LW flux at TOA assuming clear clean sky
TOA incident shortwave flux	TOA outgoing shortwave flux assuming clear clean sky
Surface incident shortwave flux	Optical thickness of high clouds
Surface incident shortwave flux assuming clear sky	Optical thickness of low clouds
Surface net downward shortwave flux	Optical thickness of mid-level clouds
Surface net downward shortwave flux assuming clear sky	Optical thickness of all clouds
Surface net downward shortwave flux assuming clean sky	High-level (above 400 hPa) cloud fraction
Surface net downward shortwave flux assuming clear clean sky	Low-level (1000-700 hPa) cloud fraction
TOA outgoing shortwave flux	Mid-level (700-400 hPa) cloud fraction
TOA outgoing shortwave flux assuming clear sky	Total cloud fraction
TOA outgoing shortwave flux assuming clean sky	

6.2.4 Two-Dimensional, Hourly, Time-averaged Assimilation and Forecast Fields – Land Surface Collection

Vegetation greenness fraction	Fractional unsaturated area
Leaf area index	Fractional saturated area
Root zone soil wetness	Fractional snow-covered area
Top soil layer wetness	Fractional wilting area
Top snow layer temperature	Surface downward PAR diffuse flux
Surface temperature of unsaturated zone	Surface downward PAR beam flux
Surface temperature of saturated zone	Sensible heat flux from land
Surface temperature of wilted zone	Latent heat flux from land
Surface snowfall	Evaporation from land
Total surface precipitation	Net downward longwave flux over land
Snow mass	Net downward shortwave flux over land
Snow depth	Downward heat flux at base of top soil layer
Bare soil evaporation	Total water store in land reservoirs
Transpiration	Energy store in all land reservoirs
Interception Loss	Total land water change per unit time
Sublimation	Total land energy change pre unit time
Overland runoff	Spurious land energy source
Baseflow	Spurious land water source
Snowmelt	Spurious snow source

6.2.5 Two-Dimensional, Hourly, Time-averaged Assimilation and Forecast Fields – Ocean Surface Collection

Specific humidity at 10 m above the surface	Net downward shortwave flux over sea-ice
Sensible heat flux from the ocean	Surface snowfall over ocean and sea-ice
Sensible heat flux from sea-ice	Surface precipitation over ocean and sea-ice
Latent heat flux from the ocean	Eastward surface wind stress over ocean
Latent heat flux from sea-ice	Northward surface wind stress over ocean
Net downward longwave flux over ocean	Eastward surface wind stress over sea-ice
Net downward longwave flux over sea-ice	Northward surface wind stress over sea-ice
Net downward shortwave flux over ocean	Fraction of sea-ice

6.2.6 Three-Dimensional, 3-Hourly, Instantaneous Pressure-Level Assimilation and Forecast Fields (3 Collections)

Sea-level pressure (2D)
Temperature
Eastward wind component
Northward wind component
Vertical pressure velocity
Surface pressure (2D)
Surface geopotential (2D)
Geopotential height
Ozone mass mixing ratio
Ertel potential vorticity
Relative humidity
Specific humidity
Cloud liquid water mixing ratio
Cloud ice mixing ratio

6.2.7 Three-Dimensional, 3-Hourly, Time-averaged Pressure-Level Assimilation and Forecast Fields – 3D Cloud Diagnostics Collection

Relative humidity
Cloud liquid water mixing ratio – large scale
Cloud ice mixing ratio – large scale
Cloud liquid water mixing ratio – anvils
Cloud ice mixing ratio – anvils
Cloud condensate mixing ratio – convective updraft
3D cloud fraction – large scale
3D cloud fraction – anvils
3D cloud fraction – convective

6.2.8 Three-Dimensional, 3-Hourly, Time-averaged Pressure-Level Assimilation and Forecast Fields – 3D Moist Processes Diagnostics Collection

Upward moist convective mass flux
Precipitation production rate – convective
Precipitation production rate – large-scale + anvil
Downward flux of liquid precipitation - convective
Downward flux of ice precipitation - convective
Downward flux of liquid precipitation – large-scale + anvil
Downward flux of ice precipitation – large-scale + anvil
Evaporation of precipitating convective condensate
Evaporation of precipitating large-scale + anvil condensate

6.2.9 Three-Dimensional, 3-Hourly, Time-averaged Pressure-Level Assimilation and Forecast Fields – 3D Radiation Diagnostics Collection

3D cloud fraction
Temperature tendency from terrestrial radiation
Temperature tendency from terrestrial radiation (clear sky)
Temperature tendency from solar radiation
Temperature tendency from solar radiation (clear sky)

6.2.10

6.2.11 Three-Dimensional, 3-Hourly, Time-averaged Pressure-Level Assimilation and Forecast Fields – 3D Turbulence Diagnostics Collection

Momentum diffusivity
Momentum diffusivity from Louis
Momentum diffusivity from Lock
Heat (scalar) diffusivity
Heat (scalar) diffusivity from Louis
Heat (scalar) diffusivity from Lock
Heat (scalar) diffusivity from Lock, radiative contribution
Heat (scalar) diffusivity from Lock, surface contribution
Richardson number

6.2.12 Three-Dimensional, 3-Hourly, Time-averaged Pressure-Level Assimilation and Forecast Fields – 3D Temperature Tendencies Collection

Temperature tendency from radiation
Temperature tendency from moist physics
Temperature tendency from turbulence
Temperature tendency from frictional heating
Temperature tendency from gravity wave drag
Temperature tendency from physics
Temperature tendency from dynamics
Temperature tendency from analysis

6.2.13 Three-Dimensional, 3-Hourly, Time-averaged Pressure-Level Assimilation and Forecast Fields – 3D Wind Tendencies Collection

U-wind tendency from moist physics	V-wind tendency from moist physics
U-wind tendency from turbulence	V-wind tendency from turbulence
U-wind tendency from gravity wave drag	V-wind tendency from gravity wave drag
U-wind tendency from dynamics	V-wind tendency from dynamics
U-wind tendency from analysis	V-wind tendency from analysis

6.2.14 Three-Dimensional, 3-Hourly, Time-averaged Pressure-Level Assimilation and Forecast Fields – 3D Moisture Tendencies Collection

Water vapor tendency from moist physics	Ice tendency from turbulence
Water vapor tendency from turbulence	Ice tendency from dynamics
Water vapor tendency from chemistry	Liquid water tendency from moist physics
Water vapor tendency from dynamics	Liquid water tendency from turbulence
Water vapor tendency from analysis	Liquid water tendency from dynamics
Ice tendency from moist physics	

6.2.15 Three-Dimensional, 3-Hourly, Time-averaged Pressure-Level Assimilation and Forecast Fields – 3D Ozone Tendencies Collection

Ozone tendency from moist physics
Ozone tendency from turbulence
Ozone tendency from chemistry
Ozone tendency from dynamics
Ozone tendency from analysis

6.2.16 6-Hourly, Instantaneous, Model-Level Analysis Collection

Surface pressure
Layer pressure thickness
Air temperature
Eastward wind component
Northward wind component
Specific humidity
Ozone mixing ratio

6.2.17 6-Hourly, Instantaneous, Pressure-Level Analysis Collection

Sea-level pressure
Surface pressure
Geopotential height
Air temperature
Eastward wind component
Northward wind component
Specific humidity
Ozone mixing ratio

6.2.18 Invariants Collection

Surface geopotential
Standard deviation of topography for gravity wave drag
Fraction of lake type in grid box
Fraction of land type in grid box
Fraction of land ice type in grid box
Fraction of ocean in grid box
Area of grid box

6.2.19 Notes

- Details of the specific collections, including definitions and units, can be found in the MERRA product file specification document, available at:
http://gmao.gsfc.nasa.gov/research/merra/MERRA_FileSpec_DRAFT_09_02_2008.pdf.
More details are also available at each collection's **info** link, under the OpenDap tab, at the web site.
- All data are at the model's native resolution ($1/4^\circ \times 1/3^\circ$), except time-averaged 3D diagnostics produced during the forecast; these are at a reduced resolution ($1/2^\circ \times 1/2^\circ$).
- The native grid has the first point in longitude centered on the dateline; in latitude the first point is at the south pole and the last at the north pole. Thus, fields are 1080 x 361.
- Reduced resolution data are on ($1/2^\circ \times 1/2^\circ$) boxes with the first box having its western edge at the dateline and its southern edge at the South Pole.

- All data are in NETCDF-4/HDF5 format.
- The 6-Hourly, Instantaneous, Model-Level Analysis Collection is provided on the 72 model levels.
- Collections on model levels include the 3D pressure thickness of the layers. Edge pressures can be computed using 1 Pa as the top pressure of the top layer. Layers are numbered from top to bottom.
- 3D pressure-level data are provided on 37 Pressure Levels:

1000	975	950	925	900	875	850	825	800	775	750	725
700	650	600	550	500	450	400	350	300	250	200	150
100	70	50	40	30	20	10	7	5	4	3	2
1											

6.3 NCEP Tendencies

T tendency from shortwave
T tendency from longwave
T tendency from vertical diffusion
T tendency from deep convection
T tendency from shallow convection
T tendency from grid scale
moistening rate from vertical diffusion
moistening rate from deep convection
moistening rate from shallow convection
moistening rate from grid scale
ozone vertical diffusion
ozone production
ozone tendency
ozone production from temperature term
zonal acceleration from vertical diffusion
zonal acceleration from gravity wave drag
zonal acceleration from convective momentum mixing
meridional acceleration from vertical diffusion
meridional acceleration from gravity wave drag
meridional acceleration from convective momentum mixing
non-convective cloud fraction